AD-A136 044 EFFICIENT FINITE ELEMENT METHODS FOR TRANSIENT NONLINEAR ANALYSIS OF SHEL..(U) NORTHWESTERN UNIV EVANSTON IL DEPT OF CIVIL ENGINEERING T BELYTSCHKO

UNCLASSIFIED AUG 83 AFOSR-TR-83-1062 F49620-82-K-0013 F/G 13/13 NL

1/2

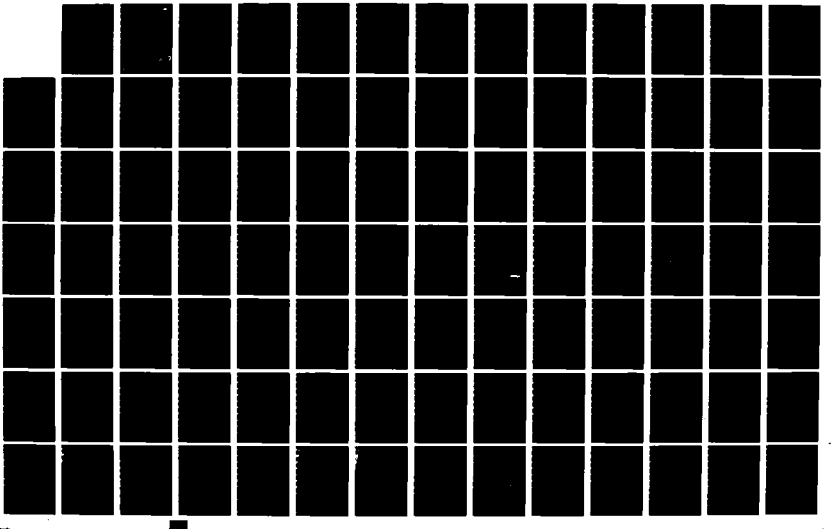

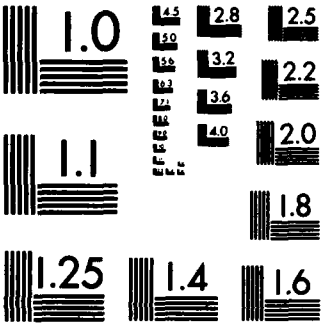

MICROCOPY RESOLUTION TEST CHART
NATIONAL BUREAU OF STANDARDS-1963-A

F49620-82-K-0013

AFOSR-TR- 83-1062

EFFICIENT FINITE ELEMENT METHODS FOR TRANSIENT NONLINEAR ANALYSIS OF SHELLS

TED BELYTSCHKO

Department of Civil Engineering
Northwestern University
Evanston, Illinois 60201

AUGUST 1983

TECHNICAL REPORT F49620-82-K-0013
~~Interim~~ Report for Period February 1982 - ~~February~~ January 1983
Annual

UNCLASSIFIED

SECURITY CLASSIFICATION OF THIS PAGE (When Data Entered)

REPORT DOCUMENTATION PAGE	READ INSTRUCTIONS BEFORE COMPLETING FORM
1. REPORT NUMBER: AFOSR-TR- 83-1062	2. GOVT ACCESSION NO.: AD-A136 044
	3. RECIPIENT'S CATALOG NUMBER
4. TITLE (and Subtitle): Efficient Finite Element Methods for Transient Nonlinear Analysis of Shells	5. TYPE OF REPORT & PERIOD COVERED: ANNUAL: 01 FEB 82-31 JAN 83
	6. PERFORMING ORG. REPORT NUMBER
7. AUTHOR(s): Ted Belytschko	8. CONTRACT OR GRANT NUMBER(s): F49620-82-K-0013
9. PERFORMING ORGANIZATION NAME AND ADDRESS: Department of Civil Engineering, Northwestern University, Evanston, Il 60201	10. PROGRAM ELEMENT, PROJECT, TASK AREA & WORK UNIT NUMBERS: 61102F, 2307/B1
11. CONTROLLING OFFICE NAME AND ADDRESS: AFOSR/NA, Bolling AFB, DC 20332	12. REPORT DATE: AUGUST 1983
	13. NUMBER OF PAGES: 171
14. MONITORING AGENCY NAME & ADDRESS(if different from Controlling Office)	15. SECURITY CLASS. (of this report): Unclassified
	15a. DECLASSIFICATION/DOWNGRADING SCHEDULE

16. DISTRIBUTION STATEMENT (of this Report)

Approved for public release; distribution unlimited

17. DISTRIBUTION STATEMENT (of the abstract entered in Block 20, if different from Report)

18. SUPPLEMENTARY NOTES

19. KEY WORDS (Continue on reverse side if necessary and identify by block number)

Finite elements, shells, structural dynamics, kinematic modes, hourglass control, reduced integration

20. ABSTRACT (Continue on reverse side if necessary and identify by block number)

The major emphasis of this project has been on the development of simple elements which require at most one quadrature point per node in a finite element mesh. Examples of these elements are triangular and quadrilateral elements with one-point quadrature and 9 node elements with 2 x 2 quadrature. A major difficulty with such elements is the rank deficiency of the element stiffness, which results in kinematic modes, which are called hourglass modes for the four node

DD FORM 1 JAN 73 1473 EDITION OF 1 NOV 65 IS OBSOLETE

UNCLASSIFIED

SECURITY CLASSIFICATION OF THIS PAGE (When Data Entered)

quadrilateral. Therefore, the first part of this research program has focused on developing an understanding of the mechanisms of rank deficiency and locking and of providing a rational and effective method for the control of kinematic modes.

The major outcome of this research has been the development of an effective procedure for controlling the kinematic modes in the four node quadrilateral plate-shell element when one quadrature point is used. In addition, the insights gained from that work have enabled us to develop a triangular plate shell element with three nodes which only requires a single quadrature point. Both of these results make possible highly efficient nonlinear transient calculations for they permit the use of very simple elements without any deleterious effects on the rate of convergence.

In addition, some unusual behavior of higher order elements, such as the 9 node plate-shell element, which we call membrane locking, has been discovered and investigated. This is a phenomenon associated with curved elements that can lead to severe errors if the number of quadrature points is too high. The importance of this finding is that many finite element workers recommend using more quadrature points when the material is nonlinear in order to represent the material nonlinearity effectively. These findings show that if recourse is taken to higher order quadrature in such elements, the performance of the element may in fact deteriorate because of the onset of membrane locking.

The results of the research conducted so far indicate that in the analysis of curved shells, an optimal integration scheme is associated with each element and deviations from this optimal integration scheme can lead to significant errors. This is of considerable importance in the use of curved shell elements in structural analysis where closed form solutions are often not available, because the damaging effects of over and underintegration often are not readily apparent. Results of the research conducted so far indicate that optimal integration schemes in the four node and nine node elements are all associated with kinematic modes. An effective method for the control of these modes for linear problems has been developed for the four-node element. The performance of the hourglass control method has been examined in linear and nonlinear problems. Although some unresolved difficulties remain to be dealt with in nonlinear material problems, the procedure is quite effective and yields a highly efficient element which is suitable for many applications in transient analysis.

Explicit Algorithms for the Nonlinear Dynamics of Shells

by

Ted Belytschko[1]

Chen-Shyh Tsay[2]

and

Jerry I. Lin[1]

1 Department of Civil Engineering
Northwestern University
Evanston, Illinois, 60201

2 Battelle Columbus Laboratories
Stress Analysis and Fracture Section
Columbus, Ohio

ABSTRACT

A finite element formulation and algorithm for the nonlinear analysis of the large deflection, materially nonlinear response of impulsively loaded shells is presented. A unique feature of this algorithm is the use of a bilinear four node quadrilateral element with single point quadrature and a simple hourglass control which is orthogonal to rigid body modes on an element level and does not compromise the consistency of the equations. The geometric nonlinearities are treated by using a corotational description wherein a coordinate system that rotates with the material is embedded at the integration point; thus the algorithm is directly applicable to anisotropic materials without any corrections for frame invariance of material property tensors. This algorithm can treat about 200 element-time-steps per CPU second on a CYBER 170/730 computer in the explicit time integration mode. Numerous results are presented for both elastic and elastic-plastic problems with large strains that show that the method in most cases is comparable in accuracy with an earlier version of this algorithm employing a cubic triangular plate-shell element, but substantially faster.

I. INTRODUCTION

In the nonlinear analysis of impulsively loaded shells, algorithms employing explicit time integration offer significant advantages in both the economy and reliability of computations. However, it is very important in these algorithms that the bending elment be quite efficient, because thousands of element nodal force evaluations are typically required in a computation.

In an earlier work, Belytschko and Marchertas [1] developed an explicit shell code SADCAT based on the Bazeley, et al element [2]. Although this element is nonconforming and meets the patch test only for restricted element arrangements [3], the code proved quite successful and economical in many applications. In addition to explicit time integration, part of the efficiency could be ascribed to a corotational formulation which considerably simplified the basic equations on an element level as compared to the Lagrangian formulations which were then popular. In Ref. [1], a computational algorithm was first developed which employed vectors to track the rotations of nodes and elements so that the arbitrarily large rotations could be treated; this was also applied to frames in [4].

However, an element which does not meet the patch test for all configurations is inherently unacceptable in a general analysis program so numerous other elements have been tried. Experiments with the Razzaque-Irons [5] element showed it was too expensive for explicit computations. Attempts with higher order quadrilateral elements proved equally disappointing.

In this paper we will report on the application of the bilinear, 4 node quadrilateral shell element with one point quadrature, as proposed by Hughes,

et al [6] under the name U1, which appears to have the necessary ingredients of simplicity, versatility, and reasonable accuracy. In the context of an explicit time integration code, a simple element appears to best because it provides the most accuracy for a given amount of computer time; higher order elements, while more accurate for a given mesh, contain very high element frequencies which severely limit the stable time step. Furthermore, they add substantially to the complexity of the computational scheme. This statement will be partially substantiated by comparing the U1 element to triangular elements with cubic fields; other studies are underway.

Even with simple elements, reduced integration is imperative in an explicit time integration code because a large part of the computational cost arises from evaluating the constitutive law at the integration points. Thus we have found that going from a single point quadrature to a 2 x 2 reduced/selective quadrature more than doubles the running time of the program for an elastic-plastic material.

Unfortunately, both reduced integration and selective/reduced integration in a bilinear plate element permit zero-energy or kinematic modes, as seen from [6] and [7]. These modes, which are called hourglassing in the finite difference literature, will often quickly destroy a solution. We will here describe the application of an hourglass control based on the work of Flanagan and Belytschko [8]. The essential feature of this hourglass control is that it is orthogonal to the straining and rigid body modes on an element level similar to the stabilization matrix scheme proposed by Belytschko, et al [9] for the selective reduced integration element. Hence its effects on the solution is minimal, although, in spite of its orthogonality on the element level, it does slightly stiffen the overall response. The U1 element was first used with hourglass control by Taylor [10], who employed the method of

Kosloff and Frazier [11].

Another feature of this work is the use of a corotational velocity-strain formulation. A corotational finite element formulation is here defined as any formulation where effects of rigid body rotation of the material are treated by embedding a coordinate system in the element or at each sampling point of the element. This provides a simple expedient for avoiding the complexities of nonlinear mechanics, for in the corotational system the rate forms of the kinematic and kinetic relations are basically linear and frame-invariant.

The attractive simplicity of a corotational formulation and its natural compatibility with the finite element method were first recognized by Argyris, et al [12], who cast their formulation in terms of the natural deformation modes of the element. Wempner [13] subsequently developed a shell theory on a similar premise. In [14], [15], [16], and [12], corotational methods were developed and applied to the nonlinear analysis of beams and shells for both static and transient nonlinear problems.

The formulation in [1] and [15] is a corotational stretch formulation, for the strain tensor defined there corresponds exactly with the "right stretch" tensor commonly used in nonlinear continuum mechanics; see [17] to [19]. A disadvantage of this formulation is that the conjugate stress is not the physical stress (Cauchy stress), but the first Kirchhoff-Piola stress. This is awkward for computer software because this stress tensor is not symmetric, and its physical interpretation is not as clear as that of the Cauchy stress. Furthermore, constitutive models today are generally developed in terms of physical stress and its conjugate strain rate, the rate of deformation or velocity-strain, so it's most efficient to perform element operations in terms of these tensors; note that the use of a corotational approach does not affect the constitutive equation routines at all.

For these reasons, our codes have recently been cast in this format, see for example [18]. The computational procedure for this formulation is actually even simpler than the corotational-stretch formulations or the natural deformation mode formulations if all computations are done directly in terms of the velocities and rates. The rate formulation does preclude the use of large time steps, but this is not a drawback in explicit time-integration codes, where numerical stability usually limits the time step to a magnitude so that errors in the integration of the rate equations are negligible. The major objection we have found to this formulation is that unless other measures of deformation are computed concurrently, the program provides no valid measure of deformation: the velocity-strain tensor itself is not integrable [19].

A word is also in order about "degenerate" shell elements, as pioneered by Ahmad and coworkers [20], [21], and recently implemented for general nonlinear analysis of shells by Hughes and Liu [22]. Although these elements have a compelling cleanliness and possess the versatility of being easily linked with continuum elements, this is achieved at some cost. Because these elements use a full continuum formulations, they require the evaluation of a full 3 dimensional constitutive equation at each integration point and the storage of the complete set of state variables associated with this 3D law. Shell formulations, on the other hand only require a plane-stress law, which effectively halves the state variables and computations. Thus, in an area where we are still "compute-bound", in that the size of computations is often limited by available computer resources, the shell elements still appear more attractive.

In Section 2 of this paper, we will define the kinematic and kinetic state variables and relations of the Mindlin theory for a corotational

description of shells. In Section 3, the finite element equations are given, followed by details of implementation, including hourglass control. In Section 5, several studies of the performance of this algorithm are reported.

In Appendix A, a triangular element is described which similarly uses only one quadrature point per element. This element so far has only been tested in linear situations, but its characteristics look quite promising. The availability of a triangular element in conjunction with a quadrilateral is quite useful since the modeling of many engineering structures requires triangles.

In Appendices B and C, the suitability of some higher order elements to these problems is examined. It is shown that unless reduced quadrature is employed in curved elements, a phenomenon called "membrane" locking is encountered which leads to poor results. On the other hand reduced quadrature in these elements also leads to kinematic modes, which need to be controlled.

II. NOMENCLATURE AND GOVERNING EQUATIONS

The geometry of the shell is defined by its reference surface, or midsurface, with coordinates denoted by x^m, y^m and z^m and by its thickness h. The velocity of the midsurface $\underset{\sim}{v}^m$ is given by

$$\underset{\sim}{v}^m = \dot{\underset{\sim}{x}}^m \text{ or } \begin{Bmatrix} v_x^m \\ v_y^m \\ v_z^m \end{Bmatrix} = \begin{Bmatrix} \dot{x}^m \\ \dot{y}^m \\ \dot{z}^m \end{Bmatrix} \tag{2.1}$$

where a superposed dot denotes a time derivative. The vectors tangent to the midsurface are $\underset{\sim}{e}_1$ and $\underset{\sim}{e}_2$ and a fiber direction is defined by $\underset{\sim}{\ell}$. The fiber direction is initially coincident with $\underset{\sim}{e}_3$, where

$$\underset{\sim}{e}_3 = \underset{\sim}{e}_1 \times \underset{\sim}{e}_2 \tag{2.2}$$

and the angle between $\underset{\sim}{\ell}$ and $\underset{\sim}{e}_3$ is assumed to remain small, so that

$$\left| \underset{\sim}{e}_3^T \underset{\sim}{\ell} - 1 \right| < \delta \tag{2.3}$$

where the order of δ depends on the magnitude of the strains and the accuracy expected; for most elastic-plastic engineering calculations, values of δ on the order of 10^{-2} are acceptable.

The triad $\underset{\sim}{e}_1$, $\underset{\sim}{e}_2$, and $\underset{\sim}{e}_3$ will be defined to be corotational in the sense that it rotates with the material except that the vectors $\underset{\sim}{e}_1$ and $\underset{\sim}{e}_2$ remain tangent to the midsurface; if the condition (2.3) is met, the difference

between the rotation of the material and the triad $\underset{\sim}{e}_i$ should be small. The location of $\underset{\sim}{e}_1$ and $\underset{\sim}{e}_2$ in the midplane will depend on the material rotation as defined subsequently. Whenever the components of a tensor are expressed in terms of the base vector $\underset{\sim}{e}_i$, it will bear a superposed "hat", as for example the stress $\hat{\underset{\sim}{\sigma}}$. The base vectors of the flobal system will be denoted by $\underset{\sim}{e}_1^g$, $\underset{\sim}{e}_2^g$ and $\underset{\sim}{e}_3^g$.

In the Mindlin [23] theory of plates and shells, the velocity of a point in the shell is defined by the velocity of the midsurface $\underset{\sim}{v}^m$ and the angular velocity vector $\underset{\sim}{\theta}$ by

$$\underset{\sim}{v} = \underset{\sim}{v}^m - \hat{z}\underset{\sim}{e}_3 \times \underset{\sim}{\theta} \tag{2.4}$$

The corotational components of the velocity strain (rate-of-deformation) $\underset{\sim}{d}$ are given by

$$d_{ij} = \frac{1}{2}\left(\frac{\partial v_i}{\partial x_j} + \frac{\partial v_j}{\partial x_i}\right) \tag{2.5}$$

Substituting (2.4) into (2.5) gives the following equations for the velocity strain

$$\hat{d}_x = \frac{\partial \hat{v}_x^m}{\partial \hat{x}} + \hat{z}\frac{\partial \hat{\theta}_y}{\partial \hat{x}}$$

$$\hat{d}_y = \frac{\partial \hat{v}_y^m}{\partial \hat{y}} - \hat{z}\frac{\partial \hat{\theta}_x}{\partial \hat{y}}$$

$$2\hat{d}_{xy} = \frac{\partial \hat{v}_x^m}{\partial \hat{y}} + \frac{\partial \hat{v}_y^m}{\partial \hat{x}} + \hat{z}\left(\frac{\partial \hat{\theta}_y}{\partial \hat{y}} - \frac{\partial \hat{\theta}_x}{\partial \hat{x}}\right) \tag{2.6}$$

$$2\hat{d}_{yz} = \frac{\partial \hat{v}_z^m}{\partial \hat{y}} - \hat{\theta}_x$$

$$2\hat{d}_{xz} = \frac{\partial \hat{v}_z^m}{\partial \hat{x}} + \hat{\theta}_y$$

The velocity strains are arranged in a column matrix

$$\hat{\underset{\sim}{\partial}}^T = [\, \hat{d}_x,\ \hat{d}_y,\ 2\hat{d}_{xy},\ 2\hat{d}_{xz},\ 2\hat{d}_{yz}] \tag{2.7}$$

The stress column matrix is given by

$$\underset{\sim}{\sigma}^T = [\hat{\sigma}_x,\ \hat{\sigma}_y,\ \hat{\sigma}_{xy},\ \hat{\sigma}_{xz},\ \hat{\sigma}_{yz}] \tag{2.8}$$

The above stress and velocity-strain matrices are conjugate in the sense that the rate of internal work per unit volume, W, is given by

$$W = \underset{\sim}{d}^T \underset{\sim}{\sigma} \tag{2.9}$$

We consider the shell in a state of plane stress, so the stresses are subdivided as follows

$$\underset{\sim}{\sigma} = \begin{Bmatrix} \underset{\sim}{\sigma}' \\ \underset{\sim}{\sigma}'' \end{Bmatrix} \tag{2.10a}$$

$$\hat{\underset{\sim}{\sigma}}'^{T} = [\hat{\sigma}_x, \hat{\sigma}_y, \hat{\sigma}_{xy}] \tag{2.10b}$$

$$\underset{\sim}{\sigma}''^{T} = [\hat{\sigma}_{xz}, \hat{\sigma}_{yz}] \tag{2.10c}$$

where $\underset{\sim}{\sigma}'$ are the inplane stresses and $\underset{\sim}{\sigma}''$ are the transverse shear stresses. The velocity-strain $\hat{d}_z$ is computed from the assumption that $\hat{\sigma}_z = 0$; the stresses $\hat{\sigma}_{xz}$ and $\hat{\sigma}_{yz}$ are treated primarily as penalty parameters to approximate the condition (2.3) and are not necessarily computed by the stress-strain law which governs the in-plane stresses. This simplifies the structure of the material law subroutine with apparently no loss in accuracy.

Note that the stresses are always computed in terms of corotational components defined by the base vectors $\underset{\sim}{e}_i$. This triad rotates exactly with the material except for the out-of-plane rotation due to the difference between the rotation of $\underset{\sim}{e}_3$ and $\underset{\sim}{\ell}$, which is assumed to be small. Thus any anisotropic material law can be expressed in rate form directly as

$$\hat{\underset{\sim}{\sigma}} = \hat{\underset{\sim}{S}} \, (\underset{\sim}{\sigma}, \hat{\underset{\sim}{d}}) \tag{2.11}$$

without any corrections for frame invariance. By contrast, a Jaumann rate formulation would require equivalent correction terms for $\hat{S}$, as exemplified in kinematic hardening models used by Key [24], where the kinematic hardening term must be updated by a Jaumann rate identical to that used to update the stresses.

III. FINITE ELEMENT EQUATIONS

The finite element equation of motion are [15]

$$\underset{\sim}{M}\ \underset{\sim}{\dot{v}} = \underset{\sim}{f}^{ext} - \underset{\sim}{f}^{int} \tag{3.1}$$

where $\underset{\sim}{M}$ is the mass matrix, $\underset{\sim}{f}^{ext}$ and $\underset{\sim}{f}^{int}$ the nodal force matrices arising from external forces and the internal element resistances respectively. The internal forces are obtained by a topologically appropriate summation

$$\underset{\sim}{f}^{int} = A \left\{ \begin{matrix} \underset{\sim}{f}^{e} \\ \underset{\sim}{m}^{e} \end{matrix} \right\} \tag{3.2}$$

where the nodal forces $\underset{\sim}{f}^{e}$ and moments $\underset{\sim}{m}^{e}$ of element e are given by the principle of virtual power

$$\delta\underset{\sim}{\theta}_I^{eT}\ \underset{\sim}{m}_I^e + \delta\underset{\sim}{v}_I^{eT}\ \underset{\sim}{f}_I^e = \delta\hat{\underset{\sim}{\theta}}_I^{eT}\ \hat{\underset{\sim}{m}}_I^e + \delta\hat{\underset{\sim}{v}}^{eT}\ \hat{\underset{\sim}{f}}_I^e \tag{3.3}$$

$$= \int_{V^e} \delta\hat{\underset{\sim}{d}}^T\ \hat{\underset{\sim}{\sigma}}\ dV$$

where V^e is the volume of element e; repeated upper case subscripts are summed over the nodes of the element, and $\underset{\sim}{m}_I^e$ and $\underset{\sim}{f}_I^e$ are given by

$$\underset{\sim}{f}_I^e = \left\{ \begin{matrix} f_{xI} \\ f_{yI} \\ f_{zI} \end{matrix} \right\} \tag{3.4a}$$

$$\underset{\sim}{m}_I^e = \left\{ \begin{matrix} m_{xI} \\ m_{yI} \\ m_{zI} \end{matrix} \right\} \tag{3.4b}$$

As stated in the introduction, we will confine ourselves to the bilinear 4 node quadrilateral element with single point quadrature; by single point quadrature we refer to the fact that only one evaluation of the moments and membrane forces is made within an element; for elastic-plastic materials, several integration points may be necessary at this point in the $\hat{z}$ direction to evaluate the moment and membrane forces from the stresses.

The reference surface of the shell is approximated in both the underformed and deformed states by the elementwise interpolation

$$\begin{Bmatrix} x^m \\ y^m \\ z^m \end{Bmatrix} = N_I \ (\xi,\eta) \begin{Bmatrix} x_I \\ y_I \\ z_I \end{Bmatrix} \tag{3.5}$$

where x_I, y_I, and z_I are the coordinates of node I.

Note that

$$\begin{aligned} v^m_{xI} &= x_I \\ v^m_{yI} &= y_I \\ v^m_{zI} &= z_I \end{aligned} \tag{3.6}$$

and the superscript "m" will be omitted in the remainder of this paper because all nodal variables pertain to the midplane

$$N_1 = \frac{1}{4} (1-\xi) (1-\eta) \tag{3.7a}$$

$$N_2 = \frac{1}{4} (1+\xi) (1-\eta) \tag{3.7b}$$

$$N_3 = \frac{1}{4}(1+\xi)(1+\eta) \tag{3.7c}$$

$$N_4 = \frac{1}{4}(1-\xi)(1+\eta) \tag{3.7d}$$

The velocity of the midsurface and the angular velocity is approximated by the same shape functions, so

$$\underset{\sim}{v}^m = N_I(\xi,\eta)\ \underset{\sim}{v}_I \tag{3.8a}$$

$$\underset{\sim}{\theta} = N_I(\xi,\eta)\ \underset{\sim}{\theta}_I \tag{3.8b}$$

Upper case indices pertain to the nodes of the element and when repeated, as in the above, are summed over the nodes of the element. The velocity strains at $\xi = 0$, $\eta = 0$ can be shown through Eqs. (2.6) and (3.8) to be given by

$$\begin{aligned}
\hat{d}_x &= B_{1I}\hat{v}_{xI} + \hat{z}B_{1I}\,\hat{\theta}_{yI} \\
\hat{d}_y &= B_{2I}\hat{v}_{yI} - \hat{z}B_{2I}\hat{\theta}_{xI} \\
2\hat{d}_{xy} &= B_{2I}\hat{v}_{xI} + B_{1I}\hat{v}_{yI} + \hat{z}(B_{2I}\hat{\theta}_{yI} - B_{1I}\hat{\theta}_{xI}) \\
2\hat{d}_{xz} &= B_{1I}\hat{v}_{zI} + N_I\hat{\theta}_{yI} \\
2\hat{d}_{yz} &= B_{2I}\hat{v}_{zI} - N_I\hat{\theta}_{xI}
\end{aligned} \tag{3.9}$$

where

$$B_{1I} = \frac{\partial N_I}{\partial \hat{x}}$$

$$B_{2I} = \frac{\partial N_I}{\partial \hat{y}} \tag{3.10}$$

If the velocity strain matrix is partitioned identically to the stress matrix, see Eq. (2.10), then Eq. (3.3) can be written as

$$\delta \underset{\sim}{\theta}_I^{eT} \underset{\sim}{m}_I^e + \delta \underset{\sim}{v}_I^{eT} \underset{\sim}{f}_I^e = \int_{V^e} (\delta \hat{d}'^T \hat{\underset{\sim}{\sigma}}' + \bar{\kappa} \delta \hat{\underset{\sim}{d}}''^T \hat{\underset{\sim}{\sigma}}'') \, dV \tag{3.11}$$

where $\bar{\kappa}$ is the shear factor; it will be treated as an arbitrary parameter in the present context since it serves primarily as a penalization to enforce the Kirchhoff normality condition as the shell becomes thin.

By using the arbitrariness of the variation and Eqs. (3.9) and (3.11) and one point quadrature, we obtain the following formulas for the nodal forces

$$\hat{f}_{xI} = A \, (B_{1I} \, \sigma_x + B_{2I} \, \sigma_{xy})$$

$$\hat{f}_{yI} = A \, (B_{2I} \, \sigma_y + B_{1I} \, \sigma_{xy}) \tag{3.12}$$

$$\hat{f}_{zI} = A \, \kappa \, (B_{1I} \, \sigma_{xz} + B_{2I} \, \sigma_{yz})$$

$$m_{xI} = A \, [B_{2I} \, m_y + B_{1I} \, m_{xy} - \frac{1}{4} \bar{\kappa} \, \sigma_{yz}]$$

$$\hat{m}_{yI} = A \, [- B_{1I} \, m_x - B_{2I} \, m_{xy}) + \frac{1}{4} \, \bar{\kappa} \, \sigma_{yz}]$$

$$\hat{m}_{zI} = 0$$

where

$$f_{\alpha\beta} = \int \hat{\sigma}_{\alpha\beta} \, d\hat{z} \tag{3.13a}$$

$$m_{\alpha\beta} = - \int \hat{z} \, \hat{\sigma}_{\alpha\beta} \, d\hat{z} \tag{3.13b}$$

and B_{iI} is evaluated at the same point as in Eq. (3.9). Details of the formulas are given in Appendix A.

IV. IMPLEMENTATION AND HOURGLASS CONTROL

A major goal in the programming of this element was to exploit the simplicity of the element to obtain relationships involving few computations so that explicit time integration could be performed efficiently. Since one point quadrature is used in the element, hourglass control is necessary. This does involve additional computations, but the techniques of [8] were adapted to the element so that the additional cost is small.

The element computations are all performed in the corotational system $(\hat{x}, \hat{y}, \hat{z})$. The function $v(x, y, z)$ is defined on the surface in terms of reference parameters ξ and η, see Eq. (3.8a). Derivatives are obtained from the following matrix equation

$$\begin{Bmatrix} v,_\xi \\ v,_\eta \\ 0 \end{Bmatrix} = \begin{bmatrix} x,_\xi & y,_\xi & z,_\xi \\ x,_\eta & y,_\eta & z,_\eta \\ y,_\xi z,_\eta - y,_\eta z,_\xi & x,_\eta z,_\xi - z,_\eta x,_\xi & x,_\xi y,_\eta - y,_\xi x,_\eta \end{bmatrix} \begin{Bmatrix} v,_x \\ v,_y \\ v,_z \end{Bmatrix} \tag{4.1}$$

where the comma followed by a subscript denotes partial differentiation with respect to that subscript. Note that the third equation in (4.1) simply indicates that the derivative of the function normal to the surface must vanish.

If Eq. (4.1) is written in terms of the corotational coordinates $\hat{x}$, $\hat{y}$, $\hat{z}$, then $\partial v/\partial \hat{z} = 0$, so it follows immediately that the differentiation formula is independent of $\partial \hat{z}/\partial \xi$ and $\partial \hat{z}/\partial \eta$. Thus, the implicit differentiation formula reduces to

$$\begin{Bmatrix} v,_\xi \\ v,_\eta \end{Bmatrix} = \begin{bmatrix} \hat{x},_\xi & \hat{y},_\xi \\ \hat{x},_\eta & \hat{y},_\eta \end{bmatrix} \begin{Bmatrix} v,_{\hat{x}} \\ v,_{\hat{y}} \end{Bmatrix} \tag{4.2}$$

If we then use the identity given in [8], we obtain

$$B_{iI} = \frac{1}{2A}\begin{bmatrix} \hat{y}_2 - \hat{y}_4 & \hat{y}_3 - \hat{y}_1 & \hat{y}_4 - \hat{y}_2 & \hat{y}_1 - \hat{y}_3 \\ \hat{x}_4 - \hat{x}_2 & \hat{x}_1 - \hat{x}_3 & \hat{x}_2 - \hat{x}_4 & \hat{x}_3 - \hat{x}_1 \end{bmatrix} \begin{matrix} i=1 \\ i=2 \end{matrix} \tag{4.3}$$

These formulas are then used directly in the evaluation of Eqs. (3.9) and (3.12), as given in Appendix A.

For the purpose of hourglass control, we follow [8] and define the matrix χ by

$$\gamma_I = h_I - (h_J \hat{x}_{\alpha J})\, B_{\alpha I} \tag{4.4a}$$

or

$$\gamma_I = h_I - [(\underset{\sim}{h}^T \hat{\underset{\sim}{x}})\, B_{1I} + (\underset{\sim}{h}^T \hat{\underset{\sim}{y}})\, B_{2I}] \tag{4.4b}$$

where

$$\dot{h}_I = [+1, -1, +1, -1] \tag{4.5}$$

In the above equations, the Greek subscripts have a range of 2 and are summed when repeated, $\hat{x}_{1I} = \hat{x}_I$, $\hat{x}_{2I} = \hat{y}_I$. Throughout this paper, repeated upper case subscripts are summed over the nodes of the element.

The hourglass generalized strain rates are obtained by

$$\dot{q}^B_\alpha = \gamma_I\, \hat{\theta}_{\alpha I} \tag{4.6a}$$

$$\dot{q}_3^B = \gamma_I \hat{v}_{zI} \tag{4.6b}$$

$$\dot{q}_\alpha^M = \gamma_I \hat{v}_{\alpha I} \tag{4.6c}$$

where the superscripts B and M denote hourglass modes associated with bending and in-plane (membrane) forces, respectively. The corresponding generalized hourglass stress rates are given by

$$\begin{aligned} \dot{Q}_\alpha^B &= C_1 \dot{q}_\alpha^B \\ \dot{Q}_3^B &= C_2 \dot{q}_3^B \\ \dot{Q}_\alpha^M &= C_3 \dot{q}_\alpha^M \end{aligned} \tag{4.7}$$

where

$$\begin{aligned} C_1 &= r_\theta \frac{Eh^3 A}{192} B_{\alpha I} B_{\alpha I} \\ C_2 &= r_w \frac{\bar{\kappa} Gh^3}{12} B_{\alpha I} B_{\alpha I} \\ C_3 &= r_M \frac{Eh\ A}{8} B_{\alpha I} B_{\alpha I} \end{aligned} \tag{4.8}$$

The constants r_θ, r_w, and r_M are generally given values between 0.01 and 0.05. For elastic-plastic materials we let $E = \frac{1}{2} \hat{C}_{\alpha\alpha}$, where $\hat{C}_{ij}$ are the constants that relate the components of the in-plane stress tensor by

$$\hat{\underset{\sim}{g}}' = \hat{\underset{\sim}{C}}\,\hat{\underset{\sim}{d}}' \tag{4.9}$$

The nodal forces corresponding to the hourglass generalized stresses are

$$\begin{aligned} \hat{m}^H_{\alpha I} &= \gamma_I\, Q^B_\alpha \\ \hat{f}^H_{zI} &= \gamma_I\, Q^B_3 \\ \hat{f}^H_{\alpha I} &= \gamma_I\, Q^M_\alpha \end{aligned} \tag{4.10}$$

where the total hourglass stresses are obtained from the rates as described in Appendix A.

An important aspect of this hourglass control procedure is that it does not effect the straining or rigid body modes for a flat element; this is shown in Appendix B. Thus if the velocities correspond to a rigid body rotation about an arbitrary point or a rigid body translation, all of the generalized hourglass strain rates vanish. When the element is warped, a rigid body motion does generate hourglass strain rates q^M_α; they may be almost entirely eliminated by a procedure described in Appendix B.

In all of the computations reported here, the central difference method was used for time integration. A lumped mass matrix was used for all computations. In addition to an augmented rotation lumped mass, as proposed in [6], a reduced shear factor $\bar{\kappa}$ as proposed in [25] was used to reduce the maximum frequency and hence increase the stable time step. This permits the increased rotatory lumped mass to be scaled so that the spectral fidelity of the finite element mesh is quite good over a large range of frequencies.

V. NUMERICAL RESULTS

Several numerical examples will be given to illustrate the performance of this quadrilateral element. All the computations were carried out on the CDC Cyber 170/730.

Example 1: Impulsively Loaded Cantilever Beam

A cantilever beam, shown in Fig. 1, is used to test the linear and nonlinear response of the quadrilateral plate element. A uniform pressure is applied in the negative z-direction as shown. The results for the linear response obtained with p = 0.01 psi are summarized in Table 1 and are compared with other elements [1] [4], and the analytic solution given by Timoshenko and Goodier [26]. The results for p = 2.85 psi, presented in Table 2, involve large displacements and highly nonlinear response. Fig. 2 illustrates the time history for the tip displacement and compares it to the result obtained with an 8 node, two dimensional isoparametric element by Shantaran et al [27].

Example 2: Simply Supported Square Plate Subjected to a Uniform Load

This problem is described in Fig. 3; all sides of the plate are simply supported. Due to the symmetry of the geometry and loading, only a quarter of the plate was modelled. The mesh consists of 25 nodes and 16 elements. Both elastic and elastic-perfectly-plastic materials were considered. The results are compared to those obtained with a triangular plate element [1] and an analytic solution by Timoshenko [28].

The elastic and elastic-plastic results are presented in Tables 3 and 4, respectively; time histories of the deflection of the center point are plotted in Fig. 4 for 3 and 5 integration points through the thickness. Note that the

number of integration points through the thickness used to evaluate Eqs. 3.13 makes a large difference in the displacement; this is also clear from Table 4.

Example 3: Impulsively Loaded Clamped Beam

A 10 in long aluminum beam clamped at both ends is loaded impulsively over a center portion, as shown in Fig. 5. The material is elastic-perfectly-plastic. Experimental results have been given for this problem by Balmer and Witmer [29]. Fig. 6 compares the computed displacement time history with the experimental results.

Example 4: Corner Supported Square Plate

The hourglass modes in static and free vibration problems have been investigated by Belytschko, Tsay and Liu [9]. Here we will demonstrate the hourglass modes and their control for a transient problem. We consider a square plate subjected to a uniform load with point supports at the four corners.

Figure 7 shows the deformed shape without hourglass control. In order to see the deformation, we have amplified the results 1000 times. This problem shows that the in-plane and w-hourglass mode [6,8] produces serious distortion of the square plate. After adding hourglass control $r_M = 10^{-3}$, $r_w = 0.03$, the quadrilateral element gives the expected deformed shapes as can be seem from Fig. 8; the amplification in this figure is 15000.

Example 5: Cylindrical Panel

A 120° cylindrical panel, loaded impulsively, is shown in Fig. 9. The problem is symmetric, so only half the panel is modelled. Note that the ends

of the panel are simply-supported and the boundaries at the sides are fixed. An initial velocity of 5650 in/sec normal to the shell's surface is applied over the region marked R_I.

We used two meshes to solve this problem, varying the number of circumferential elements from 6 to 8 with 16 elements along the length of the cylinder. The displacement of the midpoint along the crown line of the cylinder is compared with experimental results [30] and the triangular elements results [1] in Fig. 10. The results obtained for the 6 x 16 quadrilateral mesh are not satisfactory; this may be due to deficiencies of one-point quadrature for warped elements. Fig. 11 gives the permanent deformation of the crown line of the panel and Fig. 12 gives the deformation of a radial cross section as compared to the experimental and the triangular element results. Deformed shapes are given in Fig. 13.

Example 6: Spherical Cap

The problem description and a top view of the mesh are shown in Fig. 14; fourfold symmetry was used. A uniform load was applied over the cap as shown. Both elastic and elastic-plastic materials with the material properties given in Fig. 14 were considered. The results for the center-deflection time-history are compared to the results obtained by Bathe et al [31] using 8 node, axisymmetric isoparametric elements in Fig. 15. Five integration points were used through the thickness in the elastic-plastic calculations.

CONCLUSIONS

A four node quadrilateral applicable to transient plate and shell problems with material and geometric nonlinearities in an explicit codes based

on the Hughes element [6,7] has been presented. The element uses one quadrature point in the plane of the element and kinematic modes are stabilized by an hourglass control. The performance of the element with one-point quadrature is generally quite good, except when excessive warping is encountered. The hourglass control procedure described here is easily implemented and permits one-point quadrature to be used regardless of the boundary conditions, without mesh instabilities. The use of one-point quadrature, as compared to reduced-selective integration, enhances the speed of the element substantially; the element is also significantly faster than the Bazeley et al [2] element as used in [1] with 3 quadrature points and, yet it possesses comparable accuracy.

ACKNOWLEDGEMENT

The support of the Air Force Office of Scientific Research under Grant F49620-82-K0013 is gratefully acknowledged.

REFERENCES

1. Belytschko, T., and Marchertas, A.H., "Nonlinear Finite Element Method for Plates and its Application to the Dynamic Response of Reactor Fuel Subassemblises", Tran. ASME Journal Pressure Vessel Technology, 251-257, 1974.

2. Bazeley, G.P., Cheung, W.K., Irons, R.M., and Zienkiewicz, O.C., "Triangular Elements in Plate Bending-Conforming and Nonconforming Solutions in Matrix Methods and Structural Mechanics", Proc. Conf. on Matrix Methods in Structural Analysis, Wright Patterson AFB, Ohio, Oct. 1965, Report AFFDL-R-66-80, 547-576.

3. Irons, B.M., and Razzaque, A., "Experience with the Patch Test for Convergence of Finite Element", in the Mathematical Foundations of the Finite Element Method with Applications to Partial Differential Equations, ed. by A.K. Aziz, Academic Press, New York, 577-588, 1972.

4. Belytschko, T., Schwer, L., and Klein, M.J., "Large Displacement Transient Analysis of Space Frames", Intl. J. Num. Meth. Eng., Vol. 11, 65-84, 1977.

5. Razzaque, A., "Program for Triangular Bending Element with Derivative Smoothing", Intl. J. Num. Meth. Eng., vol. 5, 588-589, 1973.

6. Hughes, T.J.R., Cohen, M., and Haroun, M., "Reduced and Selective Integration Techniques in Finite Element Analysis of Plates", Nuclear Engineering and Design, Vol. 46, 203-222, 1978.

7. Hughes, T.J.R., Taylor, R.L., and Kanoknukulchai, W., "A Simple and Efficient Finite Element for Plate Element", Intl. J. Num. Meth. Eng., Vol. 11, 1529-1547, 1977.

8. Flanagan, D. and Belytschko, T., "A Uniform Strain Hexahedron and Quadrilateral with Orthogonal Hourglass Control", Intl. J. Num. Meth. Eng., vol. 17, 679-706, 1981.

9. Belytschko, T., Tsay, C.S., and Liu, W.K., "A Stabilization Marix for the Bilinear Mindlin Plate Element", Computer Methods in Applied Mech. and Eng., Vol. 29, 313-327, 1981.

10. Taylor, R.L., "Finite Element for General Shell Analysis", 5th Intl. Seminar on Computational Aspects of the Finite Element Method, Berlin, August, 1979.

11. Kosloff, D., and Frazier, G., "Treatment of Hourglass Patterns in Low Order Finite Element Codes", Numerical and Analytical Methods in Geomechanics, Vol. 2, 52-72, 1978.

12. Argyris, J.H., Kelsey, S., and Kamel, H., "Matrix Methods of Structural Analysis: a Precis of Recent Developments", in Matrix Methods of Structural Analysis, edited by E.F. de Veubeke, Agargograph, 72, Permagon Press, New York, 1964.

13. Wempner, G.A., "Finite Elements, Finite Rotations, and Small Strains of Flexible Shells", Intl. J. Solids and Structures, Vol. 5, 117-153, 1969.

14. Muraay, D.W., and Wilson, E.L., "Finite Element Large Deflection Analysis of Plates", ASCE, J. Eng. Mech. Div., 143-165, 1969.

15. Belytschko, T., and Hsieh, B.J., "Nonlinear Transient Finite Element analysis with Convected Coordinates", Intl. J. Num. Meth. Eng., Vol. 7, 255-271, 1973.

16. Belytschko, T., and Glaum L.W., "Applications of Higher Order Corotational Stretch Theories to Nonlinear Finite Element analysis", Computer and Structures, Vol. 10, 175-182, 1979.

17. Malvern, L.E., Introduction to the mechanics of a Continuous Medium, Prentice-Hall, Inc., Englewood Cliffs, New Jersey, 1969.

18. Belytschko, T., and Mullen, R., "WHAMS: a Program for Transient Analysis of Structures and Continua", Structural Mechanics Software Series, Vol. 2, 151-212, 1978.

19. Belytschko, T., "Nonlinear Analysis - Descriptions and Numerical Stability" in Shock and Vibration Computer Programs, ed. by w. Pilkey and B. Pilkey, Shock and Vibration Information Center, Washington, D.C., 537-562, 1975.

20. Ahmad, S., "Pseudo-Isoparametric Finite Elements for Shell and Plate Analysis", Proc. Conf. on Recent Advances in Stress Analysis, JECSA Royal Aeronatuical Society, 6-20 - 6-21, 1968.

21. Ahmad, S., Irons, B.M., and Zienkiewicz, O.C., "Analysis of Thick and Thin Shell Structures by Curved Finite Elements", Intl. J. Num. Meth. Eng., Vol. 2, 419-451, 1970.

22. Hughes, T.J.R., and Liu, W.K., "Nonlinear Finite Element Analysis of Shells; Part I. Three Dimensional Shells", to be published Computer Methods in Applied Mechanics and Engineering.

23. Mindlin, R.D., "Influence of Rotary Inertia and Shear on Flexural Motions of Isotropic, Elastic Plates", Journal of Applied Mechanics, Vol. 18, 31-38, 1951.

24. Key, S.W., "HONDO - a Finite Element Computer Program for the Large Deformation Dynamic Response of Axisymmetric Solid", Report SLA-74-0039, Sandia Laboratories.

25. Mindle W., and Belytschko, T., "A Study of Shear Factors in Reduced-Selective Integration Mindlin Beam Elements", Computers and Structures, Vol. 17, No. 3, 334-344, 1983.

26. Timoshenko, S. and Goodier, J.N., Theory of Elasticity, Second Edition, New York, McGraw-Hill, 1951.

27. Shantaram, D., Owen, D.R.J., and Zienkiewicz, O.C., "Dynamic Transient Behavior of Two- and Three-Dimensional Structures Including Plasticity Large Deformation Effects and Fluid Interaction", Earthquake Engineering and Structural Dynamics, Vol. 4, 561-578.

28. Timoshenko, S. and Woinowsky-Krieger, S., Theory of Plates and Shells, McGraw-Hill, New York, 1911.

29. Balmer, H.A., and Witmer, E.A., "Theoretical-Experimental Correlation of Large Dynamic and Permanent Deformation of Impulsively Loaded Simple Structures", Air Force Flight Dynamics Laboratory, Report FDP-TDR-64-108, Wright Patterson AFB, Ohio, July 1964.

30. Morino, L., Leech, J.W., and Witmer, E.A., "An Improved Numerical Calculation Technique for Large Elastic-Plastic Transient Deformations of Thin Shells: Part 2 - Evaluation and Applications", Journal of Applied Mechanics, 429-435, 1971.

31. Bathe, K.J., Ramm, E. and Wilson, E.L., "Finite Element Formulations for Large Deformation Dynamic Analysis", International Journal for Numerical Methods in Engineering, Vol. 9, 353-386, 1975.

APPENDIX A

DETAILS OF FINITE ELEMENT IMPLEMENTATION

We describe here in detail the procedure for computing the internal nodal forces $\underset{\sim}{f}_e$ for a given set of nodal coordinates and nodal velocities. Throughout this Appendix a double numerical subscript indicates a difference: $x_{32} = x_3 - x_2$, $v_{x41} = v_{x4} - v_{x1}$.

Orientation of local base vectors $\underset{\sim}{e}_i$.

The local $\underset{\sim}{e}_3$ vector is assumed to be the normal to the vectors $\underset{\sim}{r}_{31}$ and $\underset{\sim}{r}_{42}$ as shown in Fig. A.1. The components of $\underset{\sim}{e}_3$ are then given by

$$\underset{\sim}{s}_3 = \begin{matrix} y_{31}z_{42} - z_{31}y_{42} \\ z_{31}x_{42} - x_{31}z_{42} \\ x_{31}y_{42} - y_{31}x_{42} \end{matrix} \qquad \text{(A.1)}$$

$$\underset{\sim}{e}_3 = \underset{\sim}{s}_3/||s_3|| \qquad ||s|| = (s_1^2 + s_2^2 + s_3^2)^{1/2} \qquad \text{(A.2)}$$

Two procedures have been used for defining the $\hat{x}$ axis. In the first procedure, $\hat{x}$ is embedded in the element between nodes 1 and 2, side 1-2; however, since this direction is not perpendicular to $\hat{\underset{\sim}{e}}_3$ normality is enforced. This is quite accurate if the shear strains are less than 10%. While defining $\hat{x}$ to join nodes 1 and 3 would automatically satisfy normality, the use of an axis along the side is convenient because the stresses, which

are computed in the $(\hat{x}, \hat{y})$ system, are then more easily interpreted. In procedure 1, $\hat{\underset{\sim}{e}}_1$ is computed by

$$\underset{\sim}{r}_{21} = \begin{matrix} x_{21} \\ y_{21} \\ z_{21} \end{matrix} \tag{A.3}$$

$$\underset{\sim}{s}_1 = [\underset{\sim}{r}_{21} - (\underset{\sim}{r}_{21}^T \hat{\underset{\sim}{e}}_3)\, \hat{\underset{\sim}{e}}_3] \tag{A.4}$$

$$\underset{\sim}{e}_1 = \underset{\sim}{s}_1 / ||s_1|| \tag{A.5}$$

The matrix $\underset{\sim}{e}_2$ is then obtained by

$$\underset{\sim}{e}_2 = \underset{\sim}{e}_3 \times \underset{\sim}{e}_1 \tag{A.6}$$

The components of $\underset{\sim}{v}$ are transformed to the local system by

$$\hat{\underset{\sim}{v}}_I = \underset{\sim}{A}\, \underset{\sim}{v}_I = \begin{matrix} \underset{\sim}{e}_1^T \\ \underset{\sim}{e}_2^T \\ \underset{\sim}{e}_3^T \end{matrix} \underset{\sim}{v}_I \tag{A.7}$$

where $\underset{\sim}{A}$ is the matrix of direction cosines between the global and local system. The current nodal coordinates, $\underset{\sim}{x}_I$ must also be expressed in terms of the local system by Eq. (A.7) before proceeding further.

In procedure 2, the coordinate $\hat{x}$ is not embedded along the side 1-2; instead side 1-2 is associated with a coordinate $\overline{x}$ and $\hat{x}$ rotates with a spin as defined by

$$\hat{\omega}_z = \frac{1}{2} \left(\frac{\partial \hat{v}_y}{\partial \hat{x}} - \frac{\partial \hat{v}_x}{\partial \hat{y}} \right) \tag{A.8}$$

which, by Eqs. (3.8), (3.11) and (4.3), gives

$$\hat{\omega}_z = \frac{1}{2A}\left[\hat{y}_{24}\,\hat{v}_{y13} + \hat{y}_{31}\,\hat{v}_{y24} - \hat{x}_{42}\,\hat{v}_{x13} - \hat{x}_{13}\,\hat{v}_{x24}\right] \tag{A.9}$$

The rate of the angle ϕ , see Fig. A.1, is then given by

$$\dot{\phi} = \hat{\omega}_z - \hat{\omega}_z(\underset{\sim}{r}_{21}) \tag{A.10}$$

where $\hat{\omega}_z(\underset{\sim}{r}_{21})$ is the angular velocity of side 1-2, which is

$$\hat{\omega}_z(\underset{\sim}{r}_{21}) = (\hat{v}_{y2} - \hat{v}_{y1})/||r_{21}|| \tag{A.11}$$

The direction cosines between the $\bar{x},\bar{y}$ and $\hat{x},\hat{y}$ are then updated by

$$\cos(\phi^{n+1}) = \cos(\phi^n) - \Delta\phi\,\sin(\phi^n) + \frac{1}{2}\,\Delta\phi^2\,\cos(\phi^n) \tag{A.12a}$$

$$\sin(\phi^{n+1}) = \sin(\phi^n) + \Delta\phi\,\cos(\phi^n) - \frac{1}{2}\,\Delta\phi^2\,\sin(\phi^n) \tag{A.12b}$$

$$\Delta\phi = \dot{\phi}^{n+1/2}\,\Delta t \tag{A.12c}$$

Note that $\dot{\phi}$ as computed by Eq. (A.10) is at time step $n+1/2$ in the central difference method since $\underset{\sim}{v}$ in Eq. (A.9) is at time step $n+1/2$. To implement this method, cos ϕ and sin ϕ must be stored for each element since their values at the previous time step, time step n, must be known to obtain their values at n+1. A radial return is used to normalize their values i.e.,

$$s = (\cos^2(\phi^{n+1}) + \sin^2(\phi^{n+1}))^{1/2} \tag{A.13a}$$

$$\cos(\phi^{n+1}) \leftarrow \cos(\phi^{n+1})/s \tag{A.13b}$$

$$\sin(\phi^{n+1}) \leftarrow \sin(\phi^{n+1})/s \tag{A.13c}$$

The direction cosines are then modified by

$$\begin{matrix} \hat{e}_1^T \\ \hat{e}_2^T \\ \hat{e}_3^T \end{matrix} \leftarrow \begin{matrix} \cos(\phi^{n+1}) & \sin(\phi^{n+1}) & 0 \\ -\sin(\phi^{n+1}) & \cos(\phi^{n+1}) & 0 \\ 0 & 0 & 1 \end{matrix} \begin{matrix} \hat{e}_1^T \\ \hat{e}_2^T \\ \hat{e}_3^T \end{matrix} \tag{A.14}$$

where the far right hand vector is that which appears in Eq. (A.7)

Note that Eq. (A.7) must now be repeated to obtain the nodal velocities in the correct local coordinate system. The procedure introduces some error because Eq. (A.9) does not use the correct local coordinate system to compute $\hat{\omega}_z$; this can be corrected by using a two pass procedure or storing $\hat{e}_1$ for time step n; neither alternative appeared to be worth its additional cost.

The area A is computed by

$$A = \frac{1}{2}(x_{31}y_{42} + x_{24}y_{13}) \tag{A.15}$$

Computation of strain rates. Once $\hat{\underset{\sim}{\theta}}_I$ and $\hat{\underset{\sim}{v}}_I$ are obtained at nodes I, I = 1 to 4, from the global components by the transformation (A.7), the strain rates are easily obtained through Eqs. (3.9) and (4.3). The following formulas are used:

$$\hat{d}_x^m = \frac{1}{2A}\left(\hat{y}_{24}\hat{v}_{x13} + \hat{y}_{13}\hat{v}_{x24}\right)$$

$$\hat{d}_y^m = \frac{1}{2A}\left(\hat{x}_{42}\hat{v}_{y13} + \hat{x}_{13}\hat{v}_{y24}\right)$$

$$2\hat{d}_{xy}^m = \frac{1}{2A}\left(\hat{x}_{24}\,\hat{v}_{x13} + \hat{x}_{13}\hat{v}_{x24} + \hat{y}_{24}\hat{v}_{y13} + \hat{y}_{31}\hat{v}_{y24}\right) \qquad \text{(A.16)}$$

$$\kappa_x = \frac{-1}{2A}\left(\hat{y}_{24}\hat{\theta}_{y13} + \hat{y}_{31}\hat{\theta}_{y24}\right)$$

$$\kappa_y = \frac{1}{2A}\left(\hat{x}_{42}\hat{\theta}_{x13} + \hat{x}_{13}\hat{\theta}_{x24}\right) \qquad \text{(A.17)}$$

$$2\kappa_{xy} = \frac{1}{2A}\left(-\hat{x}_{42}\hat{\theta}_{y13} - \hat{x}_{13}\hat{\theta}_{x24} + \hat{y}_{24}\hat{\theta}_{x13} + \hat{y}_{31}\hat{\theta}_{y24}\right)$$

$$\hat{d}_x = \hat{d}_x^m - \hat{z}\,\kappa_x$$

$$\hat{d}_y = \hat{d}_y^m - \hat{z}\,\kappa_y \qquad \text{(A.18)}$$

$$\hat{d}_{xy} = \hat{d}_{xy}^m - \hat{z}\,\kappa_{xy}$$

The strain rates must be computed at a set of quadrature points through the thickness, $-h/2 \leq \hat{z} \leq h/2$, if a plane stress law is used.

The generalized hourglass strain-rates are only computed once in an element and the form of Eq. (4) is used directly.

Stresses. The stresses are computed by a plane-stress constitutive equation

$$\dot{\underset{\sim}{g}} = \underset{\sim}{C}\,\dot{\underset{\sim}{d}} \tag{A.19}$$

The transverse shear stresses are always computed by an elastic law. The generalized hourglass stress-rates are computed by Eq. (4.6). Note that all rates are at time $n+1/2$. The new values of the stresses are then computed by

$$\hat{\underset{\sim}{g}}^{n+1} = \hat{\underset{\sim}{g}}^{n} + \Delta^{1/2}$$

$$\underset{\sim}{Q}^{n+1} = \underset{\sim}{Q}^{n} + \;^{1/2} \tag{A.20}$$

The stresses must be computed at all integration points $\frac{-h}{2} \leq \hat{z} \leq \frac{h}{2}$ to obtain $_{\alpha\beta}$ and e generalized horuglass stresses and strain rates are computed only once each element.

Nodal forces. The nodal force contribution from an element consists of both the nodal forces arising from the physical stresses, Eqs. (3.12), and those arising from the generalized hourglass stresses, Eqs. (4.10). We will give the nodal forces for node 1:

$$\hat{f}_{x1} = \frac{1}{2}\,(\;+\,x_{42}\;\;_{xy}) + \gamma_1 Q_1^M$$

$$\hat{f}_{y1} = \frac{1}{2}\,(\;+\,y_{24}\;\;_{xy}) + \gamma_1 Q_2^M$$

$$\hat{f}_{z1} = \frac{\bar{\kappa}}{2}\;_{xz} + x_{42}\;\;_{yz}) + \gamma_1 Q_3^B \tag{A.21}$$

$$\hat{m}_{x1} = (x_{42}\ _{y} + y_{24}\ _{xy}) - \frac{1}{4}\overline{\kappa}A\ _{yz} + \gamma_1 Q_1^B$$

$$\hat{m}_{y1} = (-y_{24}\ _{x} - x_{42}\ _{xy}) + \frac{1}{4}\overline{\kappa}A\ _{xz} + \gamma_1\ Q_2^B$$

The nodal forces and moments are then transformed to the global system by the inverse of Eq. (A.7) which gives

$$\underset{\sim}{f}_I = \underset{\sim}{A}^T\ \hat{\underset{\sim}{f}}_I \qquad\qquad \underset{\sim}{m}_I = \underset{\sim}{A}^T\ \hat{\underset{\sim}{m}}_I \qquad\qquad (A.22)$$

APPENDIX B

PERFORMANCE OF HOURGLASS CONTROL IN RIGID BODY MOTION

In this Appendix it is shown that all generalized hourglass strain-rates vanish exactly for an element if all of the nodes are co-planar. This is crucial for the performance of the element with hourglass control because if the hourglass strain rates do not vanish for rigid body motions, nodal forces are generated by rigid body motions via the generalized hourglass stresses. It is also shown that this condition can be satisfied when the element is warped and the nodes are not co-planar by a slight modification of Eqs. (4.6).

In this Appendix indicial motion is used; Greek subscripts have a range of 2, Latin lower case subscripts have a range of 3, Latin upper case subscripts a range of 4.

$$s_I = [1, 1, 1, 1] \tag{B.1}$$

The following equations will be used

$$h_I s_I = 0 \tag{B.2}$$

$$B_{\alpha I} x_{\beta I} = \delta_{\alpha\beta} \tag{B.3}$$

$$B_{\alpha I} s_I = 0 \tag{B.4}$$

where $B_{\alpha I}$ is defined in Eq. (4.3) and h_I in Eq. (4.5); $\delta_{\alpha\beta}$ is the Kronecker delta. Eqs. (B.2) to (B.3) can easily be verified by simple algebra.

In rigid body motion, the nodal velocities are given by

$$v_i = e_{ijk}\ \omega_j\ x_k + v_i^o \tag{B.5}$$

where e_{ijk} is the alternator tensor, ω_j is the angular velocity and v_i^o the translational velocity. The nodal velocities can then be written as

$$\hat{v}_{iI} = \hat{\omega}_j(e_{ij\alpha}\hat{x}_{\alpha I} + e_{ij3}\zeta h_I + e_{ijk}\ r_k s_I) + v_i^o s_I \tag{B.6}$$

where $\underset{\sim}{r}$ is the vector from the center of rotation to the origin of the $\hat{x}$ coordinate system and the assumption that

$$\hat{x}_{3I} = \zeta h_I \tag{B.7}$$

has been made in writing the second term. The last two terms will be omitted henceforth since by Eqs. (B.2) and (B.3) their inner product with γ_I will always vanish. The nodal angular velocities are given by

$$\hat{\theta}_{iI} = \omega_i s_I \tag{B.7}$$

Using Eqs. (4.4), (4.6a) and (B.7), we note that

$$\dot{q}_\alpha^B = [h_I - (h_J\ \hat{x}_{\beta J})\ B_{\beta I}]\ \hat{\omega}_\alpha s_I = 0 \tag{B.8}$$

where the last equality follows immediately from Eqs. (B.2) and (B.4).

Similarly, from Eqs. (4.4), (4.6b) and (B.6), it follows that

$$\dot{q}_3^B = [h_I - (h_J \hat{x}_{\alpha J}) B_{\alpha I}] \hat{\omega}_j e_{3j\beta} \hat{x}_{\beta I} = 0 \qquad (B.9)$$

where the second term in (B.6) has been omitted immediately because $e_{3j3} = 0$. The last equality in (B.9) follows directly from the use of Eq. (B.3).

Using a similar procedure shows that

$$\dot{q}_\beta^M = 4\zeta \hat{\omega}_j e_{\beta j3} \qquad (B.10)$$

Thus, the membrane hourglass strain rates do not vanish when $\zeta \neq 0$, i.e. when the nodes are not co-planar. However, they can be made to vanish approximately by letting

$$\dot{q}_1^M = \gamma_I \hat{v}_{xI} - 4\zeta \hat{\omega}_y \qquad (B.11a)$$

$$\dot{q}_2^M = \gamma_I \hat{v}_{yI} + 4\zeta \hat{\omega}_x \qquad (B.11b)$$

Equations (B.11) do not completely eliminate $\dot{q}_\alpha^M$ in rigid body motion because the $\hat{z}$ coordinates of the nodes usually do not satisfy Eq. (B.7).

FIGURE CAPTIONS

Fig. 1. Cantilever beam (example 1): problem description and finite element mesh.

Fig. 2. Tip deflection for cantilever beam subjected to a uniform load p = 2.85 psi.

Fig. 3. Simply supported square plate (example 2): problem description and finite element mesh.

Fig. 4 Deflection of center-point of simply-supported square plate for elastic and elastic-perfectly-plastic materials using 3 and 5 integration points through the thickness for the latter.

Fig. 5. Impulsively loaded clamped beam (example 3): problem description and finite element mesh.

Fig. 6. Deflection of center point of example 3 compared to experimental results [29].

Fig. 7. Deformed mesh of corner supported plate without hourglass control.

Fig. 8. Deformed mesh of corner supported plate with hourglass control.

Fig. 9. Problem description for impulsively loaded cylindrical panel, example 5.

Fig. 10 Displacement time histories for two points of the cylindrical panel, example 5, compared to experiment [30] and earlier computed results [1].

Fig. 11 Final deformed shape of the panel, example 5, at the crown line compared to experiment [30] and earlier results [1].

Fig 12. Final deformed shape of the panel at the cross-section z = -6.28 compared to experiment [30] and earlier results [1].

Fig. 13. Computer plots of deformed cylindrical panel.

Fig. 14. Problem description for spherical cap, example 6.

Fig. 15. Center displacement of spherical cap for elastic and elastic-plastic materials compared to numerical results of Bathe, et al [31].

TABLES

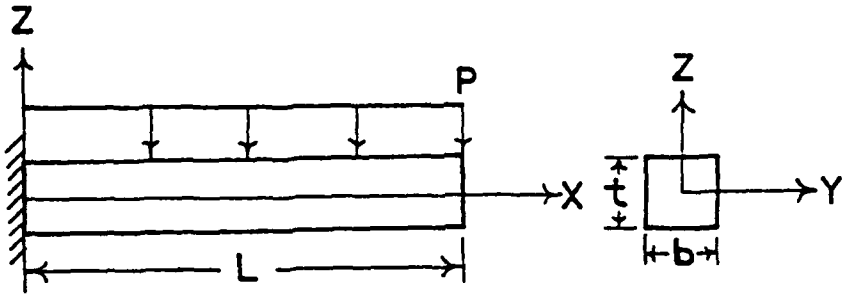

Length	L = 10. in.
Width	b = 1. in.
Thickness	t = 1. in.
Young's modulus	E = 12000. psi
Density	$\rho = .1024 \times 10^{-5}$ lb-sec^2/in^4
Poisson's ratio	$\nu = 0.2$

(a) Problem definition

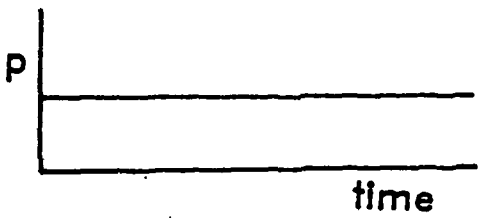

(b) Pressure load

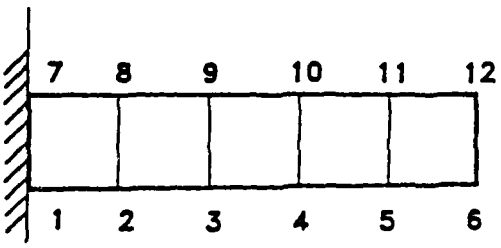

(c) Element mesh

Fig. 1. Cantilever beam (example 1): problem description and finite element mesh.

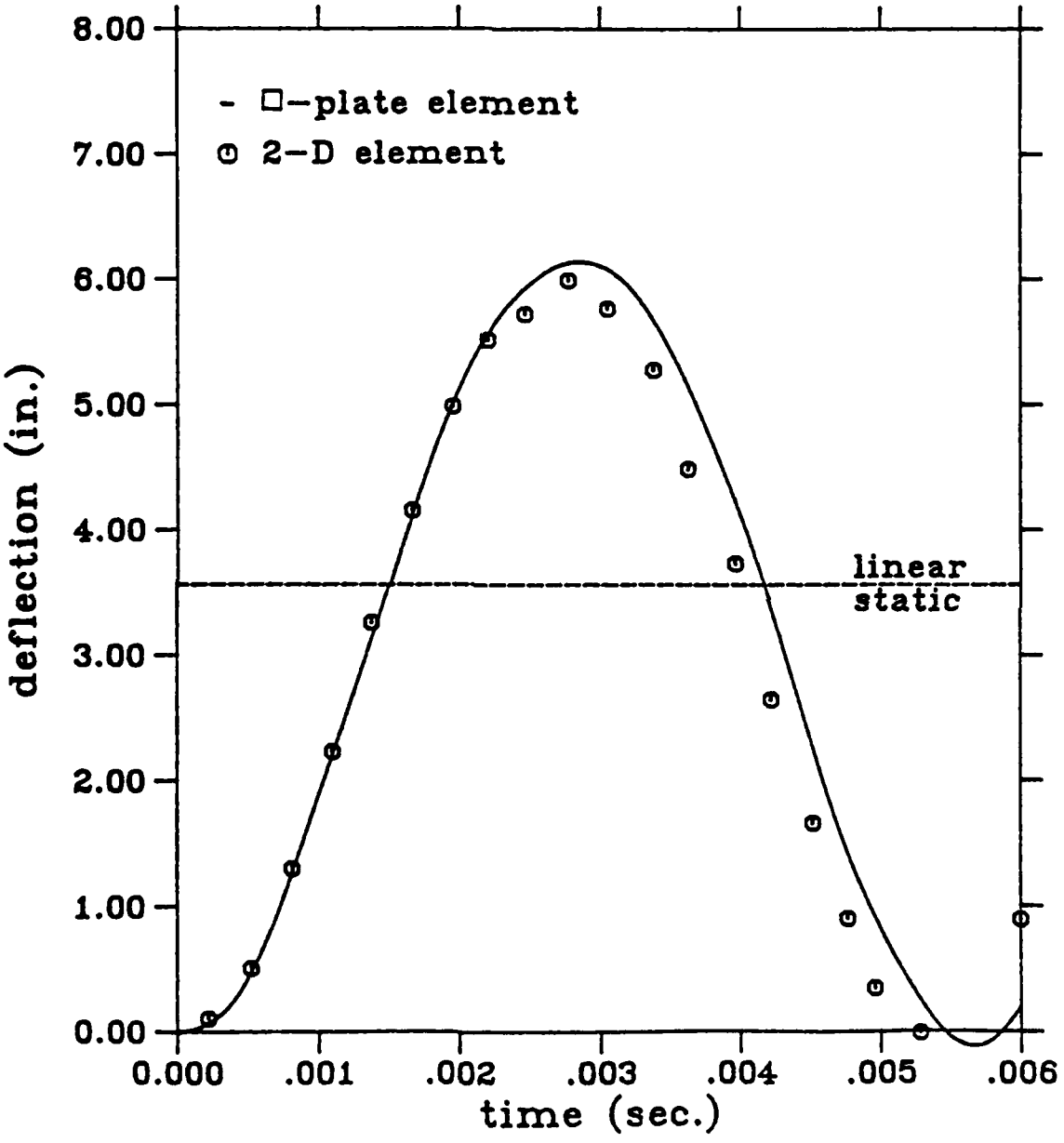

Fig. 2. Tip deflection for cantilever beam subjected to a uniform load p = 2.85 psi.

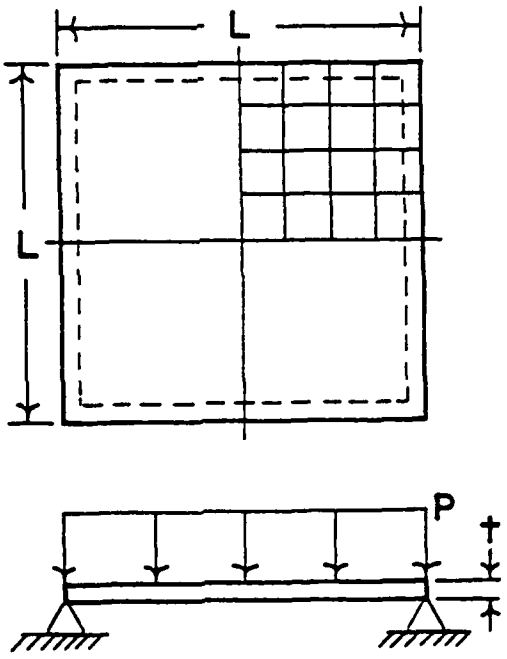

Length	L = 10. in.
Thickness	t = 0.5 in.
Young's modulus	E = 10^7 psi
Density	ρ = 2.588×10^{-4} lb−sec^2/in^4 psi
Poisson's ratio	ν = 0.3
Yield stress	σ = 30000. psi
Plastic modulus	E_p = 0. psi
Pressure load	P = 300. psi

(a) Problem definition and element mesh

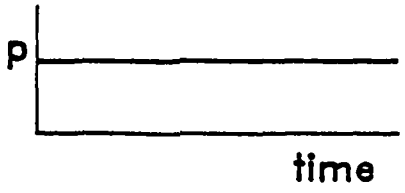

(b) Pressure load

Fig. 3. Simply supported square plate (example 2): problem description and finite element mesn.

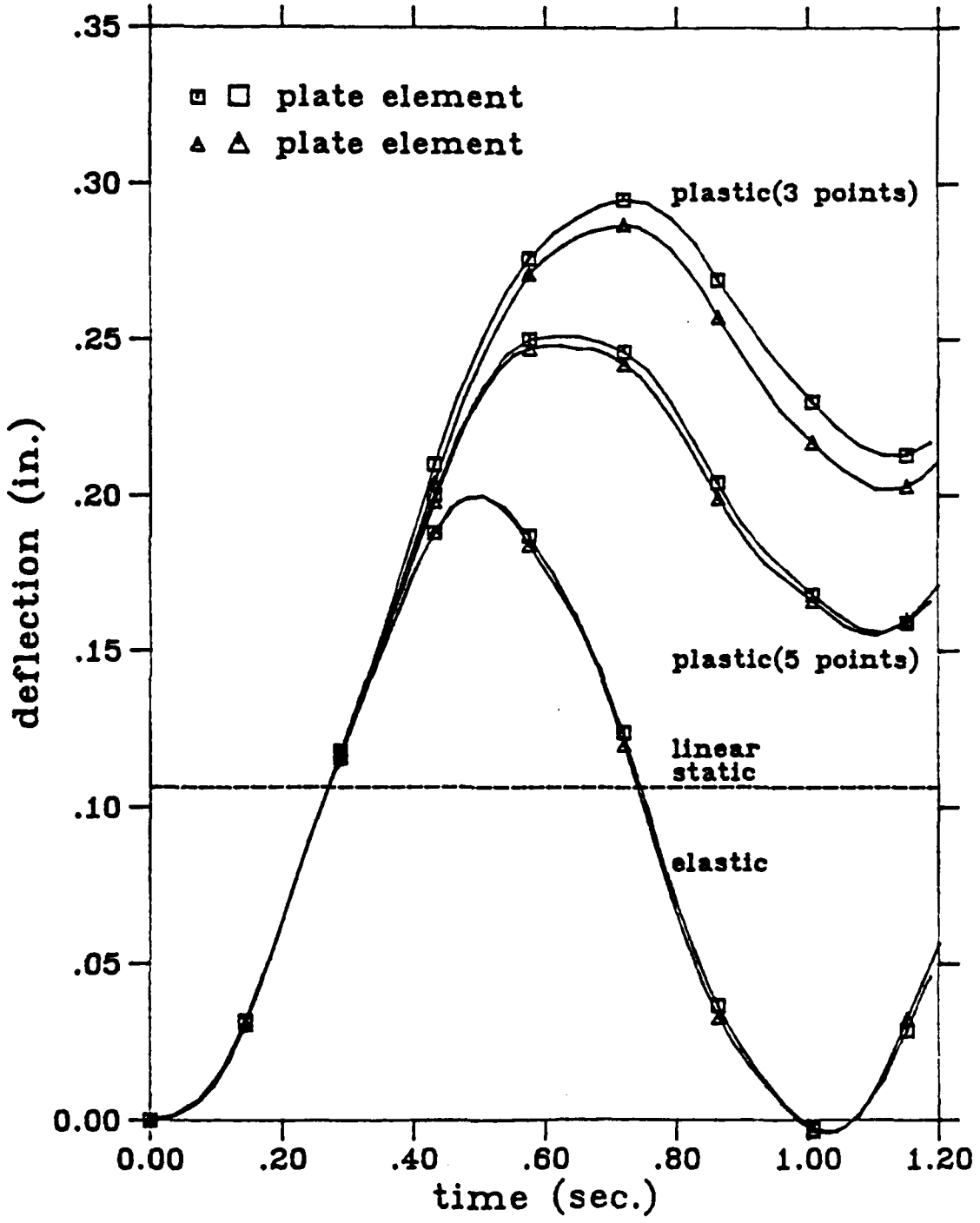

Fig. 4 Deflection of center-point of simply-supported square plate for elastic and elastic-perfectly-plastic materials using 3 and 5 integration points through the thickness for the latter.

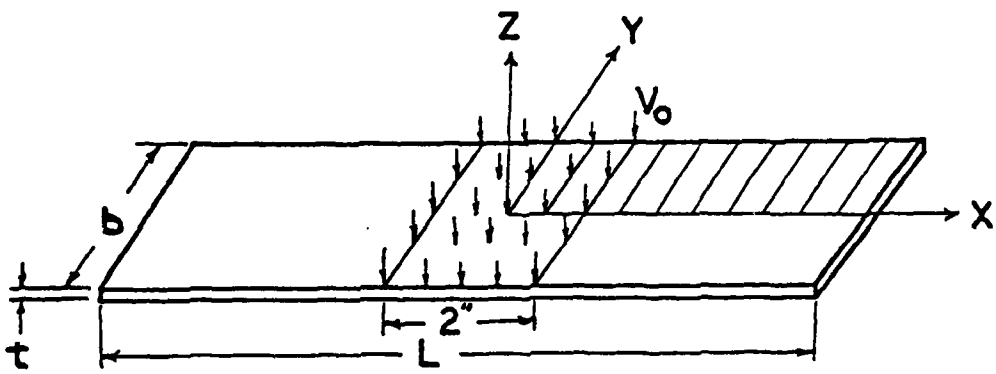

Length	L = 10. in.
Width	b = 1.2 in.
Thickness	t = .125 in.
Young's modulus	$E = 10.4 \times 10^6$ psi
Density	$\rho = 2.61 \times 10^{-4}$ lb–sec^2/in^4 psi
Poisson's ratio	$\nu = 0.3$
Yield stress	$\sigma = 41400.$ psi
Plastic modulus	$E_p = 0.$ psi
Initial velocity	$V_o = -5000.$ in/sec

Fig. 5. Impulsively loaded clamped beam (example 3): problem description and finite element mesh.

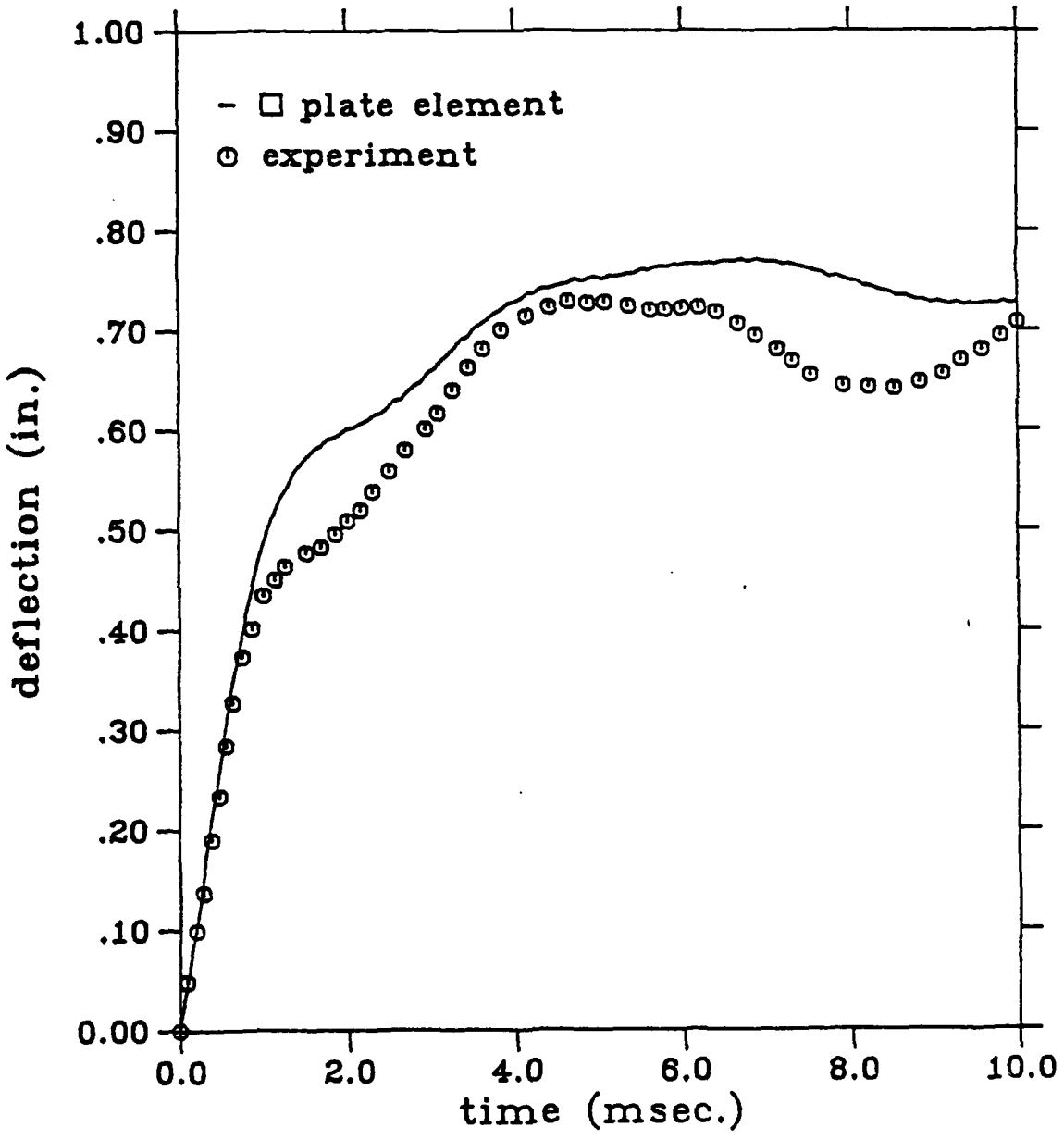

Fig. 6. Deflection of center point of example 3 compared to experimental results [29].

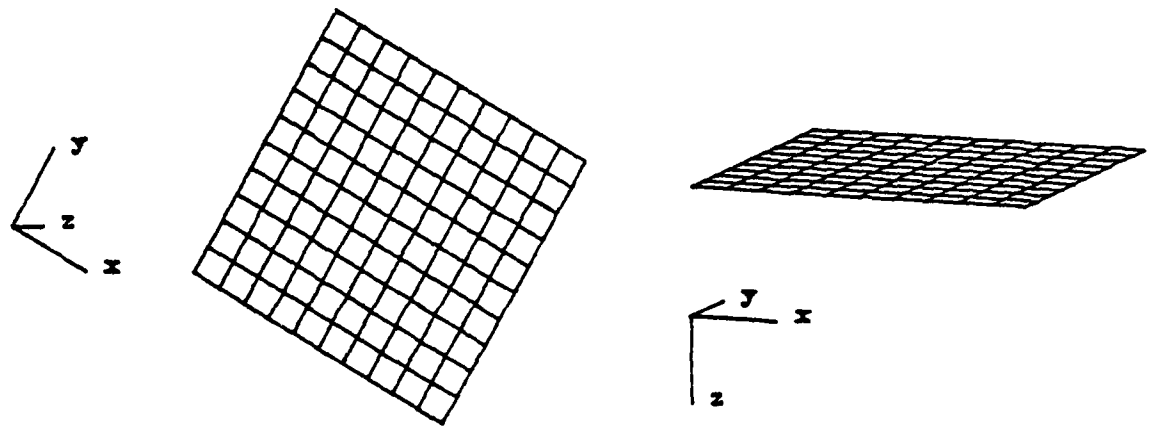

time =.400E-02

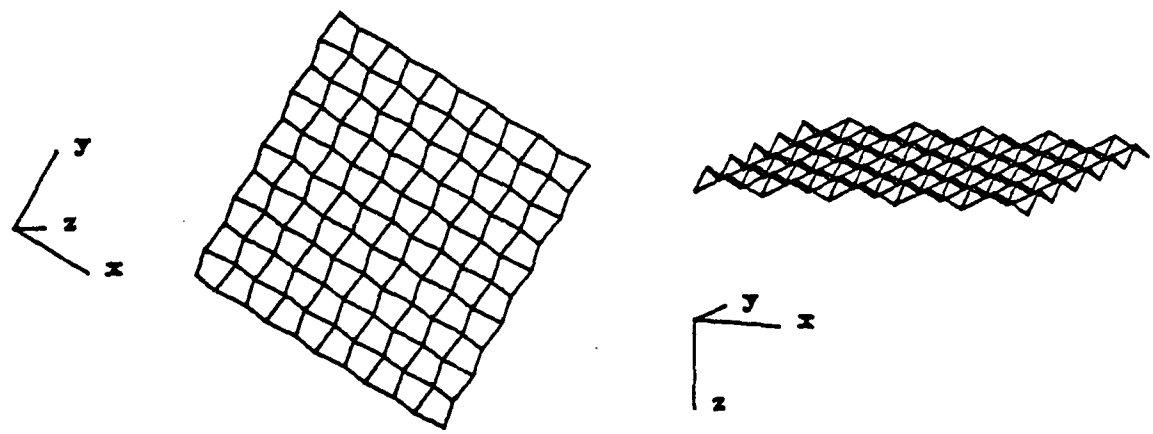

time =.800E-02

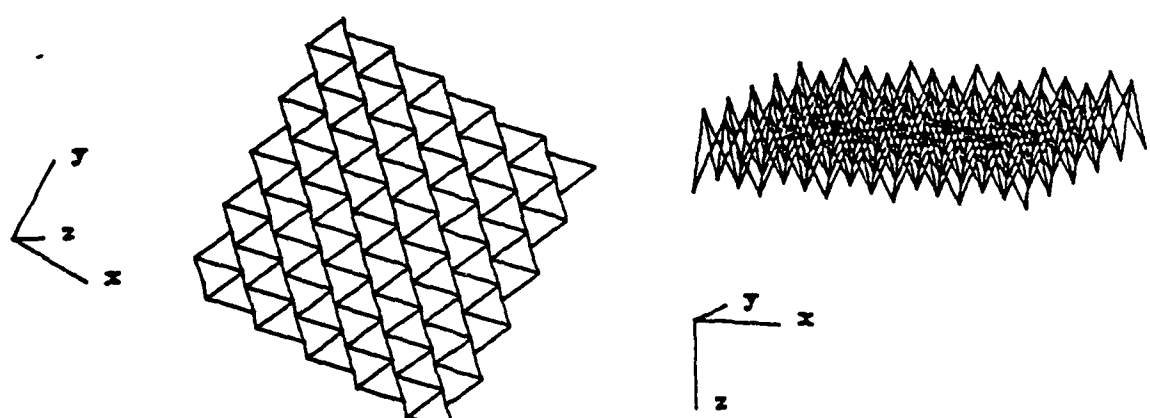

Fig. 7. Deformed mesh of corner supported plate without hourglass control.

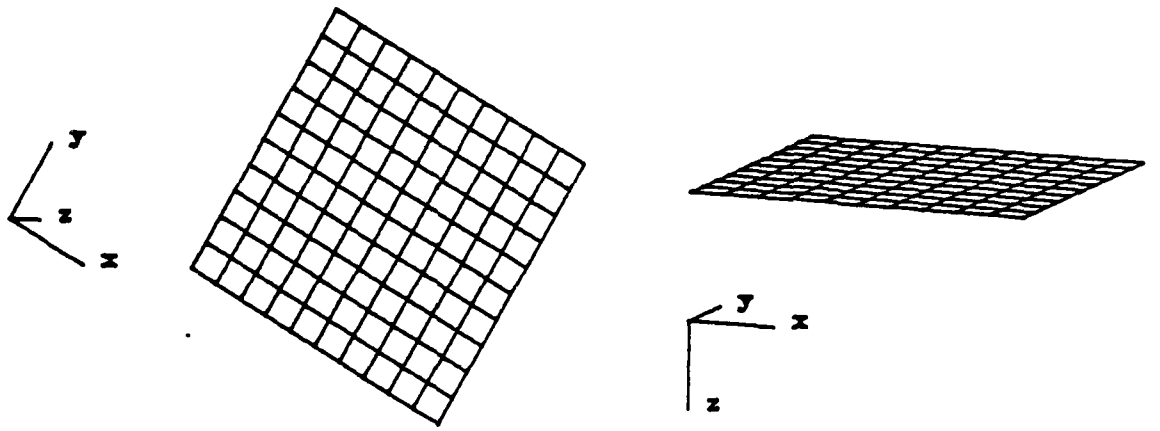

time =.400E-02

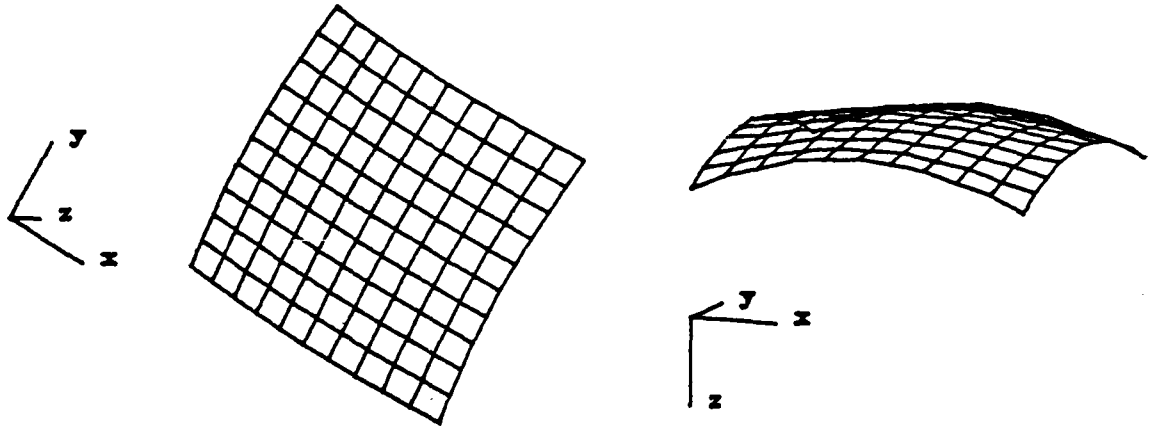

time =.800E-02

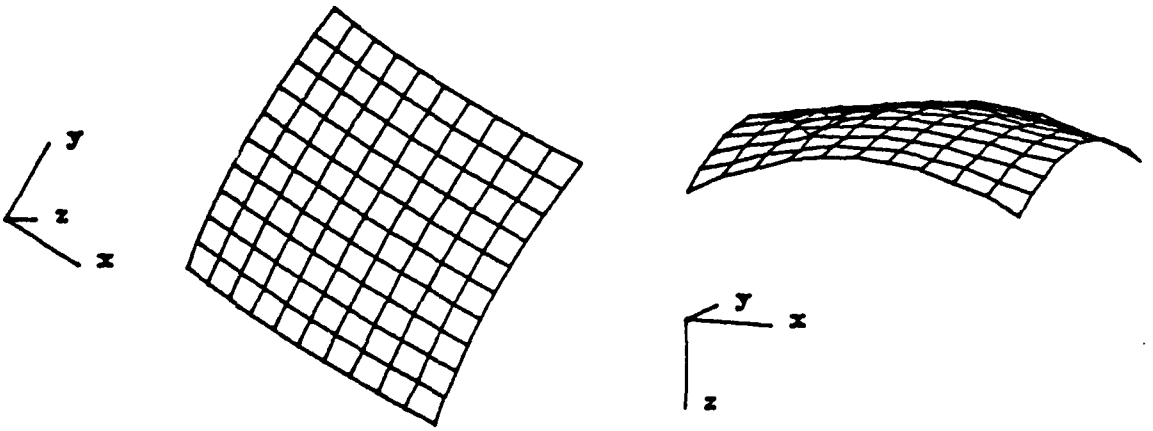

Fig. 8. Deformed mesh of corner supported plate with hourglass control.

Young's modulus	$E = 10.5 \times 10^6$
Density	$\rho = 2.5 \times 10^{-4}$ lb-sec^2/in^4
Poisson's ratio	$\nu = 0.33$
Yield stress	$\sigma = 44000.$ psi
Plastic modulus	$E_p = 0.$ psi

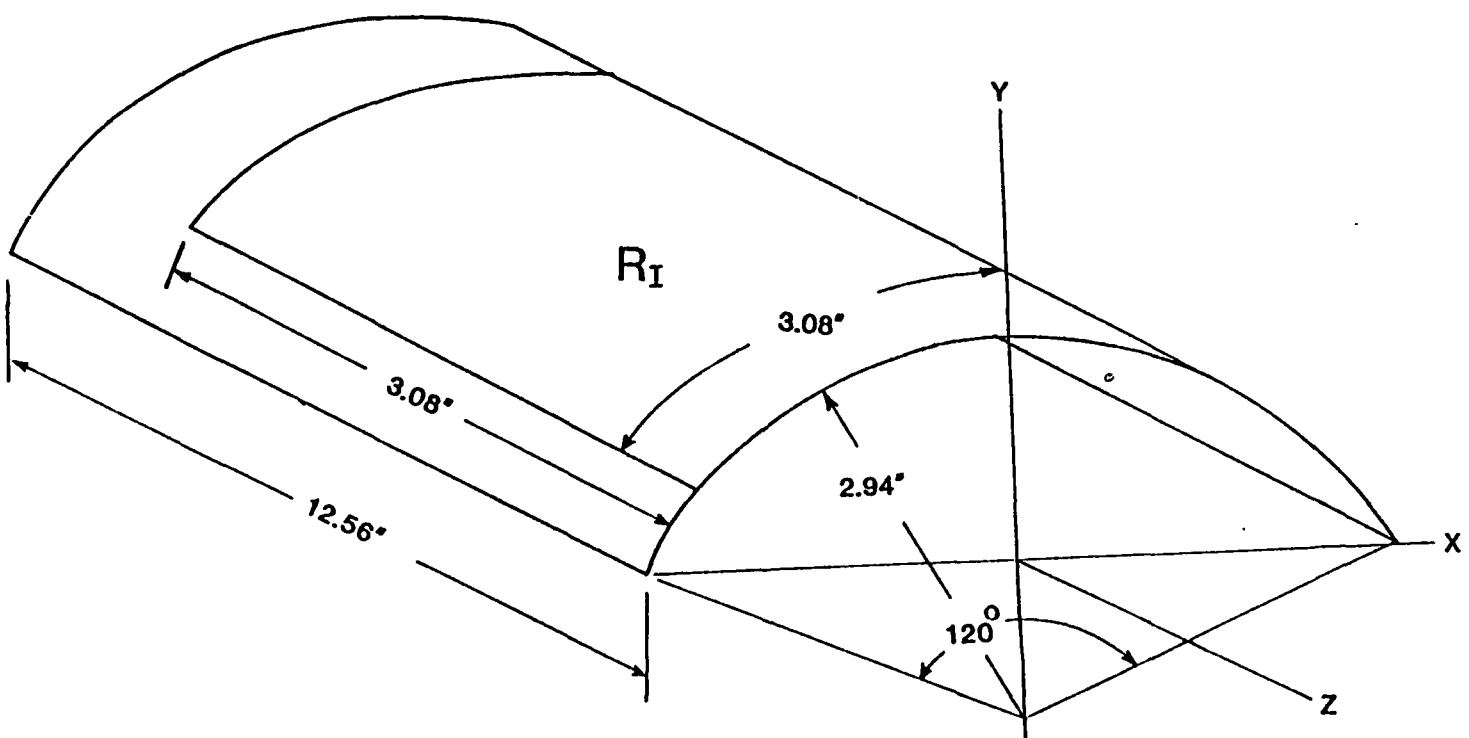

Fig. 9. Problem description for impulsively loaded cylindrical panel, example 5.

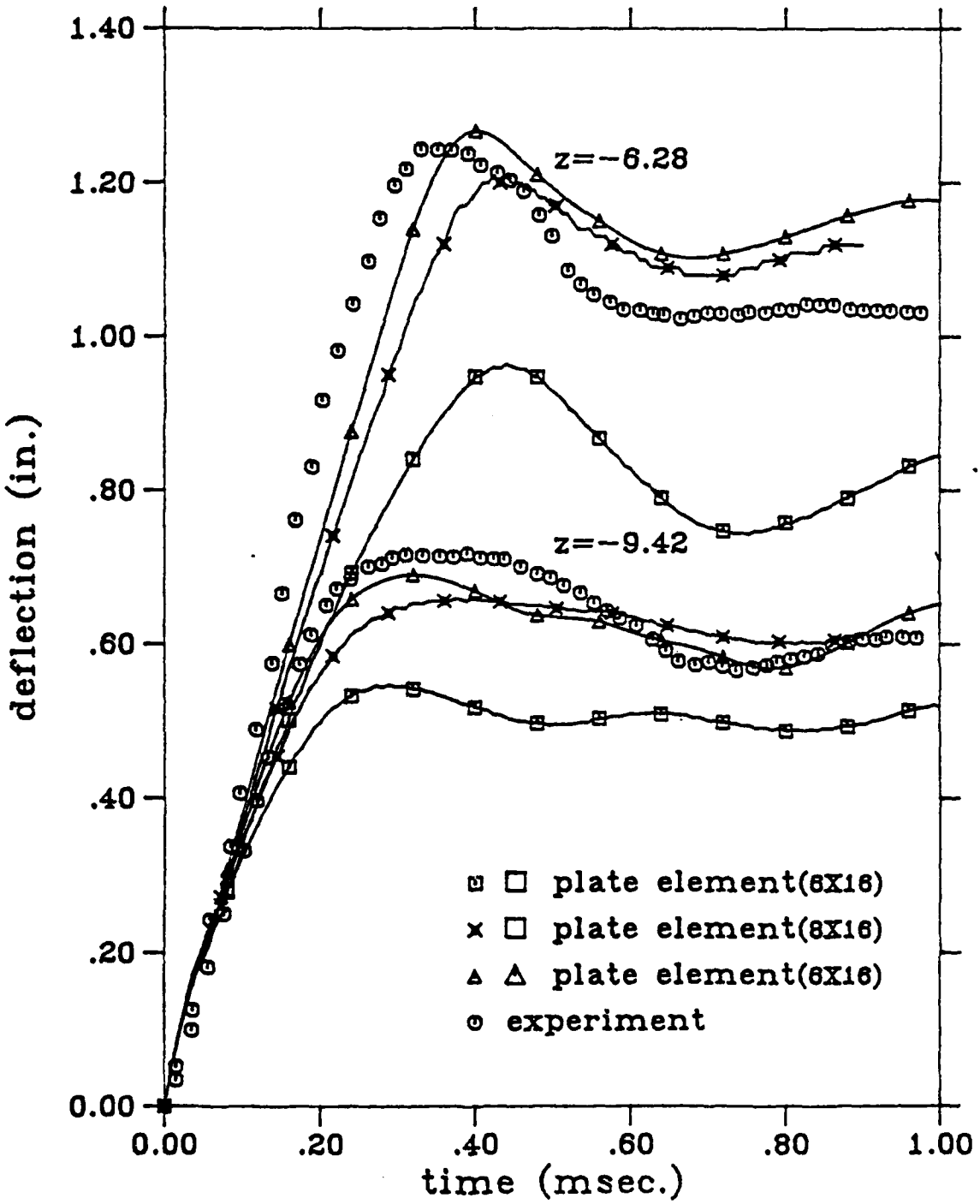

Fig. 10 Displacement time histories for two points of the cylindrical panel, example 5, compared to experiment [30] and earlier computed results [1].

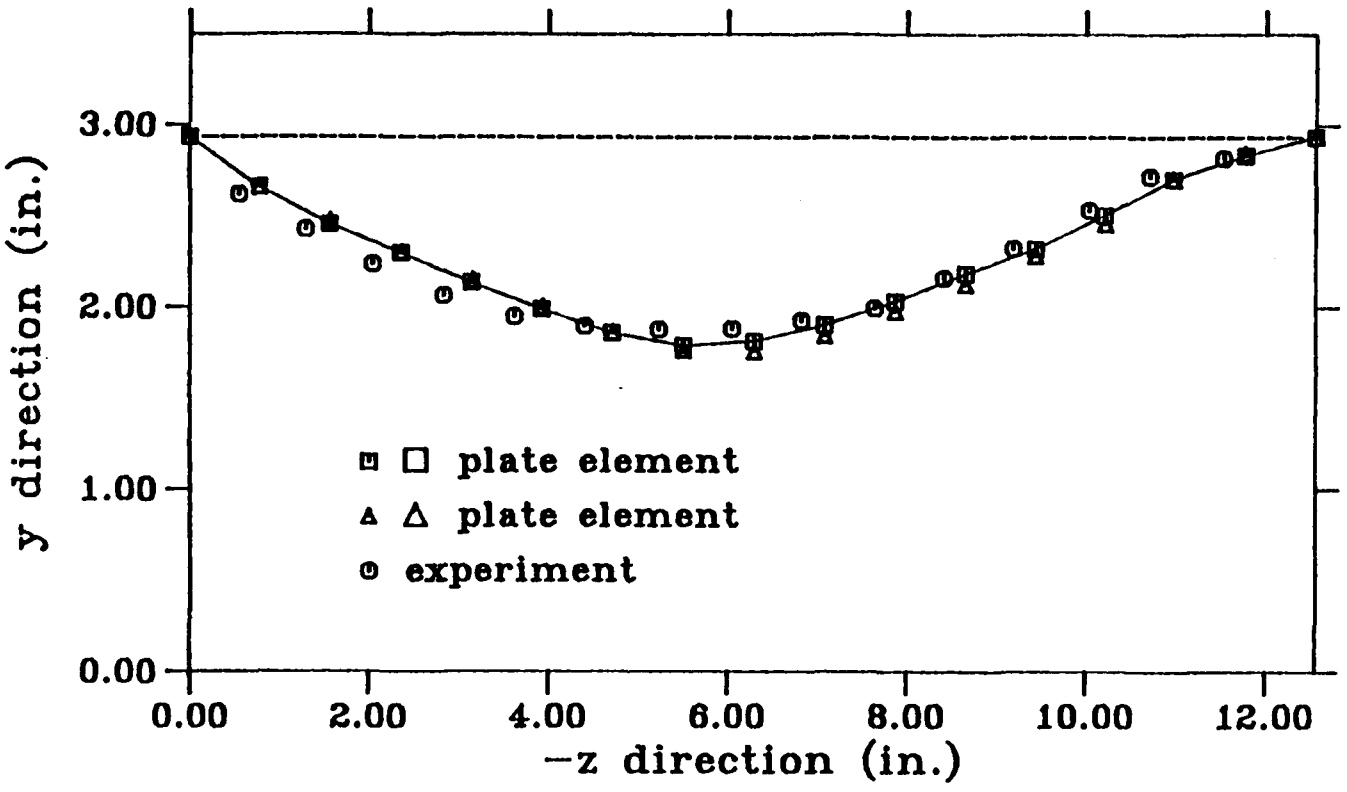

Fig. 11 Final deformed shape of the panel, example 5, at the crown line compared to experiment [30] and earlier results [1].

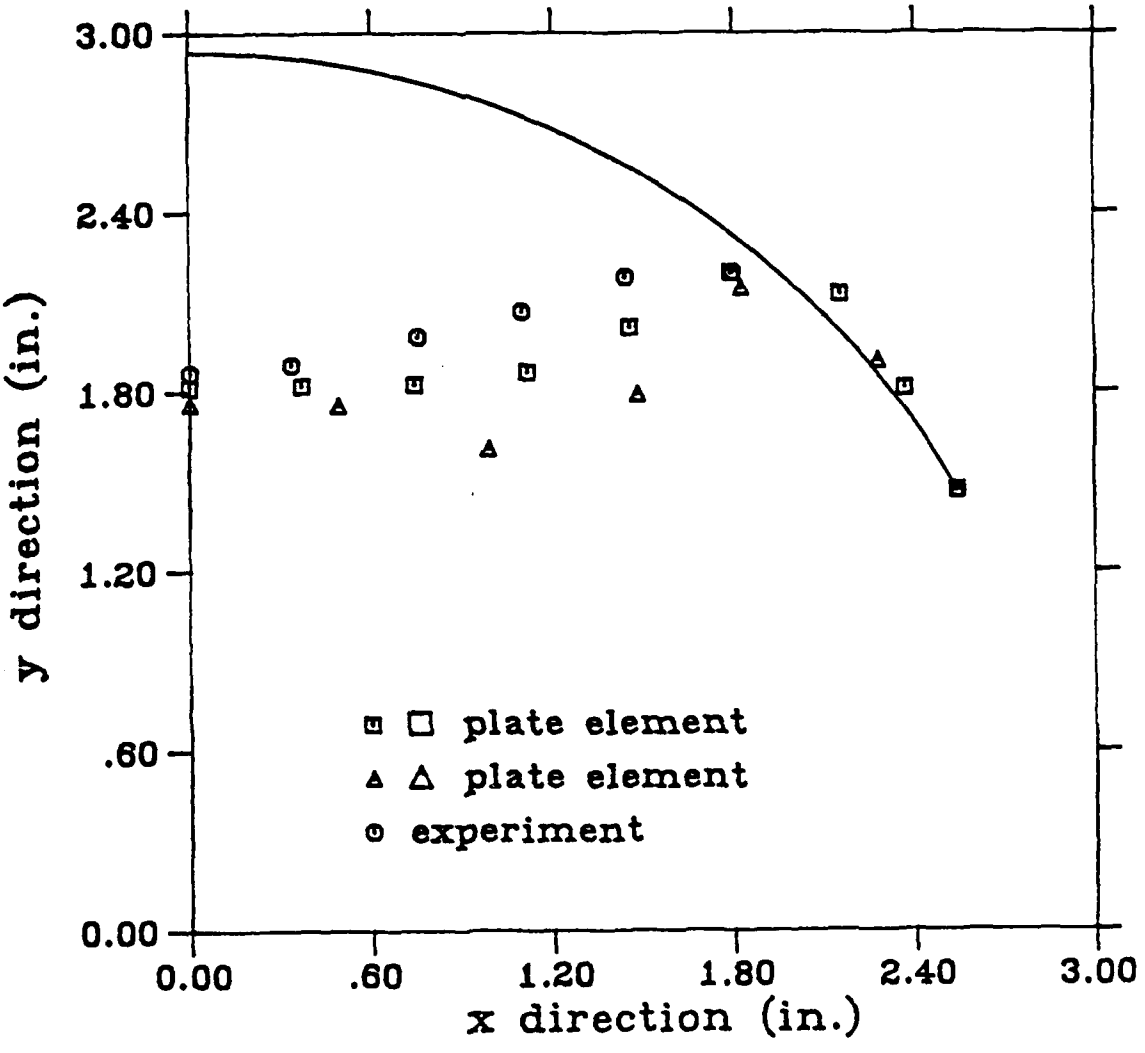

Fig 12. Final deformed shape of the panel at the cross-section z = -6.28 compared to experiment [30] and earlier results [1].

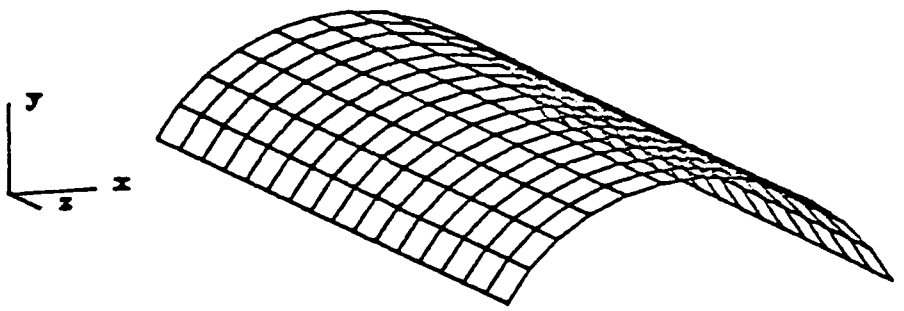

time =.378E-03

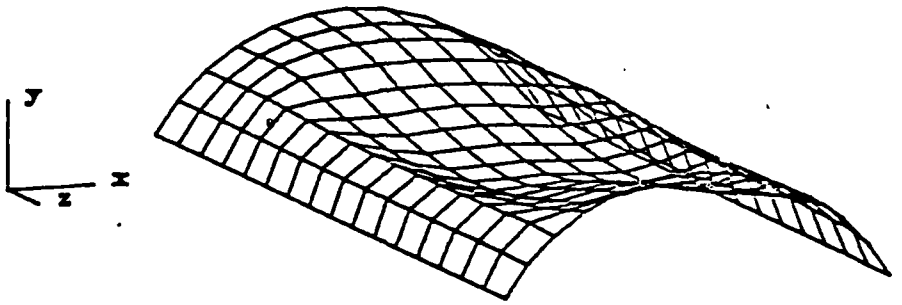

time =.600E-03

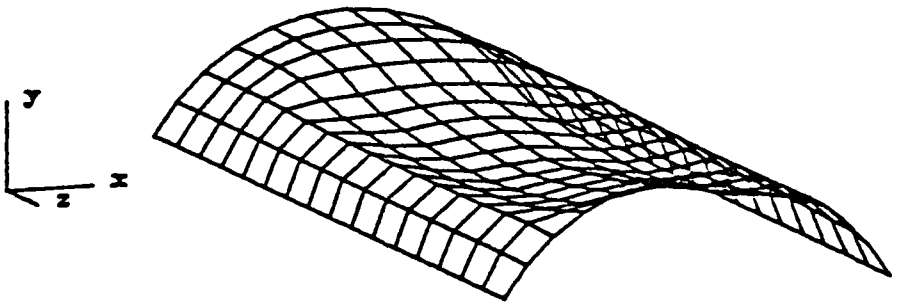

time =.100E-02

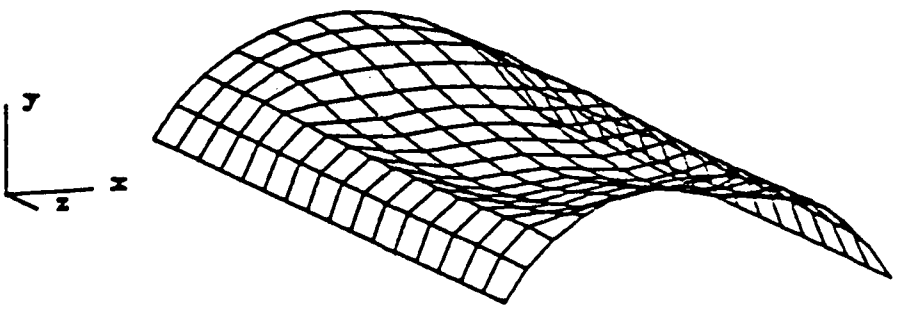

Fig. 13. Computer plots of deformed cylindrical panel.

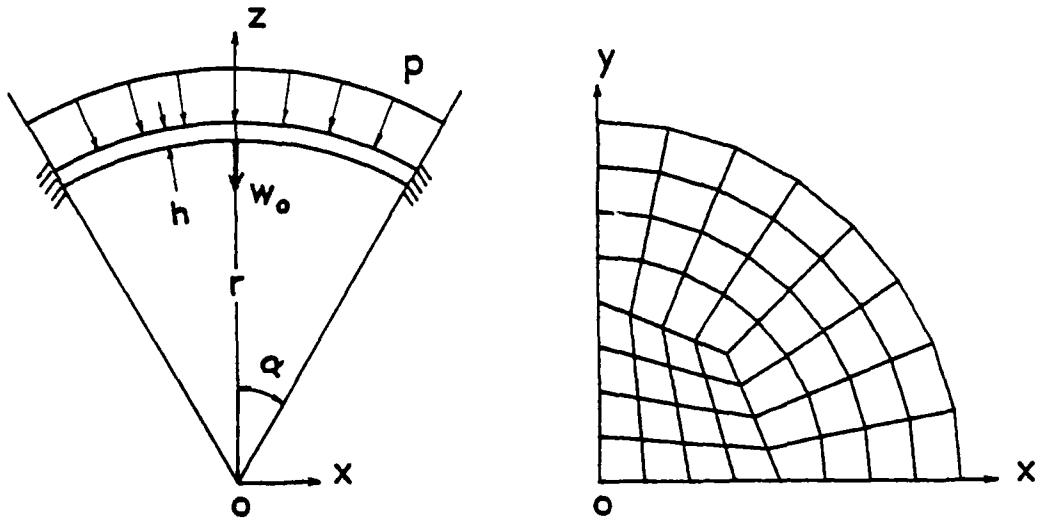

Clamped spherical cap and element mesh

Radius	r = 22.27 in.
Thickness	t = 0.41 in.
Angle	$\alpha = 28.67^{o}$
Young's modulus	$E = 10.5 \times 10^{6}$ psi
Density	$\rho = 2.45 \times 10^{-4}$ lb−sec^2/in^4 psi
Poisson's ratio	$\nu = 0.3$
Yield stress	$\sigma_Y = 24000.$ psi
Plastic modulus	$E_p = 0.21 \times 10^{6}$ psi
Pressure load	P = 600. psi

Fig. 14. Problem description for spherical cap, example 6.

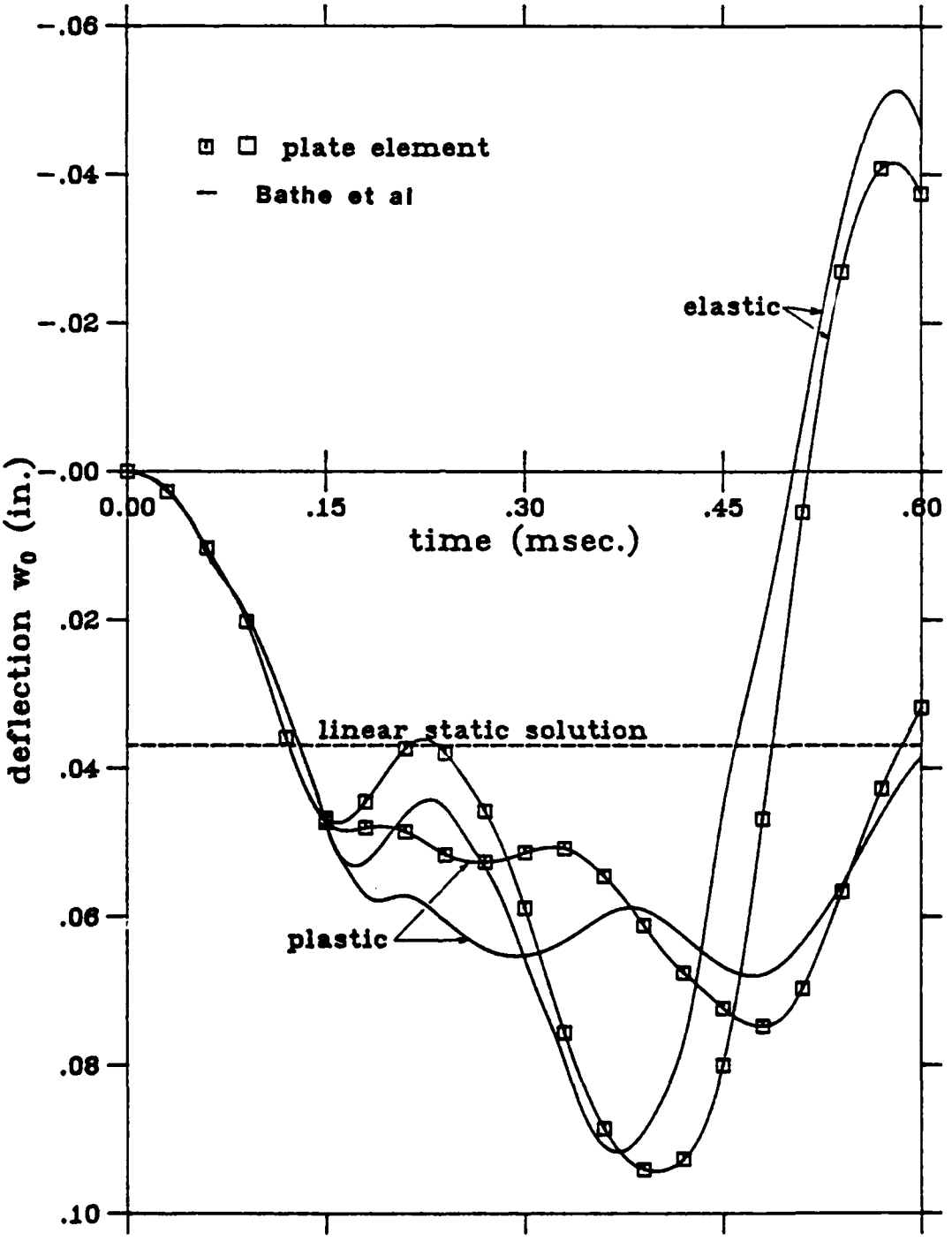

Fig. 15. Center displacement of spherical cap for elastic and elastic-plastic materials compared to numerical results of Bathe, et al [31].

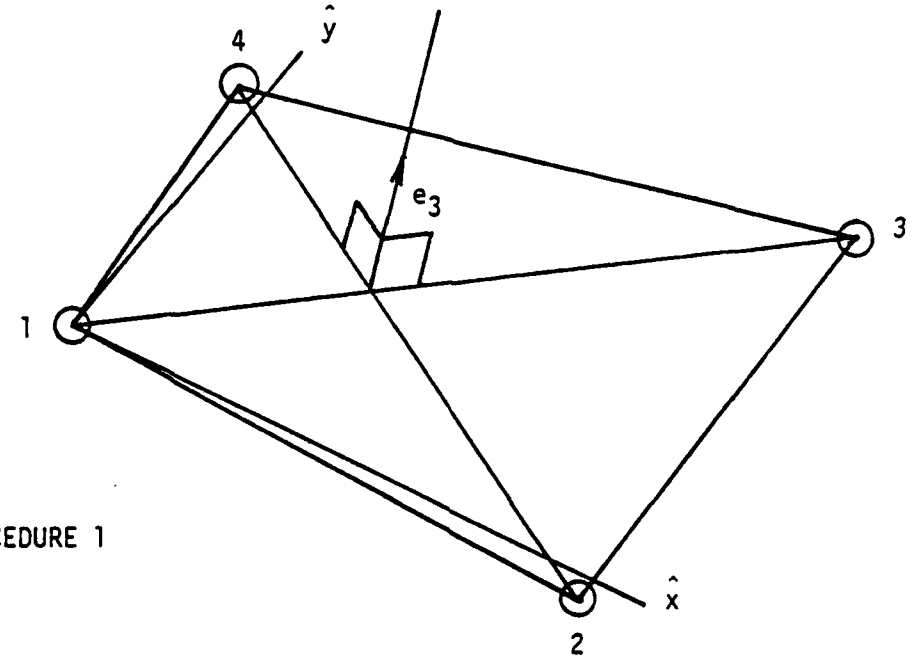

PROCEDURE 1

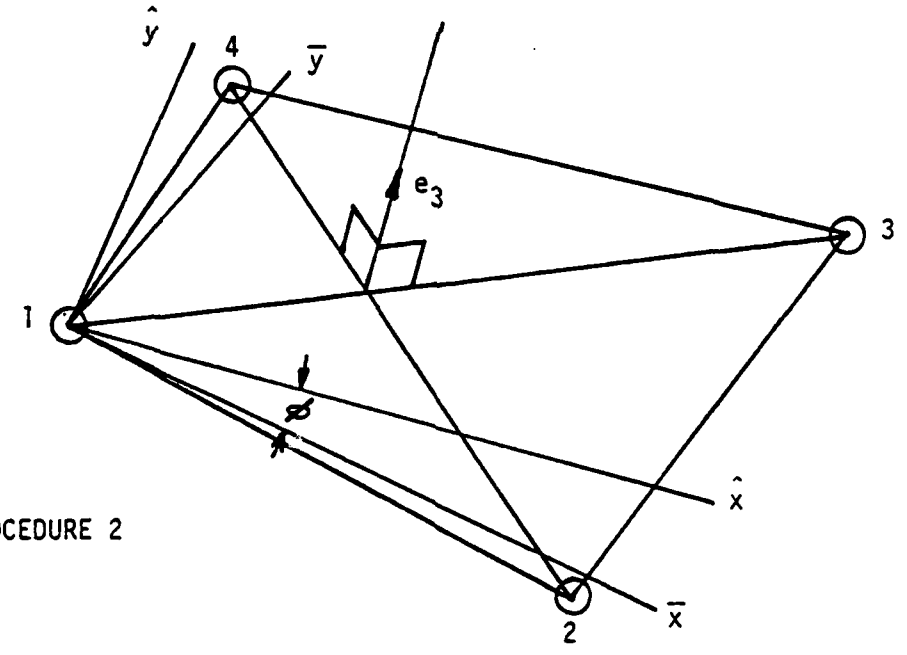

PROCEDURE 2

Fig. A1. Element coordinate systems

Table 1. Parameters and results for linear response (p = 0.01 psi) of cantilever beam, example 1.

Element Type	No. of Nodes	No. of Elements	Time Step Δt (sec)	No. of Time Steps	Max. Deflection (in)	Period (msec)	CPU Time (sec)
Euler Beam Element[4]	6	5	1.5×10^{-5}	400	0.02543	5.812	20.03
Triangular Plate Element[1]	12	20	1.5×10^{-5}	400	0.02408	5.662	126.03
Quadri-lateral Plate Element	12	5	1.5×10^{-5}	400	0.02454	5.680	25.80
Analytic [27]					0.025	5.719	

Table 2. Parameters and results for nonlinear response of cantilever beam, example 2.

Element Type	No. of Nodes	No. of Elements	Time Step Δt (sec)	No. of Time Steps	Max. Deflection (in)	Period (msec)	CPU Time (sec)
Euler Beam Element[4]	6	5	1.5×10^{-5}	400	6.321	5.812	20.03
Triangular Plate Element[1]	12	20	1.5×10^{-5}	400	6.076	5.587	126.03
Quadri-lateral Plate Element	12	5	1.5×10^{-5}	400	6.139	5.640	25.80
2-D Element[28]	22	5	0.2×10^{-5}	6600	6.0	5.600	43*

* CDC 7600

Table 3. Parameters and results for elastic, simply-supported square plate, example 2.

Element Type	No. of Nodes	No. of Elements	Time Step Δt (sec)	No. of Time Steps	Max. Deflection (in)	Period (msec)	CPU Time (sec)
Triangular Plate Element[1]	25	32	4×10^{-6}	300	0.1996	1.032	70.31
Quadri-lateral Plate Element	25	16	6×10^{-6}	200	0.2001	0.995	28.08
Analytic [29]					0.2129	1.070	

Table 4. Parameters and results for elastic-plastic, simple supported square plate, example 2.

Element Type	No. of Nodes	No. of Elements	Time Step Δt (sec)	No. of Time Steps	Max. Deflection (in.)	Period (sec)	CPU Time (sec)
Triangular Plate Element (3 layers) [1]	25	32	4×10^{-6}	300	0.3866	0.01152	124.51
Triangular Plate Element (5 layers) [1]	25	32	4×10^{-6}	300	0.2478	0.01104	143.41
Quadrila-teral Plate Element (3 layers)	25	16	6×10^{-6}	200	0.2949	0.01152	33.82
Quadrila-teral Plate Element (5 layers)	25	16	6×10^{-6}	200	0.2511	0.01116	43.64

*note: 3 layers means 3 integration points through thickness
5 layers means 5 integration points through thickness

APPENDIX A

1. INTRODUCTION

In the analysis of nonlinear problems, particularly transient nonlinear problems, computation time and memory are often crucial factors. Since element stiffness computations are repeated many times it is advantageous to have efficient and simple elements. Consequently much research is aimed at formulating accurate elements with these characteristics [1-8].

In the analysis of thin flexible structures, perhaps the most promising approach for developing simple and efficient elements is that based on independent approximations of the rotations and displacements combined with a reduced order of shear integration [3-5, 9-16]. As opposed to the C^1 continuity required in the Kirchhoff type theory, only C^0 continuity need be satisfied in this approach. Consequently lower order shape functions can be used which enhance simplicity. However, the use of the low order shape functions necessitates reduced integration of the shear contribution to the stiffness matrix, [3]; otherwise the elements are considerably too stiff. Fortunately this necessity further contributes to the efficiency of the C^0 element; reducing the number of the integration points reduces the number of computations, and along with the simple shape functions, results in extremely efficient elements. While this approach also has its drawbacks, such as possible zero energy modes, these appear only for certain boundary conditions and then can be effectively eliminated [17,18].

In some cases reduced integration may fail. For instance Batoz et.al. [7] examine three different approaches to triangular elements and in their study the SRI (selective/reduced integration) triangular element was found to be ineffective. On the other hand Hughes and Taylor [19] have developed a more successful one point quadrature triangular element by overlapping two

nodes of the quadrilateral [20], but the element's performance is mediocre for certain element arrangements.

The results of [7] and [19] show that to develop a successful C^0 element it is not sufficient to use reduced shear integration; it is necessary in fact to identify those mechamisms which are associated with excessive shear-strain energy and hence shear locking. This will be accomplished by fitting a portion of the deformation to an "equivalent Kirchhoff mode"; this portion of deformation will be called the bending mode. Although accompanied by shear strains, bending modes will not involve any shear strain energy. The remaining portion of the deformation will be called a shear mode. The proper definition of these modes is crucial for the development of a successful C^0 element. It can not always be achieved by just reducing the order of numerical integration. The triangular linear plate element is one of the best examples of this situation.

In this paper we develop a new triangular element with linear C^0 fields which is based on this concept of decomposing the deformation into well defined bending and shear modes. The element developed here shows definite improvement compared to the formulation presented in [19]. We also identify the source of the difficulties encountered in [7]. After some modifications, the basic ideas presented here can also be used for other elements.

Our presentation begins with general considerations regarding the shear and bending modes of deformation. Section 3 contains the specifications of the problem for the triangular linear plate element. Section 4 deals with major aspects regarding implementation while in Section 5 the results of numerical applications are presented including a discussion.

2. GENERAL REMARKS

The main issue in this paper is to determine an additive decomposition of the displacements and rotations of a C^0 plate element into two modes: a bending mode - associated exclusively with bending strain energy (regardless of the presence of shear strains in this mode) and a shear mode - which is associated only with the shear strain energy. Therefore the transverse deflection w and the rotations θ_x, θ_y in each element are given by

$$w = \sum_I w_I N_I^w = \sum_I (w_I^b + w_I^s) N_I^w \tag{1a}$$

$$\begin{Bmatrix} \theta_x \\ \theta_y \end{Bmatrix} = \sum_I \begin{Bmatrix} \theta_{xI} \\ \theta_{yI} \end{Bmatrix} N_I^\theta = \sum_I \left(\begin{Bmatrix} \theta_{xI}^b \\ \theta_{yI}^b \end{Bmatrix} + \begin{Bmatrix} \theta_{xI}^s \\ \theta_{yI}^s \end{Bmatrix} \right) N_I^\theta \tag{1b}$$

where the following decomposition is implied for the nodal variables

$$\underset{\sim}{\theta} = \underset{\sim}{\theta}^b + \underset{\sim}{\theta}^s \tag{1c}$$

$$\underset{\sim}{w} = \underset{\sim}{w}^b + \underset{\sim}{w}^s \tag{1d}$$

Here N_I^w and N_I^θ are the shape functions for the displacements and rotations, respectively, and where superscripts b and s designate the bending mode and the shear mode, respectively. Each of these modes can include an arbitrary amount of rigid body motion.

The decomposition is chosen so that the element behaves as closely as possible to a Kirchhoff C^1 element in the thin-structure limit. The mechanical reasoning used to accomplish this task will be presented in the next Section. In the decomposition, the shear and bending nodal variables are

linearly related to the total nodal variables, so

$$\begin{Bmatrix} \underset{\sim}{\theta}^b \\ \underset{\sim}{w}^b \end{Bmatrix} = \underset{\sim}{P}^b \begin{Bmatrix} \underset{\sim}{\theta} \\ \underset{\sim}{w} \end{Bmatrix} \tag{2a}$$

$$\begin{Bmatrix} \underset{\sim}{\theta}^s \\ \underset{\sim}{w}^s \end{Bmatrix} = \underset{\sim}{P}^s \begin{Bmatrix} \underset{\sim}{\theta} \\ \underset{\sim}{w} \end{Bmatrix} \tag{2b}$$

where $\underset{\sim}{P}^b$, $\underset{\sim}{P}^s$ are linear operators emerging from the decomposition. They can also be viewed as nonorthogonal projection operators.

Assuming the sign convention shown in Fig. 1, the kinematical relationships are

$$\underset{\sim}{\kappa} = \begin{Bmatrix} \kappa_x \\ \kappa_y \\ \kappa_{xy} \end{Bmatrix} = \begin{Bmatrix} \theta_{x,x} \\ \theta_{y,y} \\ \theta_{x,y} + \theta_{y,x} \end{Bmatrix} \tag{3a}$$

$$\underset{\sim}{\gamma} = \begin{Bmatrix} \gamma_x \\ \gamma_y \end{Bmatrix} = \begin{Bmatrix} \theta_x + w_{,x} \\ \theta_x + w_{,y} \end{Bmatrix} \tag{3b}$$

Their discretization yields:

$$\underset{\sim}{\kappa} = \underset{\sim}{B}^b \begin{Bmatrix} \underset{\sim}{\theta} \\ \underset{\sim}{w} \end{Bmatrix} \equiv [\underset{\sim}{B}^b_r, \underset{\sim}{0}] \begin{Bmatrix} \underset{\sim}{\theta} \\ \underset{\sim}{w} \end{Bmatrix} \tag{4a}$$

$$\underset{\sim}{\gamma} = \underset{\sim}{B}^s \begin{Bmatrix} \underset{\sim}{\theta} \\ \underset{\sim}{w} \end{Bmatrix} \equiv [\underset{\sim}{B}^s_r, \underset{\sim}{B}^s_d] \begin{Bmatrix} \underset{\sim}{\theta} \\ \underset{\sim}{w} \end{Bmatrix} \tag{4b}$$

with $\underset{\sim}{B}^b_r$, $\underset{\sim}{B}^s_r$, $\underset{\sim}{B}^s_d$ defined by Eqs. (1) and (3). Equations (2) and (4) can be used to find the strain fields in the bending or shear mode of deformation. Thus, in the bending mode

$$\underset{\sim}{\kappa}^b = \underset{\sim}{B}^b \begin{Bmatrix} \underset{\sim}{\theta}^b \\ \underset{\sim}{w}^b \end{Bmatrix} = \underset{\sim}{B}^b \underset{\sim}{P}^b \begin{Bmatrix} \underset{\sim}{\theta} \\ \underset{\sim}{w} \end{Bmatrix} \equiv \underset{\sim}{B}^{bb} \begin{Bmatrix} \underset{\sim}{\theta} \\ \underset{\sim}{w} \end{Bmatrix} \tag{5a}$$

$$\underset{\sim}{\gamma}^b = \underset{\sim}{B}^s \begin{Bmatrix} \underset{\sim}{\theta}^b \\ \underset{\sim}{w}^b \end{Bmatrix} = \underset{\sim}{B}^s \underset{\sim}{P}^b \begin{Bmatrix} \underset{\sim}{\theta} \\ \underset{\sim}{w} \end{Bmatrix} \equiv \underset{\sim}{B}^{sb} \begin{Bmatrix} \underset{\sim}{\theta} \\ \underset{\sim}{w} \end{Bmatrix} \tag{5b}$$

while in the shear mode

$$\underset{\sim}{\kappa}^s = \underset{\sim}{B}^b \begin{Bmatrix} \underset{\sim}{\theta}^s \\ \underset{\sim}{w}^s \end{Bmatrix} = \underset{\sim}{B}^b \underset{\sim}{P}^s \begin{Bmatrix} \underset{\sim}{\theta} \\ \underset{\sim}{w} \end{Bmatrix} \equiv \underset{\sim}{B}^{bs} \begin{Bmatrix} \underset{\sim}{\theta} \\ \underset{\sim}{w} \end{Bmatrix} \tag{6a}$$

$$\underset{\sim}{\gamma}^s = \underset{\sim}{B}^s \begin{Bmatrix} \underset{\sim}{\theta}^s \\ \underset{\sim}{w}^s \end{Bmatrix} = \underset{\sim}{B}^s \underset{\sim}{P}^s \begin{Bmatrix} \underset{\sim}{\theta} \\ \underset{\sim}{w} \end{Bmatrix} \equiv \underset{\sim}{B}^{ss} \begin{Bmatrix} \underset{\sim}{\theta} \\ \underset{\sim}{w} \end{Bmatrix} \tag{6b}$$

As mentioned earlier, only the bending mode will contribute to the bending strain energy, and only the shear mode will contribute to the shear-strain energy. Hence, each mode is uniquely associated with one of the energy

terms. The total strain energy is

$$U = \frac{1}{2}\left(\int_A (\underset{\sim}{\kappa}^b)^T \underset{\sim}{D}^b \underset{\sim}{\kappa}^b \, dA + \int_A (\underset{\sim}{\chi}^s)^T \underset{\sim}{D}^s \underset{\sim}{\chi}^s \, dA \right) \tag{7}$$

$$= \frac{1}{2} \begin{Bmatrix} \underset{\sim}{\theta} \\ \underset{\sim}{w} \end{Bmatrix}^T \left(\int_A (\underset{\sim}{B}^{bb})^T \underset{\sim}{D}^b \underset{\sim}{B}^{bb} \, dA + \int_A (\underset{\sim}{B}^{ss})^T \underset{\sim}{D}^s \underset{\sim}{B}^{ss} \, dA \right) \begin{Bmatrix} \underset{\sim}{\theta} \\ \underset{\sim}{w} \end{Bmatrix}$$

where $\underset{\sim}{B}^{bb}$, $\underset{\sim}{B}^{ss}$ are defined in Eqs. (5) and (6), A is the area of the element,

$$\underset{\sim}{D}^b = \frac{Eh^3}{12(1-\nu^2)} \begin{bmatrix} 1 & \nu & 0 \\ \nu & 1 & 0 \\ 0 & 0 & \frac{1-\nu}{2} \end{bmatrix} \tag{8}$$

$$\underset{\sim}{D}^s = \frac{Eh\psi}{2(1+\nu)} \begin{bmatrix} 1 & 0 \\ 0 & 1 \end{bmatrix} \tag{9}$$

where E is Young's modulus, ν is Poisson's ratio, h the thickness and ψ the shear correction factor. Eq. (7) leads immediately to the conclusion that in the present formulation, the element stiffness matrix is:

$$\underset{\sim}{K} = \int_A (\underset{\sim}{B}^{bb})^T \underset{\sim}{D}^b \underset{\sim}{B}^{bb} dA + \int_A (\underset{\sim}{B}^{ss})^T \underset{\sim}{D}^s \underset{\sim}{B}^{ss} \, dA \tag{10}$$

The above outline of the approach does not give any rationale for the decomposition into the bending and shear modes nor the decomposition. This crucial aspect of the formulation will be discussed in the next Section in connection with the analysis of the linear triangular element.

3. LINEAR TRIANGULAR PLATE ELEMENT

Consider a triangular plate element in the local coordinate frame shown in Fig. 2. Nodal rotations and displacements form the following vectors

$$\underset{\sim}{\theta}^T = [\theta_{x1}, \theta_{y1}, \theta_{x2}, \theta_{y2}, \theta_{x3}, \theta_{y3}] \tag{11a}$$

$$\underset{\sim}{w}^T = [w_1, w_2, w_3] \tag{11b}$$

Linear shape functions will be used within the element, so the rotations and displacements are

$$\begin{Bmatrix} \theta_x \\ \theta_y \end{Bmatrix} = \sum_{I=1}^{3} L_I \begin{Bmatrix} \theta_{xI} \\ \theta_{yI} \end{Bmatrix} \tag{12a}$$

$$w = \sum_{I=1}^{3} L_I w_I \tag{12b}$$

where L_I are area triangular coordinates.

Using Eqs (3) and (12) leads to the following forms of matrices $\underset{\sim}{B}^b$ and $\underset{\sim}{B}^s$

$$\underset{\sim}{B}^b_r = \frac{1}{x_2 y_3} \begin{bmatrix} -y_3 & 0 & y_3 & 0 & 0 & 0 \\ 0 & x_3-x_2 & 0 & -x_3 & 0 & x_2 \\ x_3-x_2 & -y_3 & -x_3 & y_3 & x_2 & 0 \end{bmatrix} \tag{13}$$

$$\underset{\sim}{B}^s_r = \begin{bmatrix} L_1 & 0 & L_2 & 0 & L_3 & 0 \\ 0 & L_1 & 0 & L_2 & 0 & L_3 \end{bmatrix} \tag{14}$$

$$\underset{\sim}{B}^s_d = \frac{1}{x_2 y_3} \begin{bmatrix} -y_3 & y_3 & 0 \\ x_3 - x_2 & -x_3 & x_2 \end{bmatrix} \tag{15}$$

The decomposition of the total displacement into its bending and shear modes will now be described. To this end, we note that modifying the shear strain energy is an effective means of improving the performance of the C^0 element in the thin plate limit, for this may eliminate the excessive energy absorption in shear which leads to locking. On the other hand, modification of the bending energy is undesirable since it may introduce additional zero energy modes (compare [3] and [18] for instance). Therefore the bending mode is chosen so that the bending strain energy in this element is unchanged by the decomposition. Since the bending energy only depends on the nodal rotations in the C^0 element, to accomplish this we can immediately establish the decomposition of $\underset{\sim}{\theta}$ as follows

$$\underset{\sim}{\theta}^b = \underset{\sim}{\theta}, \qquad \underset{\sim}{\theta}^s = \underset{\sim}{0} \tag{16}$$

To determine the decomposition of the nodal displacements $\underset{\sim}{w}$, we first define the set of "equivalent Kirchhoff configurations", which are displacement fields $w^K(x,y)$ with curvatures equal to that of the C^0 element, i.e.

$$-\frac{\partial^2 w^K}{\partial x^2} = \kappa_x = \theta_{x,x} \tag{17a}$$

$$-\frac{\partial^2 w^K}{\partial y^2} = \kappa_y = \theta_{y,y} \tag{17b}$$

$$-\frac{\partial^2 w^K}{\partial x \partial y} = \kappa_{xy} = \theta_{x,y} + \theta_{y,x} \tag{17c}$$

Note that the above implies that the bending strain energies in the C^0 element and any equivalent Kirchhoff configuration are equal.

The curvatures in this C^0 element are constant, so the set of equivalent Kirchhoff configurations is described by

$$w^K = -\frac{1}{2}\begin{bmatrix} x^2 - x_2 x - x_3(x_3 - x_2)\frac{y}{y_3}, & y^2 - y_3 y, & xy - x_3 y \\ -\alpha_x x - \alpha_y y + \beta & & \end{bmatrix} \underset{\sim}{\kappa} \tag{18a}$$

where

$$\underset{\sim}{\kappa} = \underset{\sim}{B}^b_r \, \underset{\sim}{\theta} \tag{18b}$$

with $\underset{\sim}{B}^b_r$ given in Eq. (13); α_x, α_y, and β are free parameters which account for rigid body motion. At node I, the nodal rotations associated with w^K are given by

$$\begin{Bmatrix} \theta_x \\ \theta_y \end{Bmatrix}^K_I = \begin{Bmatrix} -\frac{\partial w^K}{\partial x} \\ -\frac{\partial w^K}{\partial y} \end{Bmatrix}_I = \underset{\sim}{S}_I \, \underset{\sim}{\kappa} + \begin{Bmatrix} \alpha_x \\ \alpha_y \end{Bmatrix} \tag{19a}$$

$$\underset{\sim}{S}_I = \frac{1}{2}\begin{bmatrix} 2x_I - x_2 & 0 & y_I \\ \frac{x_3}{y_3}(x_2 - x_3) & 2y_I - y_3 & x_I - x_3 \end{bmatrix} \tag{19b}$$

The nodal displacements of an equivalent Kirchhoff configuration are

$$\underset{\sim}{w}^K \equiv \begin{Bmatrix} w_1^K \\ w_2^K \\ w_3^K \end{Bmatrix} = \begin{bmatrix} 1 & 0 & 0 \\ 1 & -x_2 & 0 \\ 1 & -x_3 & -y_3 \end{bmatrix} \begin{Bmatrix} \beta \\ \alpha_x \\ \alpha_y \end{Bmatrix} \tag{20}$$

In order for the C^0 element to perform well in the thin-structure limit, its bending mode should resemble an equivalent Kirchhoff configuration as closely as possible. Therefore, we will define the optimal bending mode as that which minimizes the following measure of the difference between an equivalent Kirchhoff configuration and the bending modes

$$f(\alpha_x, \alpha_y, \beta, w_I^b) = (\underset{\sim}{\theta}^b - \underset{\sim}{\theta}^K)^T (\underset{\sim}{\theta}^b - \underset{\sim}{\theta}^K) + (\underset{\sim}{w}^b - \underset{\sim}{w}^K)^T (\underset{\sim}{w}^b - \underset{\sim}{w}^K) \tag{21}$$

where $\underset{\sim}{\theta}^b$, $\underset{\sim}{\theta}^K$ and $\underset{\sim}{w}^K$ are given by Eqs. (16), (19), and (20), while $\underset{\sim}{w}^b$ is to be determined. The nodal displacement vector $\underset{\sim}{w}^b$ (along with $\underset{\sim}{\theta}^b$) which minimizes the function in Eq. (21) is called the optimal bending mode. It is clear that the above procedure is in fact a least square method.

The minimum of f is independent of the rigid body translation, β. Assuming $\beta = 0$ the following steps are needed to determine $\underset{\sim}{w}^b$. First, according to Eqs. (18b) and (20)

$$\underset{\sim}{\theta}^K = \underset{\sim}{A}\, \underset{\sim}{\theta} + \underset{\sim}{R}^T \begin{Bmatrix} \alpha_x \\ \alpha_y \end{Bmatrix} \tag{22}$$

where

$$\underset{\sim}{A} = \begin{Bmatrix} \underset{\sim}{S}_1 \\ \underset{\sim}{S}_2 \\ \underset{\sim}{S}_3 \end{Bmatrix} \underset{\sim}{B}_r^b \tag{23a}$$

$$\underset{\sim}{R} = \begin{bmatrix} 1 & 0 & 1 & 0 & 1 & 0 \\ 0 & 1 & 0 & 1 & 0 & 1 \end{bmatrix} \tag{23b}$$

The values of α_x and α_y which minimize the function (21) can then easily be shown to be

$$\begin{Bmatrix} \alpha_x \\ \alpha_y \end{Bmatrix} = \frac{1}{3} \underset{\sim}{R} (\underset{\sim}{I}_6 - \underset{\sim}{A}) \underset{\sim}{\theta} \tag{24}$$

where $\underset{\sim}{I}_6$ is the unit matrix of order 6. It also follows that at the minimum of f, $\underset{\sim}{w}^b = \underset{\sim}{w}^K$. Consequently, according to Eqs. (20) and (23b),

$$\underset{\sim}{w}^b = \underset{\sim}{w}^K = -\frac{1}{3} \underset{\sim}{X} (\underset{\sim}{I}_6 - \underset{\sim}{A}) \underset{\sim}{\theta} \tag{25a}$$

$$\underset{\sim}{X} = \begin{bmatrix} 0 & 0 & 0 & 0 & 0 & 0 \\ x_2 & 0 & x_2 & 0 & x_2 & 0 \\ x_3 & y_3 & x_3 & y_3 & x_3 & y_3 \end{bmatrix} \tag{25b}$$

with β assumed to be zero.

Having specified $\underset{\sim}{\theta}^b$ and $\underset{\sim}{w}^b$, the projection operators $\underset{\sim}{P}^b$ and $\underset{\sim}{P}^s$ of Eqs. (2), can be defined. In view of Eqs. (16) and (25a)

$$\underset{\sim}{P}^b = \begin{bmatrix} \underset{\sim}{I}_6 & \underset{\sim}{0} \\ -\frac{1}{3} \underset{\sim}{X} (\underset{\sim}{I}_6 - \underset{\sim}{A}) & \underset{\sim}{0} \end{bmatrix} \tag{26}$$

Moreover, since Eqs. (1) and (2) imply that

$$\underset{\sim}{P}^b + \underset{\sim}{P}^s = \underset{\sim}{I}_9 \tag{27}$$

the operator $\underset{\sim}{P}^S$ is

$$\underset{\sim}{P}^S = \begin{bmatrix} \underset{\sim}{0} & \underset{\sim}{0} \\ \frac{1}{3} \underset{\sim}{X} (\underset{\sim}{I}_6 - \underset{\sim}{A}) & \underset{\sim}{I}_3 \end{bmatrix} \tag{28}$$

The above expressions for operators $\underset{\sim}{P}_b$ and $\underset{\sim}{P}_s$ along with Eqs. (4-6) and (13-15) enable one to find the stiffness matrix defined in Eq. (10).

In Eq. (21) the function f utilizes local x and y components of rotations in both the bending mode and equivalent Kirchhoff configurations. It is worth noting, however, that the result of the minimization is independent of the local frame. To explain this, note that

$$f = \sum_{I=1}^{3} (\Delta\theta_{xI}^2 + \Delta\theta_{yI}^2) \tag{29}$$

where

$$\Delta\theta_{xI} = \theta_{xI} - \theta_{xI}^K(\alpha_x, \alpha_y) \tag{29a}$$

$$\Delta\theta_{yI} = \theta_{yI} - \theta_{yI}^K(\alpha_x, \alpha_y) \tag{29b}$$

Since at each node θ_{xI}, θ_{yI}, θ_{xI}^K, θ_{yI}^K and α_x, α_y are components of appropriate vectors (cf. Eq. (19)) so are $\Delta\theta_{xI}$, $\Delta\theta_{yI}$. Therefore, if the components are taken with respect to a different coordinate system, the function f in Eq. (30a) does not change. In particular the local x axis can coincide with any side of the triangle.

It is clear from the above, that if the nodal rotations and displacements in the total C^0 configuration coincide with those of an equivalent Kirchhoff configuration, the total configuration and the bending mode are the same. Consequently, the shear-strain energy vanishes for this element for any curvatures. We can show that this is not true of the formulation presented in [7] where just reduced integration was employed. To this end, assume that the nodal values of the rotations are given by Eq. (19a) while the nodal displacements by Eq. (20). In this case the shear strains at the centroid of the C^0 element are (compare Eq. (19b))

$$\begin{Bmatrix} \gamma_x^c \\ \gamma_y^c \end{Bmatrix} = \frac{1}{2} \begin{bmatrix} 2x_c - x_2 & 0 & y_c \\ \frac{x_3}{y_3}(x_2 - x_3) & 2y_c - y_3 & x_c - x_3 \end{bmatrix} \underset{\sim}{\kappa} \quad (30)$$

where x_c, y_c are the coordinates of the centroid. Since in the thin-structure limit, the shear strains go to zero, for the SRI element of Ref. [7] $\gamma_x^c \to 0$, $\gamma_y^c \to 0$. Thus Eq. (30) (with $\gamma_x^c = \gamma_y^c = 0$) imposes two constraints on κ_x, κ_y, κ_{xy} which result in the excessive stiffness of the SRI element.

4. IMPLEMENTATION

Both the bending and shear contributions to the stiffness matrix defined in Eq. (10) form 9 x 9 matrices which are referred to all 9 degrees of freedom. We found it more convenient to first formulate a 6 x 6 stiffness matrix, referred to a corotational frame in whic

$$\hat{\underset{\sim}{w}} = \underset{\sim}{0} \tag{31a}$$

$$\hat{\underset{\sim}{\theta}} = \underset{\sim}{T} \begin{matrix} \underset{\sim}{\theta} \\ \underset{\sim}{w} \end{matrix} \tag{31b}$$

where $\underset{\sim}{T}$ is the transformation matrix resulting from condition (31a). All of the previous considerations are obviously valid and can be specialized to the following: the bending part of the stiffness matrix is

$$\hat{\underset{\sim}{K}}^b = \int_A (\underset{\sim}{B}_r^b)^T \underset{\sim}{D}^b \underset{\sim}{B}_r^b \, dA \tag{32}$$

where $\underset{\sim}{B}_r^b$ is defined in Eq. (13). The shear related stiffness matrix is

$$\hat{\underset{\sim}{K}}^s = \frac{Eh\psi}{18(1+\nu)} \int_A (\underset{\sim}{I}_6 - \underset{\sim}{A})^T \underset{\sim}{R}^T \underset{\sim}{R} (\underset{\sim}{I}_6 - \underset{\sim}{A}) \, dA \tag{33}$$

with $\underset{\sim}{A}$ and $\underset{\sim}{R}$ defined in Eqs. (23 a,b). The stiffness matrix of Eq. (10) can then be obtained as follows

$$\underset{\sim}{K} = \underset{\sim}{T}^T (\hat{\underset{\sim}{K}}^b + \hat{\underset{\sim}{K}}^s) \underset{\sim}{T} \tag{34}$$

A similar transformation has to be performed once again (with a different $\underset{\sim}{T}$) to obtain the matrix $\underset{\sim}{K}$ in a global coordinate system.

The integrands in both Eq. (32) and Eq. (33) are constants, so the evaluation of the integral is simply the product of the area and the integrand. Computationally, it is equivalent to one-point quadrature.

The formulation presented in the previous section, utilizing x and y components of nodal rotation, is one of the frame-indifferent formulations implemented herein. It will be referred to as the LSC (least square, components) formulation. Another, natural and also frame-indifferent formulation implemented here utilizes projections of the nodal rotations onto sides of the triangle. We will refer to it as LSP (least square, projections) formulation. In this case

$$f(\alpha_x, \alpha_y, \beta, w_I^b) = (\underset{\sim}{\theta}^P - \underset{\sim}{\theta}^{PK})^T (\underset{\sim}{\theta}^P - \underset{\sim}{\theta}^{PK}) + (\underset{\sim}{w}^b - \underset{\sim}{w}^K)^T (\underset{\sim}{w}^b - \underset{\sim}{w}^K) \quad (35)$$

where,

$$\underset{\sim}{\theta}^P = \underset{\sim}{E}\,\underset{\sim}{\theta} \quad (36a)$$

$$\underset{\sim}{\theta}^{PK} = \underset{\sim}{E}\,\underset{\sim}{\theta}^K \quad (36b)$$

$$\underset{\sim}{E} = \begin{bmatrix} e_{x1} & e_{y1} & 0 & 0 & 0 & 0 \\ e_{x3} & e_{y3} & 0 & 0 & 0 & 0 \\ 0 & 0 & e_{x1} & e_{y1} & 0 & 0 \\ 0 & 0 & e_{x2} & e_{y2} & 0 & 0 \\ 0 & 0 & 0 & 0 & e_{x2} & e_{y2} \\ 0 & 0 & 0 & 0 & e_{x3} & e_{y3} \end{bmatrix} \quad (36c)$$

and e_{xI}, e_{yI} are components of a unit vector $\underset{\sim}{e}_I$ parallel to Ith side of the

triangle, Fig. 2. Note that in contrast to f in Eq. (21), the first term of Eq. (35) is not the length of the vector.

Minimization of the function (35) leads to the following result

$$\begin{Bmatrix} \alpha_x \\ \alpha_y \end{Bmatrix} = \frac{1}{3} \bar{\underset{\sim}{R}} (\underset{\sim}{I} - \underset{\sim}{A}) \underset{\sim}{e} \tag{37}$$

where

$$\bar{\underset{\sim}{R}} = 3 (\underset{\sim}{R} \underset{\sim}{E}^T \underset{\sim}{E} \underset{\sim}{R}^T)^{-1} \underset{\sim}{R} \underset{\sim}{E}^T \underset{\sim}{E} \tag{38}$$

Consequently, if $\underset{\sim}{R}$ is replaced with $\bar{\underset{\sim}{R}}$, Eqs. (32), (33) and (34) are all valid. Moreover, the simple form of matrices $\underset{\sim}{R}$, Eq. (23b), and $\underset{\sim}{E}$, Eq. (36c), enables one to perform a number of the multiplications in Eq. (38) analytically

$$\underset{\sim}{R} \underset{\sim}{E}^T \underset{\sim}{E} \underset{\sim}{R}^T = 2 \begin{bmatrix} e_{x1}^2 + e_{x2}^2 + e_{x3}^2 & e_{x1}e_{y1} + e_{x2}e_{y2} + e_{x3}e_{y3} \\ e_{x1}e_{y1} + e_{x2}e_{y2} + e_{x3}e_{y3} & e_{y1}^2 + e_{y2}^2 + e_{y3}^2 \end{bmatrix} \tag{39}$$

$$\underset{\sim}{R} \underset{\sim}{E}^T \underset{\sim}{E} =$$

$$\begin{bmatrix} e_{x1}^2 + e_{x3}^2 & e_{x1}e_{y1} + e_{x3}e_{y3} & e_{x1}^2 + e_{x2}^2 & e_{x1}e_{y1} + e_{x2}e_{y2} \\ e_{x1}e_{y1} + e_{x3}e_{y3} & e_{y1}^2 + e_{y3}^2 & e_{x1}e_{y1} + e_{y2}e_{x2} & e_{y1}^2 + e_{y2}^2 \\ & & e_{x2}^2 + e_{x3}^2 & e_{x2}e_{y2} + e_{x3}e_{y3} \\ & & e_{x2}e_{y2} + e_{x3}e_{y3} & e_{y2}^2 + e_{y3}^2 \end{bmatrix} \tag{40}$$

6. NUMERICAL RESULTS

In order to evaluate the performance of this element and to compare it with other elements, several square and circular plate problems were solved. The parameters for all examples are given in Table 1. The term simply supported here means that only the transverse displacements are constrained. The transverse load is discretized in a manner consistent with the internal force formulation; for a uniformly distributed load, one third of the total load is allocated to each of the three nodes of the element. Only a quarter of the plate is analyzed in each case because of symmetry. In the results presented (with the exception of the square, corner-supported plate), the deflection of the center of the plate is normalized with respect to the analytic value based on Kirchhoff theory [21].

The results for the square simply supported plate (Example 1) are shown in Table 2, where A, B, CD refer to the various discretization patterns presented in Figure 3. This element shows marked improvement over [19] with mesh A and a slight loss of accuracy with mesh B, so this element is less orientation-dependent. It should be noted here that for the uniform load, the consistent load formulation distributes twice as much load to the central node for mesh B as it does for mesh A, which is significant for the coarse mesh, N = 4. Table 3 presents the results obtained by distributing the load to the nodes by dividing the plate into equal square areas and allocating the resulting load to each node. For the cross-diagonal mesh, the results of this element and [19] are comparable.

Results for the circular plate are presented in Table 4; the corresponding meshes are illustrated in Figure 4. Improvement of about 4% to 10% is gained, over [19] for mesh-type A, while the cross diagonal mesh again yields results comparable to [19].

We have also compared the triangular element with the quadrilateral with one-point quadrature and a stabilization matrix, Example 3 in Table 1. In both cases the number of degrees of freedom is the same. The mesh used is of the type B, N = 64, shown in Figure 3 and the results for both uniform load and a central point load are presented in Table 5 and compared to [18]. The Kirchhoff theory solution for the uniform load case is given in [21]. The performance of these 2 elements is quite similar.

The convergence rate for this triangular element for the square (edge supported) plate and circular plate are shown in Figures 5 and 6, respectively. In both cases, the convergence rate is somewhat greater than the expected value of 2.0 [22], but no rigorous estimates of the convergence rate are available.

In this convergence study, the following measure of the error has been used

$$\|e\|_0 = \left(\int_\Omega e^2 d\Omega\right)^{1/2} \tag{41}$$

where Ω is the area of the plate,

$$e = w^A - w^{FEM} \tag{42}$$

with w^A the analytic solution based on Kirchhoff theory and w^{FEM} the finite element solution. To simplyfy the computations, w^A was evaluated at the nodal points only and then interpolated by means of linear shape functions. Thus the following difference has been actually used within each element

$$e = \sum_I \left(w_I^A - w_I^{FEM}\right) L_I \tag{43}$$

The mesh parameter ρ has been choosen to be the length of the maximum side of the biggest element.

7. CONCLUSIONS

An accurate and simple formulation for the C^0 triangular element with linear shape functions has been developed. The success of the method hinges on the identification of the bending and shear modes and the use of the least square method to properly separate the two modes. In comparison with the four node bilinear element with one point quadrature [18], the element shows comparable accuracy. However in shell problems this element may prove more effective than the quadrilateral with one point quadrature because it can more effectively handle a warped surface.

Since this method assumes a constant shear in the element, one point quadrature is sufficient for exact integration of the resulting integrals; in fact, no numerical integration is needed. Since the shear distribution in [19] is linear, a point probably exists within the element at which the shear strains developed in [19] are equal to those defined in this paper. Thus if that point is used for the reduced shear integration, the two formulations would yield equivalent stiffness matrices. The present formulation, however, does provide a rationale for a selection of the integration point.

Because the shear distribution in this element is constant, it has one zero-energy mode: in-plane rotation of the upper face of the element with respect to its midplane. This zero-energy mode, however, disappears in any mesh of two or more elements. Thus the present element can be safely used in all plate problems.

ACKNOWLEDGEMENT

The support of the Air Force Office of Scientific Research under Grant F 49620-82-K0013 is gratefully acknowledged.

REFERENCES

1. I. Fried and S.K. Yang, "Triangular Nine-Degree-of-Freedom C^0 plate Bending Element of Quadratic Accuracy," Quart. Appl. Math, 31 1978, pp. 303-312.

2. J. H. Argyris, P.C. Dunne, G.A. Malejannakis and E. Shelke, "A Simple Triangular Facet Shell Element with Applications to Linear and Nonlinear Equilibrium and Elastic Stability Problems," ISD Report No. 212, Institut fur Static and Dynamic, Stuttgart, December 1975.

3. T.J.R. Hughes, R.L. Taylor and W.Å. Kanoknukulchai, "Simple and Efficient Element for Plate Bending," Int. J. Num. Meth. Eng. 11, 1977, pp. 1529-1543.

4. O.C. Zienkiewicz, J. Bauer, K. Morgan and E. Onate, "Simple Element for Axisymmetric Shell with Shear Deformation", Int. J. Num. Meth. Eng., 11, 1977, pp. 1545-1558.

5. R.H. MacNeal, "A Simple Quadrilaterial Shell Element," Computers and Structures, 8, 1978, pp. 175-183.

6. W. Kanoknukulchai, "A Simple and Efficient Finite Element for General Shell Analysis," Int. J. Num. Meth. Eng.,14, 1979, pp. 179-200.

7. J.L. Batoz, K.J. Bathe and L.W. Ho, "A Study of Three-Node Triangular Plate Bending Elements," Int. J. Num. Meth. Eng., 15, 1980, p. 1771-1812.

8. H. Garnet, J. Crouzet-Pascal and A.B. Pifko, "Aspects of a Simple Triangular Plate Bending Element," Computers and Structures, 12, 1980, pp. 783-789.

9. O.C. Zienkiewicz, R.L.Taylor, and J.M. Too, "Reduced Integration Technique in General Analysis of Plates and Shells," Int. J. Num. Meth. Eng., 3, 1971, pp. 275-290.

10. I. Fried, "Shear in C^0 and C^1 Bending Finite Elements," Int. J. Solids Structures, 9, 1973, pp. 449-461.

11. E.D.L. Pugh, E. Hinton, and O.C. Zienkiewicz, "A Study of Quadrilateral Plate Bending Elements with Reduced Integration," Int. J. Num. Meth. Eng., 12, 1978, pp. 1059-1073.

12. T.J.R. Hughes, M. Cohen and M. Haroun, "Reduced and Selective Integration Techniques in the Finite Element Analysis of Plates," Nucl. Eng. Design, 46, 1978, pp. 203-222.

13. D.S. Malkus and T.J.R. Hughes, "Mixed Finite Element Methods-Reduced and Selective Integration Techniques: A Unification of Concepts," Comp. Meth. Appl. Mech. Eng., 15, 1978, pp. 63-81.

14. T.J.R. Hughes and M. Cohen, "The 'Heterosis' Finite Element for Plate Bending", Computers and Structures., Vol. 8, 1978,pp. 391-397.

15. H. Parish, "A Critical Survey of the 9-Node Degenerated Shell Element with Special Emphasis on Thin Shell Application and Reduced Integration," Comp. Meth. Appl. Mech. Eng., 20, 1979, pp. 323-350.

16. T.J.R. Hughes, "Generalization of Selective Integration Procedures to Anisotropic and Nonlinear Media," Int. J. Num. Meth. Eng., 15, 1980, pp. 1413-1418.

17. D.P. Flanagan and T. Belytschko, "A Uniform Strain Hexahedron and Quadrilateral with Orthogonal Hourglass Control," Int. J. Num. Meth. Eng., 17 1981, pp. 679-706.

18. T. Belytschko, C.S. Tsay, and W.K. Liu, "A Stabilization Matrix for the Bilinear Mindlin Plate Element," Comp. Meth. Appl. Mech. Eng. 29, 1981, pp. 313-327.

19. T.J.R. Hughes, and R.L. Taylor, "The Linear Triangular Bending Element," to appear in the Proceedings of the MAFELAP 1981 Conference, Brunel University, April 28-May 1, 1981.

20. T.J.R. Hughes and T.E. Tezduyar, "Finite Elements Based Upon Mindlin Plate Theory with Particular Reference to the Four-Node Bilinear Isoparametric Element," J. Appl. Mech., 48, 1981, pp. 587-596.

21. S. Timoshenko and S. Woinowsky-Krieger, "Theory of Plates and Shells," McGraw-Hill, 1959, Article 49.

22. E.B. Becker, A. F. Carey and G.T. Oden, "Finite Elements: An Introduction," Prentice-Hall, 1981.

TABLE 1

Parameters for Example Problems

Example 1. Square Plate
Uniform Road, simply supported edges

Dimensions:	10 in x 10 in
Thickness:	0.1 in
Young's modulus	10.92×10^5 psi
Poisson's ratio:	0.3

Example 2. Circular Plate
Uniform load, simply supported edge

Radius:	5 in
Thickness:	0.1 in
Young's modulus:	10.92×10^5 psi
Poisson's ratio:	0.3

Example 3. Square Plate
Uniform load and concentrated load, corner supported

Dimentions:	24 x 24 in
Thickness:	0.375 in
Young's modulus:	43.00×10^4 psi
Poisson's ratio:	0.38

TABLE 2

Center displacement and moment for simply-supported square plate subjected to uniform load.

MESH	N	NDOF	DISPLACEMENT			MOMENT		
			Ref.[19]	LSC	LSP	Ref.[19]	LSC	LSP
A	4	16	.681	.690	.690	.555	.574	.573
	16	56	.784	.919	.915	.564	.870	.855
	64	208	.947	.986	.985	.835	.978	.973
B	4	16	.883	.883	.825	.904	.951	.811
	16	56	.989	.974	.951	1.127	1.026	.977
	64	208	.999	.994	.994	1.098	1.002	.999
cross diagonal	4	28	.912	.913	.914	.919	.920	.920
	16	104	.978	.980	.980	.979	.982	.982
	64	400	.994	.998	.998	.996	.997	.998

TABLE 3

Center Displacement for simply-supported square plate; Uniform load; nodal forces proportional to the area surrounding the nodes.

MESH	N	NDOF	DISPLACEMENT	
			LSC	LSP
A	4	16	.730	.729
	16	56	.925	.920
	64	208	.989	.988
B	4	16	.770	.766
	16	56	.962	.927
	64	208	.988	.987
Cross diagonal	4	28	.913	.936
	16	104	1.035	.986
	64	400	.997	.998

TABLE 4

Center displacement and moment for simply-supported circular plate subjected to uniform load.

MESH	N	NDOF	DISPLACEMENT			MOMENT		
			Ref.[19]	LSC	LSP	Ref.[19]	LSC	LSP
A	3	12	.703	.824	.815	.576	.781	.750
	12	42	.912	.954	.954	.878	.957	.951
	48	156	.948	.989	.989	.975	.988	.987
cross diagonal	3	21	.927	.930	.930	.885	.890	.893
	12	78	.981	.982	.982	.976	.979	.979
	48	300	.976	.996	.996	.986	.994	.994

TABLE 5

Center line displacements for corner supported, square plate

Nodal point	DISPLACEMENT [in]				
	LSC		Ref.[18]		KIRCHHOFF
	UNIFORM LOAD	POINT LOAD	UNIFORM LOAD	POINT LOAD	UNIFORM LOAD
1	.11963	.14095	.11940	.14102	.12065
2	.11888	.13908	.11903	.13884	
3	.11667	.13423	.11647	.13392	
4	.11315	.12749	.11337	.12711	
5	.10855	.11955	.10843	.11919	
6	.10318	.11093	.10349	.11057	
7	.09743	.10214	.09742	.10183	
8	.09177	.09368	.09222	.09339	
9	.08678	.08602	.08689	.08576	

FIGURE CAPTIONS

Fig. 1. Sign convention.

Fig. 2. Geometry of the triangular element in a local reference frame.

Fig. 3. Discretizations of the square plate.

Fig. 4. Discretizations of the circular plate.

Fig. 5. Convergence rate for the square plate.

Fig. 6. Convergence rate for the circular plate.

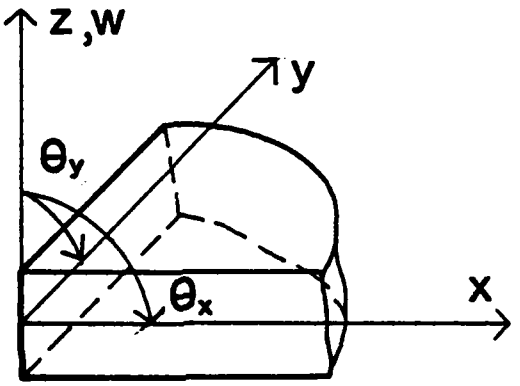
z ,w
y
θy
θx
x

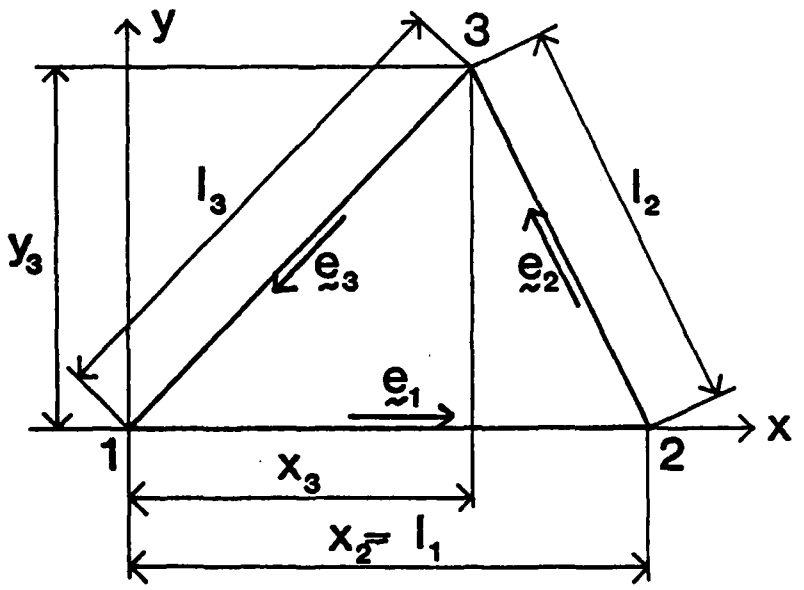
y
3
l_3
l_2
y_3
$\underset{\sim}{e}_3$
$\underset{\sim}{e}_2$
$\underset{\sim}{e}_1$
x
1
2
x_3
$x_2 = l_1$

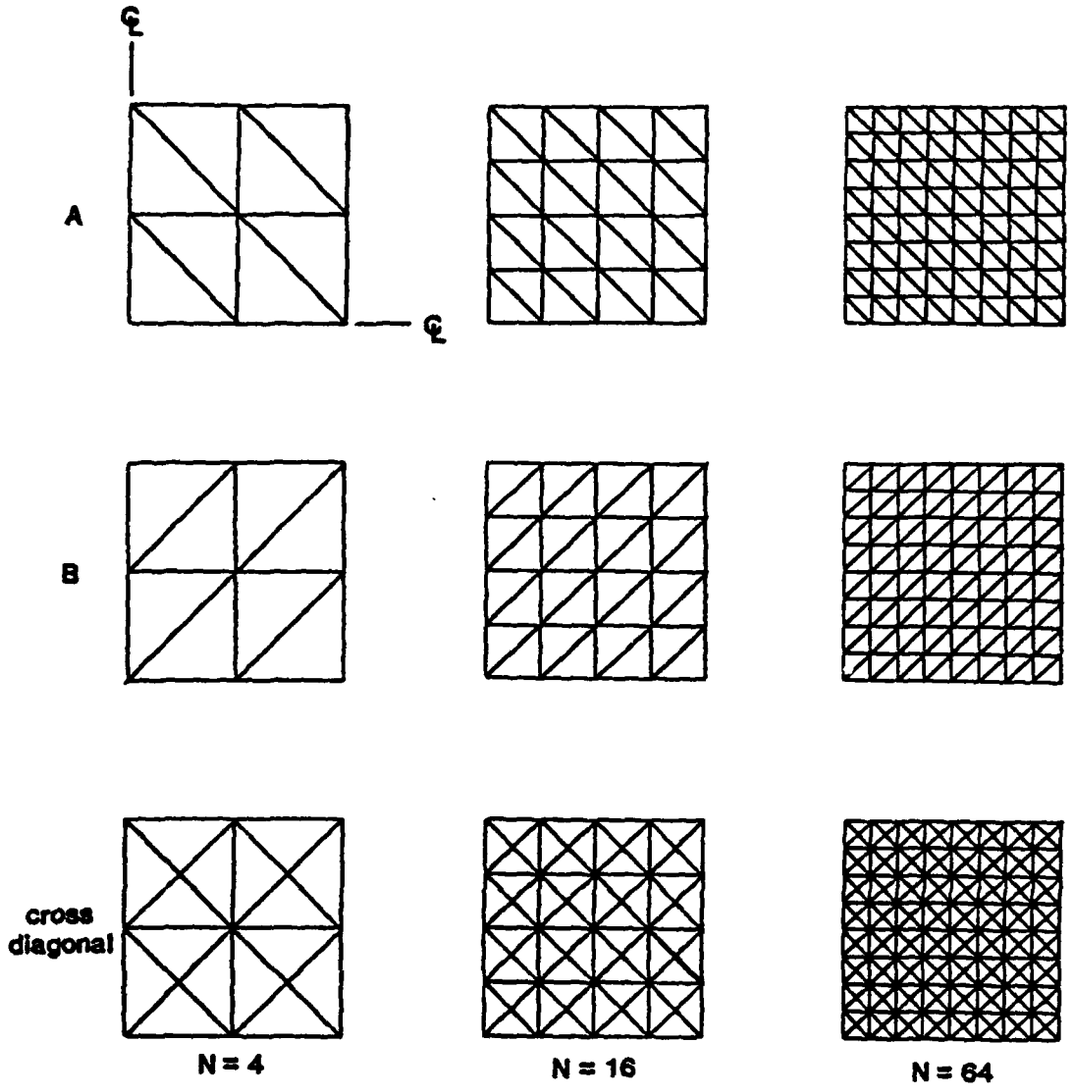
A
B
cross
diagonal
N = 4
N = 16
N = 64

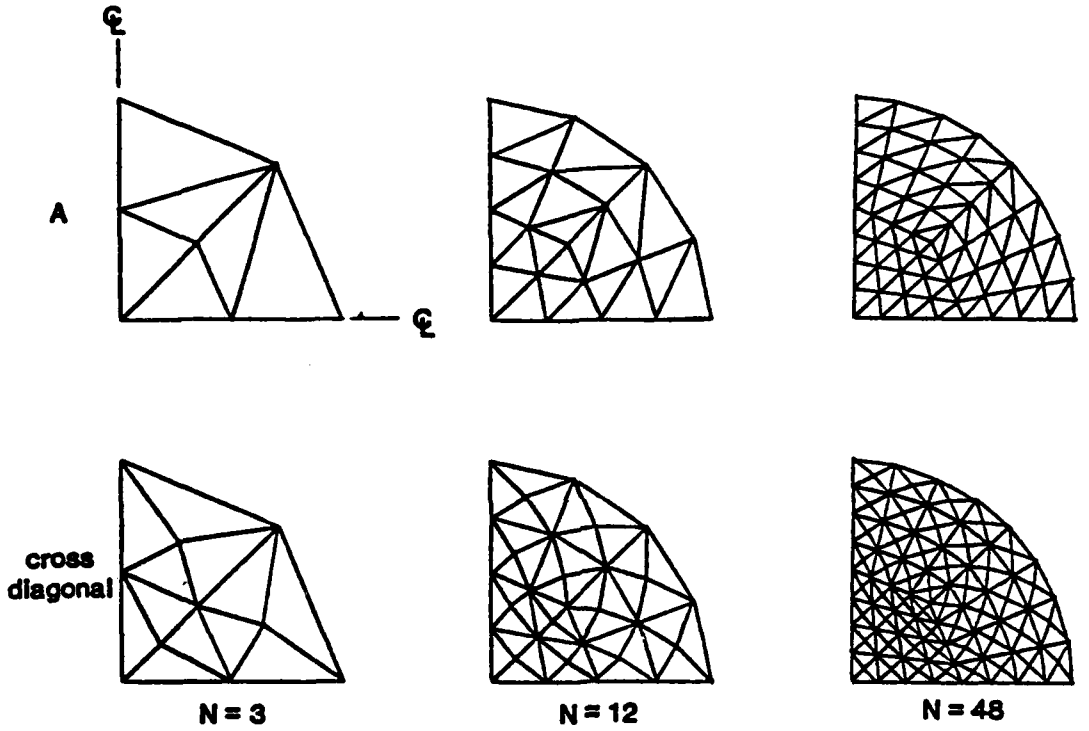
℄
A
℄
cross
diagonal
N = 3
N = 12
N = 48

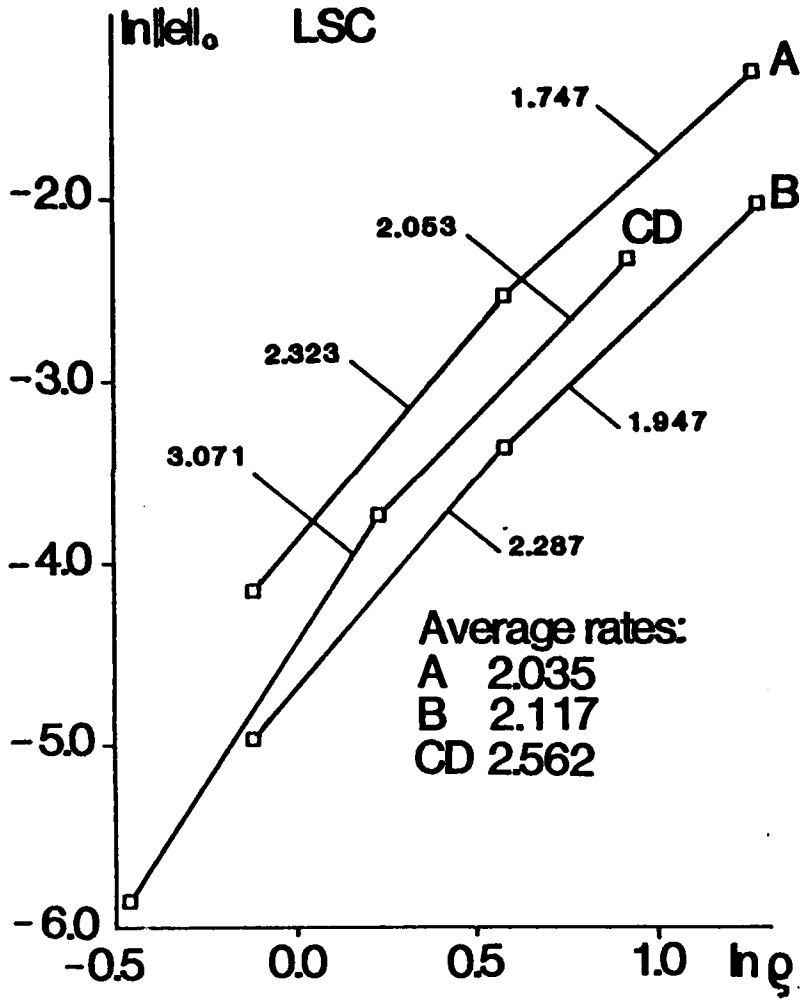
ln|el|₀ LSC
A
B
CD
1.747
2.053
2.323
3.071
1.947
2.287
-2.0
-3.0
-4.0
-5.0
-6.0
-0.5
0.0
0.5
1.0
ln ϱ
Average rates:
A 2.035
B 2.117
CD 2.562

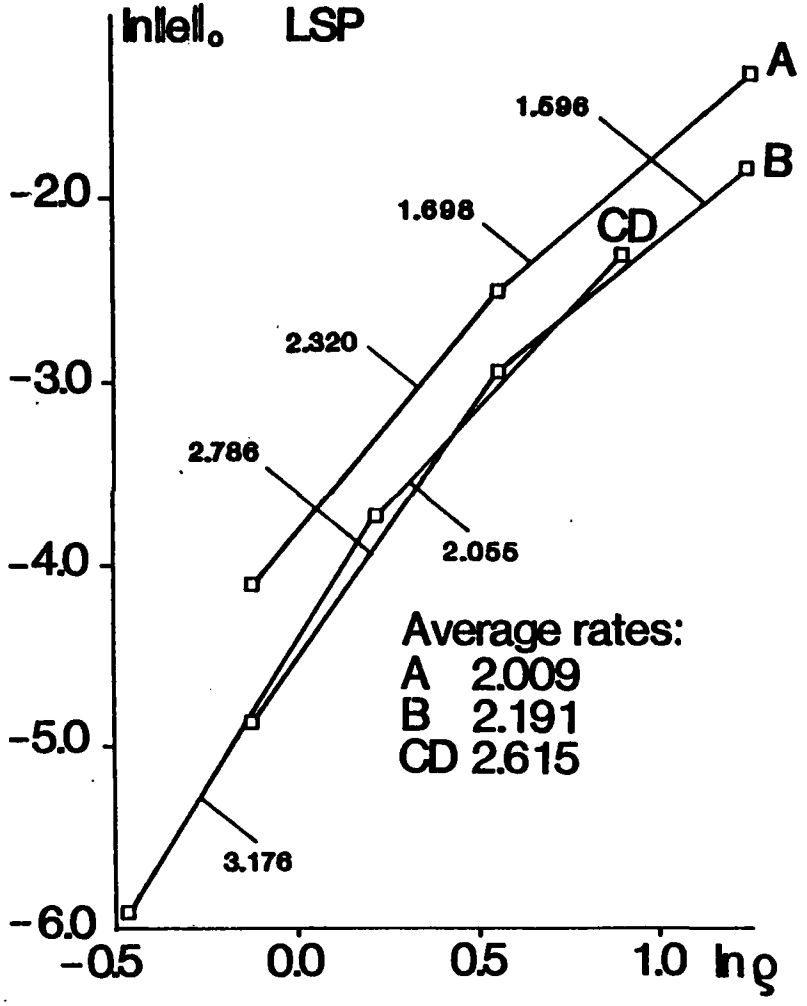
ln|el|₀ LSP
A
B
CD
1.596
1.698
2.320
2.786
2.055
3.176
-2.0
-3.0
-4.0
-5.0
-6.0
-0.5
0.0
0.5
1.0
ln ϱ
Average rates:
A 2.009
B 2.191
CD 2.615

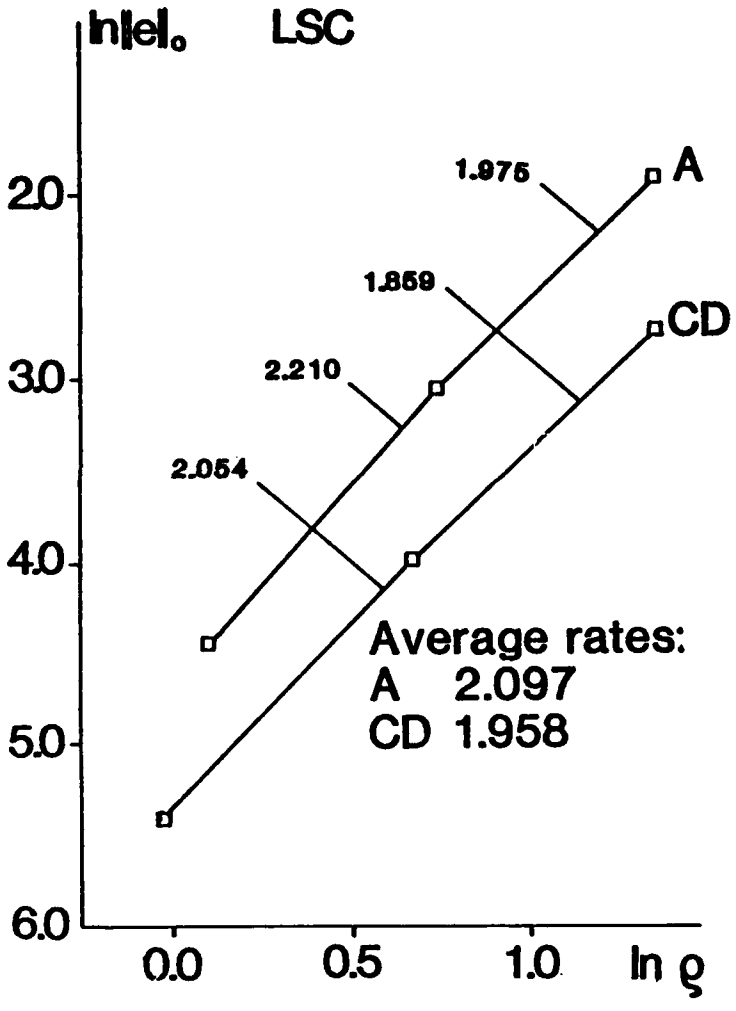
ln|e|₀
LSC
2.0
3.0
4.0
5.0
6.0
1.975
A
1.869
CD
2.210
2.054
Average rates:
A 2.097
CD 1.958
0.0
0.5
1.0
ln ς

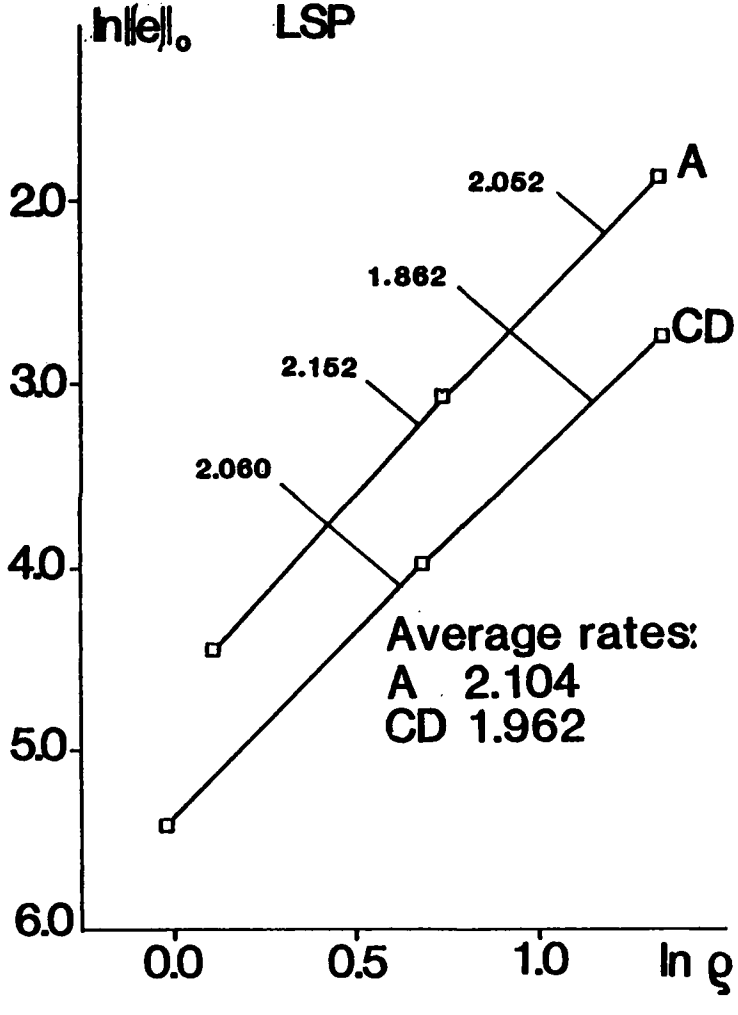
ln|e|₀
LSP
2.0
3.0
4.0
5.0
6.0
2.052
A
1.862
CD
2.152
2.060
Average rates:
A 2.104
CD 1.962
0.0
0.5
1.0
ln ς

APPENDIX B

1. Introduction

Since the early years of finite element development, the use of C^0 finite elements for the analysis of thin flexible structures has been very tempting, as the C^1 continuity required by the Kirchhoff theory is very troublesome and requires higher order shape functions [1-4]. However a rapid development of the C^0 approach started only with the application of reduced integration [5-12].

The effectiveness of this technique arises from its elimination of the excessive shear contribution to the stiffness of thin structures whose response is usually dominated by their bending properties.* However, it was not clear how much of the shear-related stiffness should be eliminated. Consequently the elements employing reduced integration were developed on a "trial and error" basis; certain interpolations and integration schemes were usually assumed and their consequences were examined, [9-12]. Elements that did not perform "well" were rejected. Although a similar approach was used in the development of Kirchhoff C^1 elements, in this case, approximations consistent with the theory usually give acceptable elements. Although their convergence properties and error characteristics may vary, they seldom fail, as for instance when the thickness of the plate decreases. This is not true of C^0 elements employing reduced integration (for instance serendipity plate elements [9-12]) and perhaps for this reason the technique is sometimes viewed more as a trick than a legitimate method. In mixed methods, [17,18], similar trial-and-error procedures have been used.

The equivalence between the reduced-integration displacement approach and well established mixed methods [19] contributed significantly to the

* A more complex phenomena occurs when a curved structure is analyzed [14-16].

legitimacy of the former. However, doubts remained as to how to create successful C^0 elements; trial-and-error approaches are still in use and consequently the resulting elements are often considered insufficiently reliable. The zero-energy modes that often accompany reduced integration can also cause severe difficulties.

A deviation from this path was originated by MacNeal [20] who, by comparing energy terms, attempted to create C^0, low order elements of accuracy equivalent to that of higher order elements. A similar approach was later used by Parish [21] to justify the use of reduced integration within 9-node Lagrange plate elements.

Another approach for improving accuracy and eliminating zero-energy modes was proposed by Hughes and Tezduyar [22] who developed a successful four-node quadrilateral plate bending element. The idea was similar to that presented in [23] and consisted in changing the discrete derivative operator $\underset{\sim}{B}$ to guarantee good behaviour of the element in thin plate limit. After the change of the matrix $\underset{\sim}{B}$ there is essentially no need for reducing the order of the integration to obtain good results. An identical approach to the analysis of perhaps the simplest plate bending element, a triangle with linear approximations of displacements and rotations, was presented by Hughes and Taylor [24]. The results for this element depended very strongly on the mesh arrangement. Consequently the reduced integration technique was applied to the shear terms along with the modified $\underset{\sim}{B}$ matrix to alleviate the dependence on the mesh orientation. However doubts arose about the correctness of the modified $\underset{\sim}{B}$ matrices. This subject has been discussed in [25], where a new approach to the modification of the $\underset{\sim}{B}$ matrix was proposed.

Another approach to C^0 elements is to use reduced integration with stabilization matrices [26,27], which eliminate the zero-energy modes. These

approaches have the same or better accuracy than [22], but the selection of stabilization parameters for nonlinear problems is an open question which is probably not trivial.

This study is aimed at identifying the factors which are most essential for the success of a C^0 flexible element. This is done by means of two elements: the linear beam element and the linear triangular plate element. The salient characteristic of the first is that all the formulations discussed lead to identical results; this is not the case for the plate element. We believe this enables one to clearly see the major features of the problem.

The next Section contains general remarks concerning C^0 flexible plate elements. The various formulations for the beam problem are given in Section 3, while the linear triangular plate element is discussed in Section 4. Numerical results and conclusions are presented in Sections 5 and 6, respectively.

AD-A136 044 EFFICIENT FINITE ELEMENT METHODS FOR TRANSIENT NONLINEAR ANALYSIS OF SHEL..(U) NORTHWESTERN UNIV EVANSTON IL DEPT OF CIVIL ENGINEERING T BELYTSCHKO

UNCLASSIFIED AUG 83 AFOSR-TR-83-1062 F49620-82-K-0013 F/G 13/13 NL

2/2

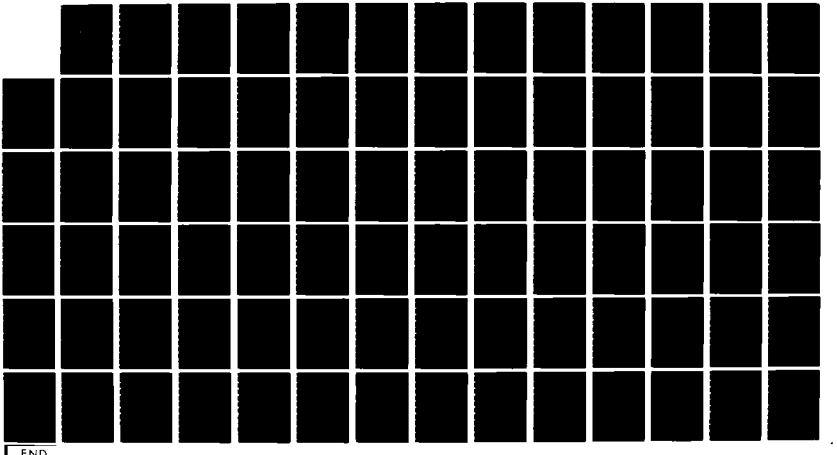

END

FILMED
1-84
DTIC

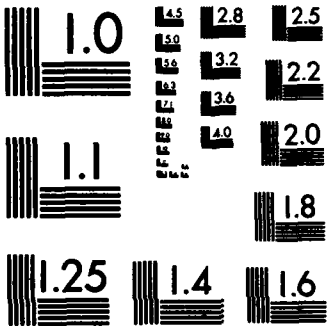

2. General Remarks

If an element of a Mindlin plate is described by independent approximations of rotations θ_x, θ_y and displacements w, the stiffness matrix $\underset{\sim}{K}$ obtained in the displacement formulation is, cf [10]:

$$\underset{\sim}{K} = \underset{\sim}{K}_b + \underset{\sim}{K}_s \tag{1a}$$

$$\underset{\sim}{K}_b = \int_A \underset{\sim}{B}_b \, \underset{\sim}{D}_b \, \underset{\sim}{B}_b \tag{1b}$$

$$\underset{\sim}{K}_s = \int_A \underset{\sim}{B}_s \, \underset{\sim}{D}_s \, \underset{\sim}{B}_s \tag{1c}$$

In the above expressions, A is the area of the element,

$$\underset{\sim}{D}_b = \frac{Eh^3}{12(1-\nu)^2} \begin{bmatrix} 1 & \nu & 0 \\ \nu & 1 & 0 \\ 0 & 0 & \frac{1-\nu}{2} \end{bmatrix} \tag{2}$$

$$\underset{\sim}{D}_s = Gh\lambda \begin{bmatrix} 1 & 0 \\ 0 & 1 \end{bmatrix} \tag{3}$$

where h is the thickness of the plate, E, G, ν are standard material

constants, λ is the shear correction factor. The matrices $\underline{B}_b$, $\underline{B}_s$ are the discrete forms of the kinematical relationships

$$\underline{\kappa} \equiv \begin{Bmatrix} \kappa_x \\ \kappa_y \\ \kappa_{xy} \end{Bmatrix} \equiv \begin{Bmatrix} \theta_{x,x} \\ \theta_{y,y} \\ \theta_{x,y} + \theta_{y,x} \end{Bmatrix} \equiv \underline{B}_b \, \underline{q} \qquad (4)$$

$$\underline{\gamma} \equiv \begin{Bmatrix} \gamma_x \\ \gamma_y \end{Bmatrix} \equiv \begin{Bmatrix} w_{,x} + \theta_x \\ w_{,y} + \theta_y \end{Bmatrix} \equiv \underline{B}_s \, \underline{q} \qquad (5)$$

where κ_x, κ_y, κ_{xy} are curvatures, γ_x, γ_y are shear deformations and $\underline{q}$ is the vector containing all elemental degrees of freedom. Positive rotations θ_x, θ_y and displacement w are shown in Figure 1.

It is known that if low order shape functions are used and if the integral in Eq. (1c) is integrated exactly, the plate elements are too stiff, or "lock", as their thickness decreases [6]. This is due to the fact that too much of the work performed by the applied forces is converted to shear-strain

energy. To alleviate this problem, the integral expressing the shear contribution to the stiffness matrix is often evaluated using quadrature schemes of lower order than that required for exact integration. By doing this, the portion of the shear strain energy associated with higher order distribution of the shear strains is removed and the performance of the element is, in general, improved.

But this is not always true. There are cases, like the triangular plate element discussed subsequently, that can not be treated in this way. Moreover, reduced integration often gives zero-energy modes that are highly undesirable. Furthermore, one can never be sure whether reduced integraton removes the correct portion of the shear strain energy. It may therefore be better to remove the troublesome terms by using mechanical arguments. This reasoning leads to a different matrix $\bar{\underset{\sim}{B}}_s$ that replaces $\underset{\sim}{B}_s$ of Eq. (1c). Depending on whether or not all the troublesome shear terms have been removed while defining the $\bar{\underset{\sim}{B}}_s$ matrix, the integral of Eq. (1c) can be integrated exactly or underintegrated [22,24]. The point is to find a general method that eliminates all the troublesome terms [25]. As pointed out in [22], mechanical reasoning may provide a $\bar{\underset{\sim}{B}}_s$ matrix which is far more effective than reduced integration.

If a mixed model is used to formulate the element stiffness matrix, internal forces, work-conjugate with the strains given in Eq. (4) and (5), are interpolated independently of displacements

$$\underset{\sim}{M} = \begin{Bmatrix} M_x \\ M_y \\ M_{xy} \end{Bmatrix} = \underset{\sim}{P}_M \underset{\sim}{\beta}_M \tag{6}$$

$$\underset{\sim}{T} = \begin{Bmatrix} T_x \\ T_y \end{Bmatrix} = \underset{\sim}{P}_T \, \underset{\sim}{\beta}_T \qquad (7)$$

where $\underset{\sim}{P}_M$, $\underset{\sim}{P}_T$ describe the distributions of $\underset{\sim}{M}$ and $\underset{\sim}{T}$ respectively. For $\underset{\sim}{\beta}_M$ and $\underset{\sim}{\beta}_T$ independent of each other (and this is often the case in practice) the two components of the stiffness matrix are (compare [16]):

$$\underset{\sim}{K}_b = \int_A \underset{\sim}{B}_b^T \underset{\sim}{P}_M \left(\int_A \underset{\sim}{P}_M^T \underset{\sim}{D}_b^{-1} \underset{\sim}{P}_M \right)^{-1} \int_A \underset{\sim}{P}_M^T \underset{\sim}{B}_b \qquad (8a)$$

$$\underset{\sim}{K}_s = \int_A \underset{\sim}{B}_s^T \underset{\sim}{P}_T \left(\int_A \underset{\sim}{P}_T^T \underset{\sim}{D}_s^{-1} \underset{\sim}{P}_T \right)^{-1} \int_A \underset{\sim}{P}_T^T \underset{\sim}{B}_s \qquad (8b)$$

Moreover, if for a given displacement field the moment distribution is exactly the one that would occur in the displacement approach i.e. if

$$\underset{\sim}{P}_M = \underset{\sim}{D}_b \, \underset{\sim}{B}_b \qquad (9)$$

then the shear-related stiffness matrix $\underset{\sim}{K}_s$ is still defined by Eq. (8b), but equation (8a) becomes

$$\underset{\sim}{K}_b = \int_A \underset{\sim}{B}_b^T \underset{\sim}{D}_b \, \underset{\sim}{B}_b \qquad (10)$$

In this case only the distribution of the shear forces has to be defined. This version of the mixed formulation will be used throughout the paper.

Malkus and Hughes [19] showed that if the kinematical description in the displacement and mixed approaches is the same, then for each reduced

integration scheme applied within a displacement approach, there exists an internal force distribution in the mixed approach such that the stiffness matrices obtained by the two methods are identical. In our case, for a shear underintegration scheme, there exists a shear force distribution $\underset{\sim}{P}_T$ such that the stiffness matrices defined by Eq. (1) and Eq. (10) are identical. This equivalence will be used later.

In subsequent chapters we will be discussing various equivalent formulations. By equivalent formulations we will mean those that result in identical stiffness matrices. In all of the problems discussed, rigid body motion will be eliminated and only the corotational stiffness matrix will be compared. This diminishes the number of degrees of freedom, yet preserves full generality of the analysis.

3. Linear Beam Element

Consider a beam of length L, width b and depth h. We assume linear distributions of rotations and displacements which depend on four nodal quantities $\bar{\theta}_1, \bar{w}_1, \bar{\theta}_2, \bar{w}_2$, where bars denote quantities defined in the global system. The corotating frame (x,y) is defined so that the transverse displacements vanish, so the deformation is totally described by the rotation field

$$\theta = \theta_1(1-\xi) + \theta_2\xi \ , \quad \xi = \frac{x}{L} \tag{11a}$$

$$\underset{\sim}{q}^T = [\theta_1, \theta_2] \tag{11b}$$

$$\theta_1 = \bar{\theta}_1 - (\bar{w}_2 - \bar{w}_1)/L \tag{11c}$$

$$\theta_2 = \bar{\theta}_2 - (\bar{w}_2 - \bar{w}_1)/L \tag{11d}$$

The curvature and shear strains are given by

$$\kappa_x = \theta_{,x} = \frac{1}{L}(\theta_2 - \theta_1) \tag{12a}$$

$$\gamma_x = \theta + w_{,x} = \theta_1(1-\xi) + \theta_2\xi \tag{12b}$$

The discrete forms of the above kinematical relations are given by

$$\underset{\sim}{B}_b = \frac{1}{L}[-1, \ 1] \tag{13a}$$

$$\underset{\sim}{B}_s = [1-\xi,\ \xi] \tag{13b}$$

i) Reduced integration displacement formulation

In this approach the integrals in Eqs. (1b) and (1c) are evaluated using $\xi = \frac{1}{2}$ as the integration point. This is exact integration for the first but reduced integration for the second integral. The resulting stiffness matrices are

$$\underset{\sim}{K}_b = \frac{Ebh^3}{12L}\begin{bmatrix} 1 & -1 \\ -1 & 1 \end{bmatrix} \tag{14a}$$

$$\underset{\sim}{K}_s = \frac{GLbh\lambda}{4}\begin{bmatrix} 1 & 1 \\ 1 & 1 \end{bmatrix} \tag{14b}$$

ii) Mixed formulation

Use of the Eqs (8) will now be made with $\underset{\sim}{B}_b$ and $\underset{\sim}{B}_s$ defined in Eqs. (13), $\underset{\sim}{P}_M$ given in Eq. (9) and $\underset{\sim}{P}_T$ defining a constant distribution of the shear force, e.g.

$$\underset{\sim}{P}_T = [1] \tag{15}$$

Exact integration of the resulting formulas yields the matrix $\underset{\sim}{K}_b$ given in Eq.

(14a) and matrix $\underset{\sim}{K}_s$ given in Eq. (14b). A constant shear distribution in the mixed method is therefore equivalent to the reduced midpoint integration in the displacement approach.

iii) Displacement formulation with the modified matrix $\underset{\sim}{B}_s$

The above two formulations are well-known [6,19]. Here we present another formulation based on a concept developed as follows. First note that in pure bending, a Kirchhoff-type element in which the curvature is constant undergoes equal but opposing nodal rotations. If, in the thin structure limit, the present C^0 element (which also gives constant distribution of the curvature) is to behave like its counterpart in the Kirchhoff theory, the symmetric part of deformation that preserves curvature and is shown in Fig. 2b, should be associated with no shear strain energy. The remaining, antisymmetric deformation, Fig. 2c, does not change the curvature and is characterized by

$$\underset{\sim}{\theta}_1^s = \underset{\sim}{\theta}_2^s = \frac{1}{2}(\theta_1 + \theta_2) \tag{16}$$

Associating only this mode with the shear strain energy we arrive at the matrix

$$\bar{\underset{\sim}{B}}_s = \left[\frac{1}{2}, \frac{1}{2}\right] \tag{17}$$

which reflects the shear strain distribution in the antisymmetric part of deformation. Moreover, since the relationship between $\bar{\underset{\sim}{B}}_s$ of Eq. (17) and $\underset{\sim}{B}_s$ of Eq. (13b) is

$$\bar{\underset{\sim}{B}}_s = \underset{\sim}{B}_s \ (\xi = \tfrac{1}{2}) \tag{18}$$

use of $\bar{\underset{\sim}{B}}_s$ in Eq. (1c) instead of $\underset{\sim}{B}_s$ and exact integration is equivalent to the reduced midpoint integration presented as formulation (i). Consequently once again the matrix $\underset{\sim}{K}_s$ is given in Eq. (14b). The matrix $\underset{\sim}{B}_b$ remains unchanged, which means that $\underset{\sim}{K}_b$ is still given by Eq. (14a).

iv) Displacement formulation with a modified distribution of the transverse displacements

Now the symmetric portion of deformation, discussed in the previous formulation will be introduced more explicitly; a quadratic transverse displacement field will be associated with it. Thus we assume

$$w^K = \frac{L}{2} (\theta_2 - \theta_1) (1-\xi) \xi \tag{19}$$

while the rotation field is still described by Eq. (11b). This displacement field will be used within the standard displacement approach, not employing any reduced integration whatsoever. Therefore the problem reduces to the evaluation of $\underset{\sim}{B}_b$ and $\underset{\sim}{B}_s$ and to the exact integration prescribed by Eqs. (1).

According to Eqs. (12a,b) κ_x does not change and neither does $\underset{\sim}{B}_b$ while

$$\gamma_x = \theta + w,_x^K = \theta_1(1-\xi) + \theta_2\xi + \frac{1}{2} (\theta_2 - \theta_1) (1 - 2\xi) \tag{20}$$
$$= \frac{1}{2} (\theta_1 + \theta_2)$$

This results in the following matrix

$$\underset{\sim}{B}_s^w = \left[\frac{1}{2}, \frac{1}{2}\right] \tag{21}$$

Since $\underset{\sim}{B}_b$ remains unchanged and $\underset{\sim}{B}_s^w$ is the same as $\underset{\sim}{\bar{B}}_s$ of Eq. (18), the last two formulations are equivalent. Furthermore, as opposed to the previous formulation, no simplifications ("tricks") have been used in the present one.

Note, that in the thin structure limit, when the constraint $\gamma_x = 0$ is enforced, Eq. (20) yields

$$\theta_1 = -\theta_2 \tag{22}$$

This is consistent with the quadratic distribution of the transverse displacement given in Eq. (19) and shows that all of the above formulations attain the accuracy of the quadratic Kirchhoff-type element. However, the quadratic Kirchhoff element, developed without any shear deformation, would be associated with a complicated assembly procedure since the two nodal rotations would not be independent.

v) Mixed formulation with the modified distribution of the transverse displacements

A quadratic distribution of displacements, Eq. (19) and a constant distribution of the shear deformation can be used to show that the mixed formulation leads to precisely the same results as those in the formulation (iv). This can be immediately concluded from Fraeijs de Veubeke's limitation principle, [28], since in the kinematic approach presented in (iv) the shear distribution is also constant, Eq. (20).

vi) Displacement formulation based on the optimal bending configuration

A detailed discussion of the approach is given in [25]; its basic idea is

the following. In order for a flexural C^0 element to perform well in the thin-structure limit, there must exist a properly defined deformed configuration associated with bending strain energy and no shear strain energy. This configuration will be called the bending mode. The additional deformation required to bring this mode to the total deformed configuration will be called the shear mode; it is associated with a shear strain energy and no bending energy. Since the assumed coordinate system is corotational only for the total configuration, the bending and the shear mode may be characterized by nonzero nodal displacements. However, at each node, the sum of the displacements describing the two modes has to vanish whereas the sum of the rotations should give the initial rotations. Both modes are described by the linear shape functions. Their proper definition is essential for a successful development of a C^0 element.

Existing works clearly indicate that shear strain energy should be modified to achieve good behavior of the C^0 elements in the thin-structure limit. Moreover, they indicate that the modification of the bending strain energy (introduced for instance by reduced bending integration) is not desirable since it usually introduces additional zero-energy modes. For that reason, the bending strain energy in the total configuration and in its bending mode should be the same. To insure that this requirement is fulfilled, the nodal rotations in the bending mode are assumed to be the same as in the total configuration. This implies that the nodal rotations in the shear mode are zero; thus the shear strains that should be taken into account are completely defined by nodal displacements in the shear mode.

Even without a quantitative formulation the following remarks can be made. First, it is clear that the shear strain described above involves only the first derivatives of the transverse displacements. The polynomials

describing the distribution of the shear strains are therefore one order lower than those resulting from a given displacement and a nonzero rotation field. Second, although the first remark indicates that certain shear strains have been removed, they do not have to be the same as those removed by reduced shear integration. The present approach is based on mechanical reasoning and can serve as a guide to the appropriate reduced quadrature.

To determine the bending mode, we consider a set of "equivalent" Kirchhoff configurations: they are characterized by a curvature identical with that in the total configuration. They can be described by superposing the quadratic displacement field of Eq. (19) and a linear field resulting from a rigid body motion. Then we select the Kirchhoff configuration whose nodal rotations are closest - in an average sense - to the already defined rotations in the bending mode (being equal to the total rotations). By identifying the nodal displacements in this particular equivalent Kirchhoff configuration with the displacements in the bending mode we define the optimal bending configuration (or bending mode).

Since only rotations are compared in the evaluation of the nodal displacements, the rigid body translation is irrelevant. Thus, rotation around the node 1 of magnitude α is considered. The difference between rotations is measured by a sum of squares, so we miminize

$$\phi(\alpha) = (\Delta\theta_1)^2 + (\Delta\theta_2)^2 \tag{23}$$

where

$$\Delta\theta_1 = \theta_1 - \left(\alpha - \frac{1}{2}(\theta_2 - \theta_1)\right) = \frac{1}{2}(\theta_1 + \theta_2) - \alpha$$

$$\Delta\theta_2 = \theta_2 - \left(\alpha - \frac{1}{2}(\theta_1 - \theta_2)\right) = \frac{1}{2}(\theta_1 + \theta_2) - \alpha \qquad (24)$$

with respect to α . It turns out for this case α can easily be chosen so that $\phi = 0$, which is obviously the minimum

$$\alpha = \frac{1}{2}(\theta_1 + \theta_2) \qquad (25)$$

This defines a particular Kirchhoff configuration shown on Fig. 3. To transform the configuration to the original configuration the nodal points have to be displaced by

$$\Delta w_1 = 0 \qquad \Delta w_2 = \alpha L \qquad (26)$$

These are nodal displacements in the shear mode that result in the following shear deformation

$$\gamma = \alpha \qquad (27)$$

In view of Eq. (25) the modified matrix $\underset{\sim}{\bar{B}}_s$ is

$$\underset{\sim}{\bar{B}}_s = \left[\frac{1}{2}, \frac{1}{2}\right] \qquad (28)$$

and it coincides with the one given in Eq. (17). Consequently the present formulation is equivalent to all the previous ones.

We have illustrated these concepts in terms of a beam element for simplicity. It is also interesting to note that all of the preceding beam

formulations give the same results. In the next Section we will discuss these formulations in application to the triangular linear plate element. In this case they are not all equivalent. The results will suggest the formulation which can be safely used in a wide class of problems.

4. Triangular linear plate element

The triangular linear plate element will be considered in the local corotational frame of reference, Fig. 4, such that the nodal transverse displacements are zero. Its deformation is therefore described by the nodal rotations

$$\underset{\sim}{\theta}^T = [\theta_{x1}, \theta_{y1}, \theta_{x2}, \theta_{y2}\ \theta_{x3}, \theta_{y3}] \tag{29}$$

whereas the rotations within the element, θ_x and θ_y, are distributed linearly

$$\begin{Bmatrix} \theta_x \\ \theta_y \end{Bmatrix} = \sum_{i=1}^{3} \underset{\sim}{\theta}_i L_i \tag{30}$$

with

$$\underset{\sim}{\theta}_i^T = [\theta_{xi}, \theta_{yi}] \tag{31}$$

and L_i denoting the area coordinates. Using the above expressions and utilizing Eqs. (4) and (5) one arrives at

$$\underset{\sim}{B}_b = \begin{bmatrix} -\frac{1}{x_2} & 0 & \frac{1}{x_2} & 0 & 0 & 0 \\ 0 & \frac{x_3-x_2}{x_2x_3} & 0 & -\frac{x_3}{x_2y_3} & 0 & \frac{1}{y_3} \\ \frac{x_3-x_2}{x_2x_3} & -\frac{1}{x_2} & -\frac{x_3}{x_2x_3} & \frac{1}{x_2} & \frac{1}{y_3} & 0 \end{bmatrix} \tag{32}$$

$$\underset{\sim}{B}_s = \begin{bmatrix} L_1 & 0 & L_2 & 0 & L_3 & 0 \\ 0 & L_1 & 0 & L_2 & 0 & L_3 \end{bmatrix} \tag{33}$$

i) Reduced integration displacement formulation

Note that $\underset{\sim}{B}_b$ defined in Eq. (32) is constant while $\underset{\sim}{B}_s$ of Eq. (33) is linear. Thus, one point centroidal integration gives the exact value for $\underset{\sim}{K}_b$ and underintegrates $\underset{\sim}{K}_s$. The expressions defining the two matrices are

$$\underset{\sim}{K}_b = A\, \underset{\sim}{B}_b^T\, \underset{\sim}{D}_b\, \underset{\sim}{B}_b \tag{34a}$$

$$\underset{\sim}{K}_s = A\, \underset{\sim}{B}_s^c\, \underset{\sim}{D}_s^T\, \underset{\sim}{B}_s^c \tag{34b}$$

where A is the area of the triangle and $\underset{\sim}{B}_s^c$ is the matrix $\underset{\sim}{B}_s$, Eq. (33), evaluated at the centroid ($L_1 = L_2 = L_3 = \frac{1}{3}$).

ii) Mixed formulation

We assume that $\underset{\sim}{P}_M$ is chosen according to Eq. (9) and that $\underset{\sim}{K}_b$ is given by Eq. (10). Both components of the shear terms are independently assumed to be constant within the element, so

$$\underset{\sim}{P}_T = \begin{bmatrix} 1 & 0 \\ 0 & 1 \end{bmatrix} \tag{35}$$

and then Eq. (8b) reduces to

$$\underset{\sim}{K}_s = \int_A \underset{\sim}{B}_s^T \left(\int_A \underset{\sim}{D}_s^{-1} \right)^{-1} \int_A \underset{\sim}{B}_s \tag{36}$$

Since $\underset{\sim}{B}_s$ is a linear function over the triangle, one point centroidal integration evaluates the first and the last integral exactly. Furthermore $\underset{\sim}{D}_s$ is constant so

$$\underset{\sim}{K}_s = A\, \underset{\sim}{B}_s^{cT} \left(A\, \underset{\sim}{D}_s^{-1} \right)^{-1} A\, \underset{\sim}{B}_s^{c} = A\, \underset{\sim}{B}_s^{cT}\, \underset{\sim}{D}_s\, \underset{\sim}{B}_s^{c} \tag{37}$$

which is identical with Eq. (34b). This formulation is therefore equivalent to the previous one.

Both formulations as well as their equivalence were reported in [29]. However the approach turned out to be ineffective. Further search for an appropriate approach to a linear C^0 triangular element has led to the formulations presented in the following.

iii) Displacement formulations with the modified matrix $\underset{\sim}{B}_s$

Both the curvatures and the shear strains along side of the element depend on the projection of the total rotation on the particular side. For the linear rotation field defined in Eq. (31) the projections θ_i, i = 1,2,3, are

$$\theta_i = \theta_{i,i}(1-\xi_i) + \theta_{i+1}\, \xi_i \tag{38}$$

with

$$\theta_{i,i} = \underset{\sim}{\theta}_i^T\, \underset{\sim}{e}_i \qquad \theta_{i,i+1} = \underset{\sim}{\theta}_{i+1}^T\, \underset{\sim}{e}_i \tag{39}$$

where for i=3, i+1 should be identified with node 1, $\underset{\sim}{\theta}_i$ is specified in Eq.

(31), $\underline{e}_i$ are the unit vectors shown on Fig. 4 and ξ_i (0,1) parametizes the i-th side of the triangle. Thus the curvatures and the shear strains associated with each side are

$$\kappa_i = \theta_{i,\xi_i} = \frac{1}{\ell_i} (\theta_{i,i+1} - \theta_{i,i}) \tag{40a}$$

$$\gamma_i = \theta_i = \theta_{i,i} (1-\xi_i) + \theta_{i,i+1}\xi_i \tag{40b}$$

The above equations are analogous to Eq. (12a,b). One can therefore draw the following conclusion: if the present plate element is to behave well in the thin plate limit, the linear portion of the shear deformation for each side has to be related to a deformation associated with no shear strain energy (this led to success in the analysis of beams). The portion of the shear strains that should be associated with the strain energy is therefore (compare Eq. (16))

$$\gamma_i^s = \theta_i^s = \frac{\theta_{i,i} + \theta_{i,i+1}}{2} = \theta_i \ (\xi_i = \frac{1}{2}) \tag{41}$$

These values, considered for i = 1,2,3, define the modified shear deformation over the entire triangle

$$\underline{\gamma}^s = \underline{\theta}^s = \sum_{i=1}^{3} L_i \underline{\theta}^s \tag{42}$$

where

$$(\underline{\theta}^s)^T = [(\underline{\theta}_1^s)^T, (\underline{\theta}_2^s)^T, (\underline{\theta}_3^s)^T] \tag{43a}$$

$$(\underset{\sim}{\theta}_i^s)^T = [\theta_{xi}^s, \theta_{yi}^s] \tag{43b}$$

can be obtained by inverting the relationships

$$\gamma_i^s = (\underset{\sim}{\theta}_i^s)^T \underset{\sim}{e}_i = (\underset{\sim}{\theta}_{i+1}^s)^T \underset{\sim}{e}_i, \quad i=1,2,3 \tag{44}$$

Taking into account Eqs.(39), (41), (42) and (44) as well as the particular position of the reference frame, Fig. 4, one arrives at

$$\bar{\underset{\sim}{B}}_s^T = \begin{bmatrix} \frac{1}{2}(L_1 + L_2 + \frac{x_3}{x_2} L_3) & \frac{x_2 - x_3}{2y_3}(L_2 + \frac{x_3}{x_2} L_3) \\ \frac{y_3}{2x_2} L_3 & \frac{1}{2}(L_1 + \frac{x_2 - x_3}{2x_2} L_3) \\ \frac{1}{2}(L_1 + L_2 + \frac{x_2 - x_3}{x_2} L_3) & -\frac{x_3}{2y_3}(L_1 + \frac{x_2 - x_3}{x_2} L_3) \\ -\frac{y_3}{2x_2} L_3 & \frac{1}{2}(L_2 + \frac{x_3}{x_2} L_3) \\ \frac{1}{2} L_3 & \frac{x_3}{2y_3} L_1 - \frac{x_2 - x_3}{2y_3} L_2 \\ 0 & \frac{1}{2} \end{bmatrix} \tag{45}$$

The approach presented above was first proposed by Hughes and Tezduyar, [22], for the analysis of the quadrilateral element, and then was used by Hughes and Taylor, [24], in the analysis of the triangular element. Since the shear strain distribution defined by $\bar{\underset{\sim}{B}}_s$ in Eq. (45) is linear, no single-point integration (associated with constant shear strains over the element) can be equivalent to the present approach. Therefore this formulation is clearly different from the two previous ones. Yet, the derivation of $\bar{\underset{\sim}{B}}_s$ as well as the difference between Eqs. (33) and (45) clearly indicates that some portion of the shear strain energy has been removed.

Although use of $\bar{\underset{\sim}{B}}_s$ instead of $\underset{\sim}{B}_s$ in Eq. (10) should not require reduced integration, exact integration has been found to lead to results very strongly dependent on the mesh orientation, [24]; consequently one point quadrature has been applied by Hughes and Taylor, [24], but the integration point has been selected so that its location (and the results) depend on the local numbering of nodes. Fig. 5 shows three locations of the integration point P,P',P" for three different numbering of nodes 123, 1'2'3' and 1",2",3". It is therefore clear that the integration point has not been selected properly. More importantly, however, the above analysis indicates that the matrix $\bar{\underset{\sim}{B}}_s$ should be defined in a better way; a correct definition of $\bar{\underset{\sim}{B}}_s$ should not necessitate any reduced integration. These problems will be discussed subsequently.

iv) Displacement fromulation with a modified distribution of the transverse displacements

Here, a displacement formulation equivalent to the previous one, but not employing any corrections like those of the last formulation, will be

presented. To this end we introduce the quadratic transverse displacement

$$w^K = -\frac{1}{2}\left[x^2 - x_2 x - x_3(x_3 - x_2)\frac{y}{y_3},\ y^2 - y_3 y,\ xy - x_3 y\right]\underline{\kappa} \qquad (46)$$

where

$$\underline{\kappa} = \underline{B}_b\,\underline{\theta} \qquad (47)$$

and $\underline{B}_b$ is given by Eq. (32). In the corotational description adopted here, the displacement w^K vanishes at all nodal points. The approximation of the rotation field is linear, as it is given by Eq. (30).

Upon substition of the above functions into Eqs. (4) and (5), one obtains $\underline{B}_b$ given in Eq. (32) and

$$\underline{B}_s^w = \underline{B}_s - \underline{B}_s^b \qquad (48)$$

where $\underline{B}_s$ is given by Eq. (33) and

$$\underline{B}_s^b = \frac{1}{2}\begin{bmatrix} 2x - x_2 & 0 & y \\ (x_2 - x_3)\dfrac{x_3}{y_3} & 2y - y_3 & x - x_3 \end{bmatrix}\underline{B}_b \qquad (49)$$

Further evaluation of the above equations leads to the conclusion that

$$\underset{\sim}{B}_s^w = \overline{\underset{\sim}{B}}_s \tag{50}$$

which proves the equivalence between the previous formulation and the present one.

The structure of the Eq. (48) clearly shows that, within this formulation, $\chi = 0$ indicates that the Kirchhoff mode described by Eq. (46) is realized. Thus, in the thin-plate limit, quadratic accuracy could be expected. However, all the remarks made with regard to the previous, equivalent formulation are also pertinent here. This means that for some mesh arrangements the results obtained with the present formulation are very poor unless reduced integration in employed.

V) Mixed formulation with the modified distribution of the transverse displacements

If the kinematics presented in the previous formulation and the constant shear forces related to the matrix $\underset{\sim}{P}_T$ of Eq. (35) are used in Eq. (8b)

$$\underset{\sim}{K}_s = A \left(\overline{\underset{\sim}{B}}_s^c\right)^T \underset{\sim}{D}_s \overline{\underset{\sim}{B}}_s^c \tag{51}$$

where $\overline{\underset{\sim}{B}}_s^c$ is the matrix $\overline{\underset{\sim}{B}}_s$ evaluated at the centroid.

The above result indicates that if reduced integration is to be applied along with the modified matrix $\overline{\underset{\sim}{B}}_s$, the centroid should be selected as a point of integration rather than one of the points shown on Fig. 5(in [24] the word "centroid" has a different meaning).

vi) Displacement formulation based on the optimal bending configuration

The idea here is the same as in the related section concerning beams. Namely, for given nodal rotations, the transverse displacements have to be found which, along with the rotations, form the bending mode that is associated with no shear strain energy. This displacement mode is assumed to be defined by the position of an equivalent Kirchhoff configuration in which the nodal rotations are, in an average sense, closest to the given rotations. The difference between the given nodal displacements and the computed ones defines the shear strain energy that has to be taken into account.

In this case the displacement field describing basic equivalent Kirchhoff configuration is given by Eqs. (46) and (47). The nodal rotations for this field are

$$\underset{\sim}{\theta}^K = \begin{Bmatrix} \underset{\sim}{B}^b_{s1} \\ \underset{\sim}{B}^b_{s2} \\ \underset{\sim}{B}^b_{s3} \end{Bmatrix} \underset{\sim}{\theta} \qquad (52)$$

where $\underset{\sim}{B}^b_{s1}$, $\underset{\sim}{B}^b_{s2}$, $\underset{\sim}{B}^b_{s3}$ are obtained by evaluating the matrix $\underset{\sim}{B}^b_s$ given in Eq. (49) at the nodal points 1,2,3 respectively. Any other equivalent Kirchhoff configuration can be obtained by the rigid body motion given in Eq. (46). Since the rigid body translation is here irrelevant only two rotations of the magnitude α_x and α_y will be considered. In this case the difference between

given nodal rotations and those of an equivalent Kirchhoff configuration is

$$\Delta\underset{\sim}{\theta} = \underset{\sim}{\theta}^{K} + \alpha_x \underset{\sim}{d}_x + \alpha_y \underset{\sim}{d}_y - \underset{\sim}{\theta} \tag{53}$$

where

$$\underset{\sim}{d}_x^T = [1,\ 0,\ 1,\ 0,\ 1,\ 0] \tag{54a}$$

$$\underset{\sim}{d}_y^T = [0,\ 1,\ 0,\ 1,\ 0,\ 1] \tag{54b}$$

The function

$$f(\alpha_x, \alpha_y) = (\Delta\underset{\sim}{\theta})^T (\Delta\underset{\sim}{\theta}) \tag{55}$$

is then minimized with respect to α_x, α_y. The result is

$$\alpha_x = \frac{1}{3}(\theta^s_{x1} + \theta^s_{x2} + \theta^s_{x3}) \quad , \quad \theta^s_{xi} = \theta_{xi} - \theta^K_{xi} \tag{56a}$$

$$\alpha_y = \frac{1}{3}(\theta^s_{y1} + \theta^s_{y2} + \theta^s_{y3}) \quad , \quad \theta^s_{yi} = \theta_{yi} - \theta^K_{yi} \tag{56b}$$

The quantities on the right hand side of the expressions defining α_x and α_y form the vector

$$(\underset{\sim}{\theta}^s)^T = [\theta^s_{x1},\ \theta^s_{y1},\ \theta^s_{x2},\ \theta^s_{y2},\ \theta^s_{x3},\ \theta^s_{y3}] \tag{57}$$

which, in view of Eqs. (30), (33), (48), (50) and (52), is

$$\underset{\sim}{\theta}^{s} = \begin{Bmatrix} \overline{\underset{\sim}{B}}_{s1} \\ \overline{\underset{\sim}{B}}_{s2} \\ \overline{\underset{\sim}{B}}_{s3} \end{Bmatrix} \underset{\sim}{\theta} \equiv \underset{\sim}{P}_s \underset{\sim}{\theta} \tag{58}$$

The matrices $\overline{\underset{\sim}{B}}_{s1}$, $\overline{\underset{\sim}{B}}_{s2}$, $\overline{\underset{\sim}{B}}_{s3}$ are the nodal values of the matrix $\overline{\underset{\sim}{B}}_s$ of Eq. (45)

Because of the corotational description adopted here the initial nodal displacements are zero, so the transformation of the bending mode to the total one results in

$$\gamma = \begin{Bmatrix} \gamma_x \\ \gamma_y \end{Bmatrix} = \begin{Bmatrix} \alpha_x \\ \alpha_y \end{Bmatrix} \tag{59}$$

So, in view of Eqs. (55), (57) and (59), the modified matrix $\overline{\underset{\sim}{B}}_s$ is

$$\overline{\underset{\sim}{B}}_s = \frac{1}{3} \begin{Bmatrix} \underset{\sim}{d}_x^T \\ \underset{\sim}{d}_y^T \end{Bmatrix} \underset{\sim}{P}_s \tag{60}$$

and it describes a constant distribution of the shear deformation over the element.

Note, that matrix $\overline{\underset{\sim}{B}}_s$ of Eq. (45) defines a linear field of rotations over the element and, by virtue of Eqs. (56) and (58), α_x and α_y is just one third of its nodal values. Thus

$$\overline{\underset{\sim}{B}}_s = \overline{\underset{\sim}{B}}^{c}_s \tag{61}$$

Therefore, the present approach once again confirms that in [24] the centroid should be taken as the integration point. More importantly, the formulation seems to capture the predominant mechanical behavior of the element so that no reduced integration is needed in conjunction with the present approach. Its more detailed analysis is presented in [25].

5. Numerical examples

Numerical solutions to a clamped beam and to a simply supported circular plate, both under uniform loading, are presented. If C^0 plate elements are used in the analysis of thin plates, two different models of the classical simply-supported boundary conditions are possible: SS1, in which only the transverse displacement is constrained and SS2, in which both the transverse displacement and tangential rotations are constrained. In the present case the SS1 condition has been employed. Geometrical and mechanical data for the beam and plate problems is given in Tables 1 and 2, respectively.

The central displacements, normalized with respect to the analytic solution, are reported in Table 3 for the beam and Table 4 for the plate.

The number of elements in Table 3 refers to half of the beam since symmetry is used. It can be seen that the improvement in the results obtained by changing the number of elements from 1 to 2 is significant. Doubling the number of elements to 4 does not change the displacement much, and the accuracy attained is already satisfactory. The difference between the 1-element and 2-element solutions is attributed to the fact that a single element can only model the antisymmetric mode of deformation shown in Fig. 2, which is associated with shear strain energy. For a thin structure, this is a highly energy-absorbing mode which results in a stiff model.

In Table 4, the number of elements is for a quarter of the plate; the related element arrangements are shown on Fig. 6. It is clear that the first two formulations fail while formulation (vi), and the equivalent formulation (v) gives the best results; the role of the proper decomposition of the total C^0 configuration into its bending and shear mode is therefore apparent. The formulations (iii) and (iv) yield results equivalent to those obtained with one-point quadrature introduced in [24]. However a different selection of the

integration point, resulting from the formulation (v) or (vi), gives significant improvement, especially for coarse meshes.

6. Conclusions

In this paper two basic and simple C^0 elements have been investigated: the beam element and the triangular plate element (this is the simplest but by no means the easiest plate element); both with linear approximations for rotations and displacements. The purpose of this investigation was to show that the proper additive decomposition of the deformation into its bending mode, which is free of shear strain energy, and the shear mode, is crucial for a successful development of C^0 structural elements. This is clearly seen in the analysis of the triangular linear plate element. In this case, almost all the formulations are different and in most cases yield unacceptable results. Good results are obtained only after a proper definition of the bending mode. However it is important to emphasize that the proper definition of the bending mode can not be achieved simply through the use of reduced integration.

The analysis of the beam element shows that under fortuitous circumstances reduced integration may work. In the beam reduced integration automatically selects the proper bending mode of deformation. This is probably the case in many other C^0 elements, as for instance the Lagrange family of plate elements which are based on reduced integration. Even if the optimal bending mode of deformation is not selected by reduced integration, in all the cases where this approach works, the reduced integration probably selects a bending mode which is sufficiently close to the optimal one to yield adequate results. There are however cases, like the Serendipity family of plate elements, where the reduced integration fails, [9, 12]. We believe that this happens because of inadequate selection of the bending mode of deformation.

Of the formulations presented herein, the one based on the optimal

bending configuration and originated in [25] is the most promising, at least for simple elements. The fact that it leads to matrices not requiring any reduced integration indicates that it removes all obstacles to the correct behavior of the elements in the thin-structure limit.

ACKNOWLEDGMENT

TO AIR FORCE

The support of the Air Force Office of Scientific Research under contract F49620-82-K0013 is greatfully acknowledged.

References

1. S. Utku, "Stiffness Matrices for Thin Triangular Elements of Nonzero Gaussian Curvature", AIAA Journal 5, 1967, pp. 1659-1667.

2. G.A. Wempner, J.T. Oden and D. Kross, "Finite Element Analysis of Thin Shells", Journal of Engineering Mechanics Division, ASCE, Vol. 94, No. EM6, 1968, pp. 1273-1294.

3. I. Fried, "Shear in C^0 and C^1 Bending Finite Elements", Int. J. Solids Struct., 9, 1973, pp. 449-460.

4. O.C. Zienkiewicz, "The Finite Element Method", 3rd Edition, McGraw-Hill, London, 1977.

5. O.C. Zienkiewicz, R.L. Taylor and J.M. Too, "Reduced Integration Technique in General Analysis of Plates and Shells", Int. J. Num. Meth. Eng., 3, 1971, pp. 275-290.

6. T.J.R. Hughes, R.L. Taylor and W.A. Kanoknukulchai, "Simple and Efficient Element for Plate Bending", Int. J. Num. Meth. Eng. 11, 1977, pp. 1529-1543.

7. O.C. Zienkiewicz, J. Bauer, K. Morgan and E. Onate, "Simple Element for Axisymmetric Shells with Shear Deformations", Int. J. Num. Meth. Eng., 11, 1977, pp. 1545-1558.

8. W. Kanoknukulchai, "A Simple and Efficient Finite Element for General Shell Analysis", Int. J. Num. Meth. Eng., 14, 1979, pp. 179-200.

9. E.D.L. Pugh. Hinton and O.C. Zienkiewicz, "A Study of Plate Bending Elements with Reduced Integration", Int. J. Num. Meth. Eng., 12, 1978, pp. 1059-1073.

10. T.J.R. Hughes, M. Cohen and M. Haroun, "Reduced and Selective Integration Techniques in the Finite Element Analysis of Plates", Nucl. Eng. Design, 46, 1978, pp. 203-222.

11. E. Hinton, E.M. Salonen and N. Bicanic, "A Study of Locking Phenomena in Isoparametric Elements", Third MAFELAP Conference, Brunel University, Uxbridge, 1978.

12. E. Hinton and N. Bicanic, "A Comparisn of Lagrangian and Serendipity Mindlin Plate Elements for Free Vibration Analysis", Computers and Structures, 10, 1979, pp 483-494.

13. T.J.R. Hughes and M. Cohen, "The Heterosis Finite Element for Plate Bending", Computers and Structures, 9, 1978, pp. 445-450.

14. S.W. Lee and T.H.H. Pian, "Improvement of Plate and Shell Finite Elements by Mixed Formulations", AIAA Journal 16, 1978, pp. 29-34.

15. G. Prathap and G.R. Bhashyam, "Reduced Integration and the Shear-Flexible Shear Element", Int. J. Num. Meth. Eng., 18, 1982, pp. 195-210.

16. H. Stolarski and T. Belytschko, "Locking and Shear/Membrane Complementarity in Displacement, Hybrid and Mixed Finite Element Models", to appear in Comp. Meth. Appl. Mech. Eng.

17. R.L. Spilker and N.I. Munir, "The Hybrid-Stress Model for Thin Plates", Int. J. Num. Meth. Eng., 15, 1980, pp 1239-1260.

18. R.L. Spilker and N.I. Munir, "A Serendipity Cubic-Displacement Hybrid-Stress Element for Thin and Moderately Thick Plates", Int. J. Num. Meth. Eng, 15, 1980, pp. 1261-1278.

19. D.S. Malkus and T.J.R. Hughes, "Mixed Finite Elements Methods - Reduced and Selective Integration Techniques: A Unification of Concepts", Comp. Meth. Appl. Mech. Eng., 15, 1978, pp. 63-81.

20. R.H. MacNeal, "A Simple Quadrilateral Shell Element", Computers and Structures, 8, 1978, pp. 175-183.

21. H. Parish, "A Critical Survey of the 9-Node Degenerated Shell Element with Special Emphasis on Thin Shell Application and Reduced Integration", Computer Meth. Appl. Mech. Eng., 20, 1979, pp. 323-350.

22. T.J.R. Hughes and T.E. Tezduyar, "Finite Elements Based Upon Mindlin Plate Theory with Particular Reference to the Four Node Bilinear Isoparametric Element", J.A.M., 48, 1981, pp. 587-596.

23. T.J.R. Hughes, "Generalization of Selective Integration Procedures to Anisotropic and Nonlinear Media", Int. J. Num. Meth. Eng., 15, 1980, pp. 1413-1418.

24. T.J.R. Hughes and R.L. Taylor, "The Linear Triangular Bending Element", to appear in the Proceedings of the MAFELAP 1981 Conference, Brunel University, April 28 - May 1, 1981.

25. T. Belytschko, H. Stolarski and N. Carpenter, "An Accurate Triangular Plate Element with One Point Quadrature", submitted for publication

26. D.P. Flanagan and T. Belytschko, "A Uniform Strain Hexahedron and Quadrilateral with Orthogonal Hourglass Control", Int. J. Num. Meth. Eng., 17, 1981, pp. 679-706.

27. T. Belytschko, C.S. Tsay and W.K. Liu, "A Stabilization Matrix for the Bilinear Mindlin Plate Element", Comp. Meth. Appl. Mech. Eng., 29, 1981, pp. 313-327.

28. B. Fraeijs de Veubeke, "Displacement and Equilibrium Models in the Finite Element Method", in: O. C. Zienkiewicz and G.S. Holister (eds), Stress Analysis, Wiley, London, 1965.

29. J.L. Batoz, K.J. Bathe and L. W. Ho, "A Study of Three-Node Triangular Plate Bending Elements", Int. J. Num. Meth. Eng 15, 1980, p. 1771-1812.

TABLE 1

Data for the beam problem

length	10 in
height	1 in
width	1 in
Young modulus	10.92×10^5 psi
Poisson ratio	0.3
shear connection factor	5/6

TABLE 2

Data for the plate problem

radius	5 in
thickness	0.1 in
Young modulus	10.92×10^5 psi
Poisson ratio	0.3
shear correction factor	5/6

TABLE 3

Central displacement
for a clamped beam

No. of elements / Formulation	1	2	4
(i) to (vi)	0.126	0.874	1.062

Notation:

i) reduced integration displacement formulation

ii) mixed formulation

iii) displacement formulation with a modified matrix $\underline{B}$

iv) displacement formulation with a modified distribution of the transverse displacements

v) mixed formulation with a modified distribution of the transverse displacement

vi) displacement formulation based on the optimal bending configuration

TABLE 4

Central displacement
for simply supported circular plate

No. of elements / Formulation	6	24	96
i), ii)	0.063	0.150	0.398
iii), iv)	0.722	0.917	0.981
ref. [24]	0.703	0.912	0.948
v), vi)	0.824	0.954	0.989

Notation as for the Table 3.

Figure Captions

Fig. 1. Sign convention.

Fig. 2. Linear beam element:
a) total deformed configuration
b) symmetric part of deformation
c) antisymmetric part of deformation

Fig. 3. Linear beam element:
a) total deformed configuration
b) equivalent Kirchhoff configuration
c) shear mode of deformation

Fig. 4. Geometry of triangular plate element.

Fig. 5. Position of the integration point in ref. [24] for various local node numbers.

Fig. 6. Discretization of the circular plate example.

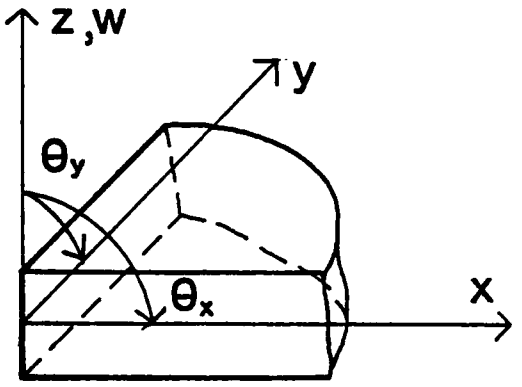

FIG. 1

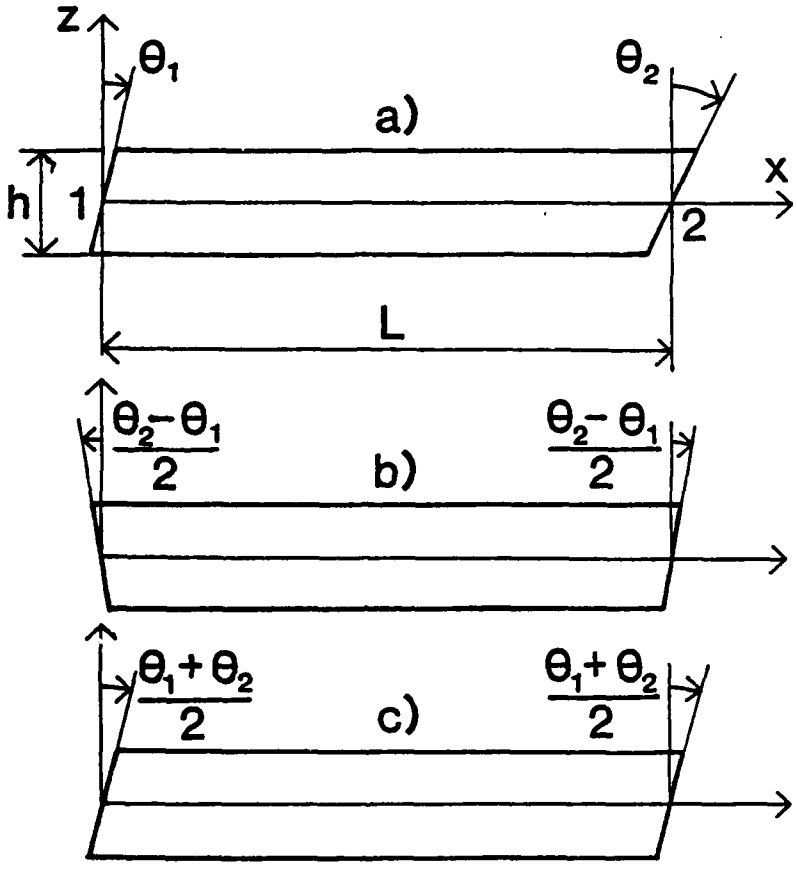

FIG. 2

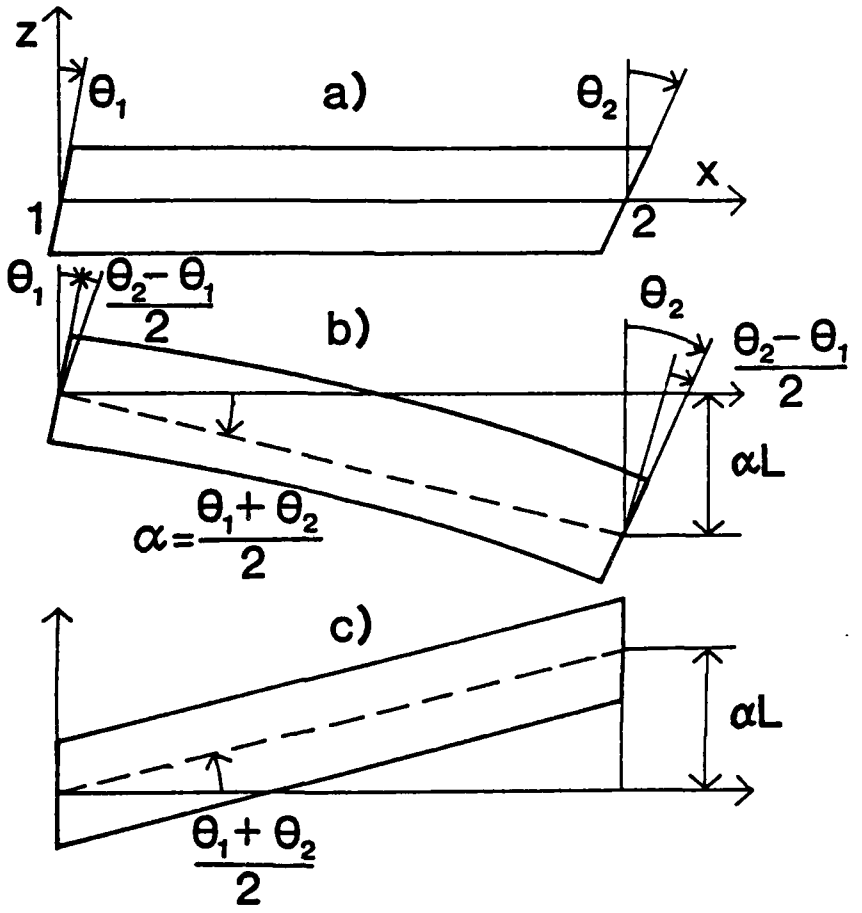

FIG. 2

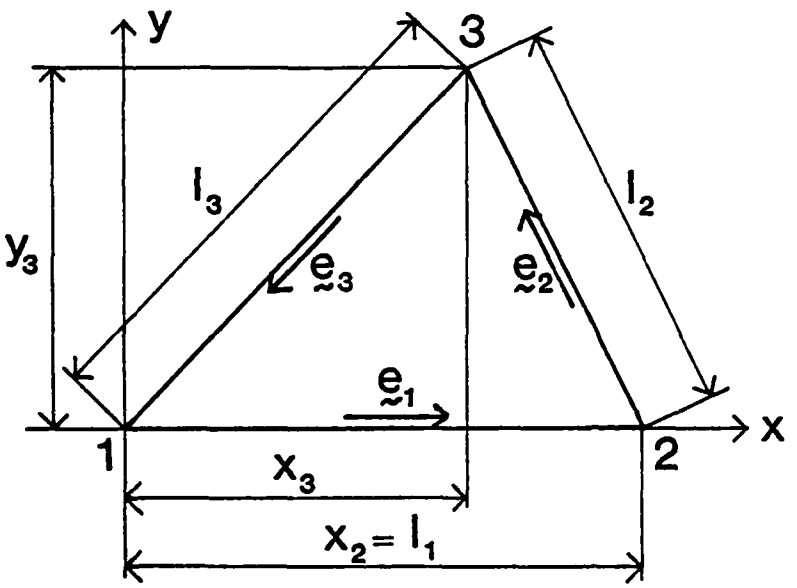
y
3
l_3
l_2
y_3
$\underset{\sim}{e}_3$
$\underset{\sim}{e}_2$
$\underset{\sim}{e}_1$
x
1
2
x_3
$x_2 = l_1$

FIG 4

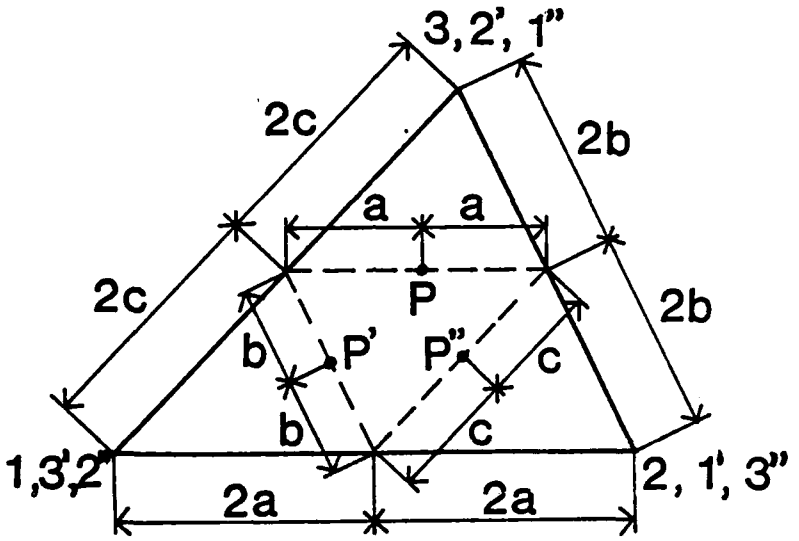

FIG. 5

FIG. 6

Section 1

INTRODUCTION

In Ref. [1] a phenomena called membrane locking was identified and analyzed for curved C^1 beam elements with linear axial and cubic transverse displacement fields. Membrane locking results from the inability of an element to bend without stretching: since any bending deformation of the element is then accompanied by stretching of the midline, membrane energy is always generated in bending, thus increasing the bending stiffness. Although the study employed a very simple beam model, it is clear that membrane locking must also appear in shells, (compare [2-9]).

However, the success of widely employed C^0 elements, [10-15] with reduced shear integration and the claims for hybrid and mixed elements [16-19] led to the conjecture that membrane locking may be circumvented in these elements. Therefore, a similar study has been made of these elements.

It has been found that reduced shear integration in curved C^0 elements does mitigate the effects of membrane locking. Indeed, a complex interdependence was found between shear and membrane underintegration: reduced integration in either the shear or membrane energies leads to improved accuracy in the bending response. In fact curved C^0 elements with full membrane integration perform quite well if reduced shear integration is used. However, reduced shear integration is accompanied by a deterioration of membrane-flexural coupling, which is one of the essential features of a curved element; it also leads to the appearance of kinematic modes.

Mixed finite elements are shown to also exhibit membrane and shear locking; in view of the equivalence theorems [20],[21], this is not

surprising. However, for a beam, hybrid methods are not subject to membrane locking because the general solution to the equilibrium equations can be constructed. This cannot be accomplished for arbitrary shells, but it may provide the insight needed for a rational construction of reduced-integration displacement elements which avoid locking. We are convinced such displacement elements provide the most viable approach to practical computations; the extra calculations associated with hybrid and mixed elements are hard to justify when displacement elements yield the same results.

In Section 2, the governing equations for a beam based on shallow shell theory and the variational formulations which pertain in this context to displacement, hybrid, and mixed elements are presented. Using a specific beam element, the interrelationship of membrane and shear locking is demonstrated in both mixed and displacement elements in Section 3. Both analytical methods and numerical results are used. In Section 4, isoparametric beam elements are examined; it appears that the cubic element avoids locking, though the cost of its counterpart in shell analysis is quite daunting. Conclusions are presented in Section 4.

Section 2

GOVERNING EQUATIONS AND VARIATIONAL FORMS

Consider a curved beam of height h, width b = 1, which is approximated by a sequence of chords, parametrized by x; in each chord the shape of the beam is described by a function w(x) as shown in Fig. 1. If w(x) is small, the behavior of the beam can be described by the theory of shallow structures wherein the following equations apply:

i. kinematic relations [22-25]

$$\varepsilon = u_{,x} + w_{,x}\, v_{,x} \tag{1a}$$

$$\kappa = -\phi_{,x} \tag{1b}$$

$$\gamma = -\phi + v_{,x} \tag{1c}$$

where u and v are the x and y components of the displacement field and ϕ is the rotation of the cross-section; ε, κ, and γ are the membrane (midplane) strain, change of curvature and shear deformation, respectively; commas denote derivatives.

ii. constitutive equations (elastic)

$$n = D_1 \varepsilon \qquad D_1 = Eh \tag{2a}$$

$$m = D_2 \kappa \qquad D_2 = \frac{Eh^3}{12} \tag{2b}$$

$$q = D_3 \gamma \qquad D_3 = \bar{\kappa} G h \tag{2c}$$

or

$$\underset{\sim}{s} = \underset{\sim}{D}\,\underset{\sim}{\varepsilon} \tag{2d}$$

where

$$\underset{\sim}{s}^T = \left[n,\ m,\ q\right] \tag{2e}$$

$$\underset{\sim}{\varepsilon}^T = \left[\varepsilon,\ \kappa,\ \gamma\right] \tag{2f}$$

$$\underset{\sim}{D} = \begin{bmatrix} D_1 & 0 & 0 \\ & D_2 & 0 \\ \text{sym} & & D_3 \end{bmatrix} \tag{2g}$$

and n, m and q are the membrane (axial) force, moment and shear on the cross-section of the beam.

iii. equations of equilibrium

$$n_{,x} = 0 \tag{3a}$$

$$m_{,x} - q = 0 \tag{3b}$$

$$q_{,x} + (nw_{,x})_{,x} - p = 0 \tag{3c}$$

iv. boundary conditions

$$n = n^* \nu_x \qquad \text{or} \quad (u = u^* \text{ and } \delta u = 0) \tag{4a}$$

$$m = -m^* \nu_x \qquad \text{or} \quad (\phi = \phi^* \text{ and } \delta\phi = 0) \tag{4b}$$

$$q + nw_{,x} = q^* \nu_x \qquad \text{or} \quad (v = v^* \text{ and } \delta v = 0) \tag{4c}$$

where asterisks denote prescribed values, the prefix δ a variation, and ν_x is

the unit normal to the end, which takes on values of -1 and +1 at the left and right hand ends. The conditions in the left column of the above (which are on the forces) are the natural boundary conditions, the ones on the right the essential boundary conditions.

Hu-Washizu Functional

The Hu-Washizu function for Eqs. (1-3) is given by

$$H = U - \int_C pv\, dx - \sum_{i=1}^{2} (n^* u + m^* \phi + q^* v) \Big|_{x = x_i} \qquad (5a)$$

$$- \int_C [n\,(\epsilon - u_{,x} - w_{,x} v_{,x}) + m(\kappa + \phi_{,x}) + q(\gamma + \phi - v_{,x})]\, dx$$

where x_1 and x_2 are the two ends of the beam and U the internal energy, which is given by

$$U = \frac{1}{2} \int_C (D_1 \epsilon^2 + D_2 \kappa^2 + D_3 \gamma^2)\, dx \qquad (5b)$$

In (5), the kinematic variables (u, ϕ, v, ϵ, κ, γ) are all independent, as are the kinetic variables (n, m, q); (u, ϕ, v) must be C^0 functions; (ϵ, κ, γ, n, m, q) must be C^{-1}, C^{-1} functions are piecewise continuous functions which are allowed to be discontinuous across element interfaces.

For the finite element formulation, these independent variables are approximated by shape functions $\underset{\sim}{S}$, $\underset{\sim}{N}$, and $\underset{\sim}{E}$ as follows

$$\begin{Bmatrix} n \\ m \\ q \end{Bmatrix} = \begin{Bmatrix} \underset{\sim}{S}_n \\ \underset{\sim}{S}_m \\ \underset{\sim}{S}_q \end{Bmatrix} \underline{\beta} = \underset{\sim}{S}\, \underline{\beta} \qquad (6)$$

$$\begin{Bmatrix} u \\ \phi \\ v \end{Bmatrix} = \begin{Bmatrix} \underset{\sim}{N}_u \\ \underset{\sim}{N}_\phi \\ \underset{\sim}{N}_v \end{Bmatrix} \underset{\sim}{d} = \underset{\sim}{N}\,\underset{\sim}{d} \tag{7}$$

$$\begin{Bmatrix} \varepsilon \\ \kappa \\ \gamma \end{Bmatrix} = \begin{Bmatrix} \underset{\sim}{E}_\varepsilon \\ \underset{\sim}{E}_\kappa \\ \underset{\sim}{E}_\gamma \end{Bmatrix} \underset{\sim}{e} = \underset{\sim}{E}\,\underset{\sim}{e} \tag{8}$$

where $\underset{\sim}{d}$ is the matrix of nodal displacements and $\underset{\sim}{s}$ and $\underset{\sim}{e}$ are the discrete variables for the stress and strain fields, respectively.

We also introduce the strains associated with the displacement field

$$\begin{Bmatrix} \hat{e} \\ \hat{\kappa} \\ \hat{\gamma} \end{Bmatrix} = \begin{Bmatrix} u_{,x} + w_{,x} v_{,x} \\ -\phi_{,x} \\ -\phi + v_{,x} \end{Bmatrix} = \begin{Bmatrix} \underset{\sim}{B}_\varepsilon \\ \underset{\sim}{B}_\phi \\ \underset{\sim}{B}_\gamma \end{Bmatrix} \underset{\sim}{d} = \underset{\sim}{B}\,\underset{\sim}{d} \tag{9}$$

where the kinematic relations (1) are used in the first equality and the elements of the $\underset{\sim}{B}$ matrix are obtained by evaluating the expressions in the second term with the displacements approximated by Eq. (7).

Substitution of Eqs. (6-9) into (5) provides the discrete form of the Hu-Washizu functional

$$H = U - \underset{\sim}{d}^T \underset{\sim}{f}^{ext} + \underset{\sim}{s}^T(\overline{\underset{\sim}{B}}\,\underset{\sim}{d} - \overline{\underset{\sim}{E}}\,\underset{\sim}{e}) \tag{10a}$$

$$U = \frac{1}{2}\,\underset{\sim}{e}^T\,\overline{\underset{\sim}{D}}\,\underset{\sim}{e} \tag{10b}$$

$$\overline{\underset{\sim}{D}} = \int_C \underset{\sim}{E}^T\,\underset{\sim}{D}\,\underset{\sim}{E}\,dx \tag{10c}$$

$$\overline{\underset{\sim}{B}} = \int_C \underset{\sim}{S}^T\,\underset{\sim}{B}\,dx \tag{10d}$$

$$\overline{\underset{\sim}{E}} = \int_C \underset{\sim}{S}^T \underset{\sim}{E}\, dx \tag{10e}$$

$$\underset{\sim}{f}^{ext} = \int_C p\, \underset{\sim}{N}_v^T\, dx + \sum_{i=1}^{2} (n^* \underset{\sim}{N}_u + m^* \underset{\sim}{N}_\phi + q^* \underset{\sim}{N}_v) \Big|_{x = x_i} \tag{10f}$$

This functional yields the following discrete equations:

i. strain-displacement

$$\overline{\underset{\sim}{B}}\, \underset{\sim}{d} = \overline{\underset{\sim}{E}}\, \underset{\sim}{e} \tag{11}$$

ii. constitutive

$$\overline{\underset{\sim}{E}}^T\, \underset{\sim}{\beta} = \overline{\underset{\sim}{D}}\, \underset{\sim}{e} \tag{12}$$

iii. equilibrium

$$\overline{\underset{\sim}{B}}^T\, \underset{\sim}{\beta} = \underset{\sim}{f}^{ext} \tag{13}$$

Since the parameters $\underset{\sim}{e}$ and $\underset{\sim}{\beta}$ are associated with C^{-1} functions, the corresponding element matrices $\underset{\sim}{e}_e$ and $\underset{\sim}{\beta}_e$ can be local to each element. The procedure for obtaining the governing equations is then the following. Using Eq. (12), it follows that

$$\underset{\sim}{e}_e = \overline{\underset{\sim}{D}}^{-1}\, \overline{\underset{\sim}{E}}^T\, \underset{\sim}{\beta}_e \tag{14}$$

which, when introduced into Eq. (11), gives

$$\underset{\sim}{\beta}_e = (\overline{\underset{\sim}{E}}\ \overline{\underset{\sim}{D}}^{-1}\ \overline{\underset{\sim}{E}}^T)^{-1}\ \ \overline{\underset{\sim}{B}}\ \underset{\sim}{d}_e \tag{15}$$

Now the use of equilibrium, Eq. (13) leads to the final result

$$\underset{\sim}{K}\ \underset{\sim}{d} = \underset{\sim}{f}^{ext} \tag{16a}$$

$$K = \sum_e \underset{\sim}{L}_e^T\ \underset{\sim}{K}_e\ \underset{\sim}{L}_e \tag{16b}$$

where $\underset{\sim}{L}_e$ is the convectivity array, the element stiffness matrix is given by

$$\underset{\sim}{K}_e = \overline{\underset{\sim}{B}}^T\ (\overline{\underset{\sim}{E}}\ \overline{\underset{\sim}{D}}^{-1}\ \overline{\underset{\sim}{E}}^T)^{-1}\ \overline{\underset{\sim}{B}} \tag{17}$$

The heart of this stiffness lies in the term $\overline{\underset{\sim}{D}}$, see Eq. (10b), which corresponds in form to the usual stiffness except that $\underset{\sim}{E}$ has replaced $\underset{\sim}{B}$.

Displacement Formulation and Selective Reduced Integration

In the displacement formulation

$$\begin{Bmatrix} \varepsilon \\ \kappa \\ \gamma \end{Bmatrix} = \begin{Bmatrix} \hat{\varepsilon} \\ \hat{\kappa} \\ \hat{\gamma} \end{Bmatrix} \quad ; \quad \begin{Bmatrix} n \\ m \\ q \end{Bmatrix} = \underset{\sim}{D} \begin{Bmatrix} \hat{\varepsilon} \\ \hat{\kappa} \\ \hat{\gamma} \end{Bmatrix} \tag{18}$$

which leads to the following identities (compare Eqs. (6), (8), (9))

$$\underset{\sim}{E}\ \underset{\sim}{e} = \underset{\sim}{B}\ \underset{\sim}{d} \qquad\qquad \underset{\sim}{S}\ \underset{\sim}{\beta} = \underset{\sim}{D}\ \underset{\sim}{B}\ \underset{\sim}{d} \tag{19}$$

and in Eqs. (10a) the coefficient of $\underset{\sim}{\beta}$ vanishes and $\underset{\sim}{e}$ can be eliminated to

give

$$H = \frac{1}{2} \underset{\sim}{d}^T \underset{\sim}{K} \underset{\sim}{d} - \underset{\sim}{d}^T \underset{\sim}{f}^{ext} \tag{20a}$$

and

$$\underset{\sim}{K}_e = \int_{C_e} \underset{\sim}{B}^T \underset{\sim}{D} \underset{\sim}{B} \, dx \tag{20b}$$

This stiffness matrix for an element can be written (see Eqs. (9) and (10g))

$$\underset{\sim}{K}_e = \int_{C_e} (D_1 \underset{\sim}{B}_\varepsilon^T \underset{\sim}{B}_\varepsilon + D_2 \underset{\sim}{B}_\phi^T \underset{\sim}{B}_\phi + D_3 \underset{\sim}{B}_\gamma^T \underset{\sim}{B}_\gamma) \, dx \tag{21}$$

membrane flexural shear

Here the membrane, flexural and shear terms are identified. The crucial feature of a curved beam is that $w_{,x}$ does not vanish, so transverse displacements v(x) may contribute to the membrane energy; see Eq. (9). Moreover, for many combinations of shape functions, <u>any</u> transverse deflection will contribute to the membrane energy; consequently pure bending deformations, which are often called inextensional modes of deformation, can not be replicated by the finite element. The concomitant increased stiffness is called "membrane" locking [1].

Mixed Formulation

In the mixed formulation, the constitutive equation and strain-displacement equations are combined so that the independent fields are the stresses and displacements. Thus Eqs. (2d), (6) and (8) are combined

$$\underset{\sim}{E}\ \underset{\sim}{e} = \underset{\sim}{D}^{-1}\ \underset{\sim}{S}\ \underset{\sim}{\beta} \tag{22}$$

The resulting functional H_e^m is obtained by substituting Eq. (22) into the first and last term of Eq. (10a), which gives

$$H_e^m = -\frac{1}{2}\ \underset{\sim}{\beta}^T\ \overline{\underset{\sim}{D}}_c^{-1}\ \underset{\sim}{\beta} + \underset{\sim}{\beta}^T\ \overline{\underset{\sim}{B}}\ \underset{\sim}{d} - \underset{\sim}{d}^T\ \underset{\sim}{f}^{ext} \tag{23a}$$

$$\overline{D}_c = \int_{C_e} \underset{\sim}{S}^T\ \underset{\sim}{D}^{-1}\ \underset{\sim}{S}\ dx \tag{23b}$$

The stationary conditions of this discrete functional are

$$\overline{\underset{\sim}{B}}\ \underset{\sim}{d}_e = \overline{\underset{\sim}{D}}_c\ \underset{\sim}{\beta}_e \tag{24a}$$

$$\overline{\underset{\sim}{B}}^T\ \underset{\sim}{\beta}_e = \underset{\sim}{f}_e^{ext} \tag{24b}$$

where

$$\overline{\underset{\sim}{B}} = \int_{C_e} \underset{\sim}{S}^T\ \underset{\sim}{B}\ dx \tag{24c}$$

The element stiffness is obtained by combining Eqs. (24a) and (24b) so that a relationship is obtained between $\underset{\sim}{f}_e$ and $\underset{\sim}{d}_e$, which yields that

$$\underset{\sim}{K}_e = \overline{\underset{\sim}{B}}^T\ \overline{\underset{\sim}{D}}_c^{-1}\ \overline{\underset{\sim}{B}} \tag{25}$$

The possibility of locking can be deduced immediately from Eq. (25). Let

$$\underset{\sim}{S} = \underset{\sim}{D}\,\underset{\sim}{B} \qquad (\dim \underset{\sim}{\beta} = \dim \underset{\sim}{d}) \tag{26}$$

Substituting into Eq. (25), we obtain a $\underset{\sim}{K}_e$ which is identical to the displacement formulation stiffness, Eq. (20b). This result, which was obtained in a more sophisticated way in [20], shows that the mixed method is equivalent to the displacement method when the shape functions for the stresses are obtained by Eq. (26); compare the conditions for equivalence in [19]. Hence locking should occur in mixed models (contrary to the implications of [19]), and reduced integration may be necessary; this will be shown later.

The counterpart of Eq. (21), which is obtained from Eqs. (24a) and (24b) is that for a mixed model

$$\underset{\sim}{K}_e = \overline{\underset{\sim}{B}}^T\, \overline{\underset{\sim}{D}}_c^{-1}\, \overline{\underset{\sim}{B}} \tag{27}$$

Reduced quadrature, if needed, will be used only on $\overline{\underset{\sim}{B}}$; all terms of $\overline{\underset{\sim}{D}}_c$ will be integrated exactly.

Hybrid Formulation

In the hybrid method, all stress shape functions are assumed to satisfy the homogeneous equilibrium equations, which allows the second term in Eq. (23a) to be replaced by a boundary integral. We will not consider this form explicitly but instead derive the hybrid method directly from Eq. (23a). Details are given in the next Section.

Section 3

CUBIC-LINEAR ELEMENT

Stiffness Formulation.

This element, shown in Fig. 1, employs cubic shape functions for the transverse deflection v, quadratic shape functions for the rotations of the cross-section ϕ, and linear shape functions for the axial displacements u. This type of element is often used in explicit time integration because its maximum frequency for commonly used element dimensions is lower than if a cubic is used for u, thus providing a larger stable time step [9].

The study of the element is facilitated by considering only the nodal degrees of freedom which are associated with deformational modes, thus excluding all rigid body modes. The deformational degrees of freedom are

$$\underset{\sim}{d}^T = [u_{21}, \phi_1, \phi_2, \alpha_1, \alpha_2] \tag{28a}$$

$$u_{21} = u_2 - u_1 \tag{28b}$$

where u_{21} is the axial displacement of the right end relative to the left one, ϕ_i are rotations of the nodal cross-sections and α_i are the rotations of the tangents to the middle line at nodal points. The shape functions and the initial shape w(x) are:

$$\underset{\sim}{N} = \begin{Bmatrix} \underset{\sim}{N}_u \\ \underset{\sim}{N}_\phi \\ \underset{\sim}{N}_v \end{Bmatrix} = \begin{bmatrix} \zeta & 0 & 0 & 0 & 0 \\ 0 & 1-\zeta & \zeta & 3(\zeta^2-\zeta) & 3(\zeta^2-\zeta) \\ 0 & 0 & 0 & L(\zeta-2\zeta^2+\zeta^3) & L(\zeta^3-\zeta^2) \end{bmatrix} \tag{28c}$$

$$w = L\,\alpha_1^o\,(\zeta - 2\zeta^2 + \zeta^3) + L\,\alpha_2^o\,(\zeta^3 - \zeta^2) \qquad (28d)$$

Note that these shape functions exclude rigid body motion and are expressed in a corotational system. The $\underset{\sim}{B}$ matrix resulting from Eq. (9), is

$$\underset{\sim}{B} = \begin{Bmatrix} \underset{\sim}{B}_u \\ \underset{\sim}{B}_\phi \\ \underset{\sim}{B}_v \end{Bmatrix} = \begin{bmatrix} \frac{1}{L} & 0 & 0 & w_{,x}(3\zeta^2-4\zeta+1) & w_{,x}(3\zeta^2-2\zeta) \\ 0 & \frac{1}{L} & -\frac{1}{L} & -\frac{3}{L}(2\zeta-1) & -\frac{3}{L}(2\zeta-1) \\ 0 & -(1-\zeta) & -\zeta & 1-\zeta & \zeta \end{bmatrix} \qquad (29)$$

where L is the length of the element and $\zeta \in [0,1]$ is the dimensionless parameter of its chord. The orders of the membrane and shear terms for this element are given in Table 1, along with the number of Gauss quadrature points required for exact integration of these polynomials.

Analysis of Reduced Integration in C^0 Displacement Element

Here an analysis of the element stiffness will be presented to demonstrate the effects of reduced membrane and shear integration. Of the rotational degrees of freedom, only ϕ must be continuous across interelement boundaries, so α_i is local to each element and can be eliminated on the element level. The elimination results in a 3x3 corotational stiffness matrix $\hat{\underset{\sim}{K}}$

$$\begin{Bmatrix} f_{x2} \\ m_{\phi 1} \\ m_{\phi 2} \end{Bmatrix} = \begin{bmatrix} \hat{K}_{11} & \hat{K}_{12} & \hat{K}_{13} \\ \hat{K}_{21} & \hat{K}_{22} & \hat{K}_{23} \\ \hat{K}_{31} & \hat{K}_{32} & \hat{K}_{33} \end{bmatrix} \begin{Bmatrix} u_{21} \\ \phi_1 \\ \phi_2 \end{Bmatrix} \qquad (30)$$

This matrix completely defines the axial and flexural properties of the element. All other nodal forces are found through global equilibrium of the element. The entries $\hat{K}_{22}$, $\hat{K}_{23}$, $\hat{K}_{32}$, $\hat{K}_{33}$ reflect bending properties of the element while $\hat{K}_{12}$, $\hat{K}_{13}$ represent membrane-bending coupling; in the absence of this coupling, $\hat{K}_{12} = \hat{K}_{13} = 0$. To make the analysis tractable, it is assumed that Poission's ratio $\nu = 1/3$ and

$$\alpha_1^o = \alpha, \qquad \alpha_2^o = -\alpha(1+\varepsilon) \tag{31a}$$

where ε is a small number. Moreover, we assume that

$$\frac{L\alpha}{h} = O(1) \ , \qquad \alpha^2 = O(\varepsilon) \tag{31b}$$

and only terms of order ε are retained in the final expressions. These assumptions are satisfied in many practical applications where $\frac{h}{L} \sim 0.1$ and $\alpha \sim 0.1$. Within this accuracy we obtain

$$m_{\phi 1} = \hat{K}_{22}\ \phi_1 + \hat{K}_{23}\ \phi_2 \tag{32}$$

The coefficients $\hat{K}_{22}$ and $\hat{K}_{23}$, for various reduced integration schemes are given in Tables 2 and 3, respectively.

For $\phi_2 = 0$, these stiffness terms are shown in Figs. 2 and 3 as a function of the element slenderness h/L. As expected, for a fixed value of α, the bending stiffness of the curved beam approaches that of the straight beam as h/L increases. For reduced membrane integration, the stiffness is

very close to the Euler-Bernoulli theory. At the same time, a clear difference between curved and straight beams is retained,

Reduced shear integration, on the other hand, shifts the stiffness towards that of a straight beam. The effects of curvature appear only for very slender elements, and from Figure 3, it is apparent that this is also true for other values of α. Thus reduced integration of either shear or membrane terms reduces the bending stiffness and yields acceptable results whenever bending is the predominant mode.

Remark 1. For the case $\alpha_1^o = \alpha_2^o$, reduced shear integation leads to singularity of the submatrix which has to be inverted to eliminate α_i. Consequently, α_i cannot be uniquely expressed in terms of the remaining degrees of freedom. The nodal forces however, in this case depend only on the mean value of α_i which is defined uniquely. To avoid this difficulty (which indicates the presence of a zero energy mode) this submatrix has been integrated exactly in this analysis; reduced integration is used for all other shear contributions.

Remark 2. This element reduces to the Euler-Bernoulli element studied in Ref. [1] if $\alpha_i = \phi_i$.

Hybrid Formulation

The general solution of the homogeneous form of Eqs. (3) is

$$n = \beta_1$$

$$q = -\beta_1 w_{,x} + \beta_2 \qquad (33)$$

$$m = -\beta_1 w + \beta_2 x + \beta_3$$

The parameters β_1, β_2, β_3 can easily be interpreted as $-n_1^*$, $-t_1^*$, m_1^*, Fig. 1, whereas the form of Eq. (33) results in

$$\underset{\sim}{S} = \begin{bmatrix} 1 & 0 & 0 \\ -w & x & 1 \\ -w_{,x} & 1 & 0 \end{bmatrix} \tag{34}$$

Note that the development of a general equilibrium solution such as (33), while feasible for curved beams, would be impossible for curved shells.

The parameters β_1, β_2, β_3 can be obtained from one of the stationary conditions of the functional (23), namely Eq. (24a), which gives

$$\left(\int_{C_e} \underset{\sim}{S}^T \underset{\sim}{D}^{-1} \underset{\sim}{S}\, dx\right) \underset{\sim}{\beta} = \left(\int_{C_e} \underset{\sim}{S}^T \underset{\sim}{B}\right) dx\, \underset{\sim}{d} \tag{35}$$

The right hand side of the above equation can, in this case, be evaluated without assuming any approximation for the displacement field, giving

$$\left(\int_{C_e} \underset{\sim}{S}^T \underset{\sim}{B}\, dx\right) \underset{\sim}{d} = \int_{C_e} \underset{\sim}{S}^T \begin{Bmatrix} \hat{\lambda} \\ \hat{\kappa} \\ \hat{\gamma} \end{Bmatrix} dx = \int_{C_e} \begin{Bmatrix} \hat{\lambda} - w\hat{\kappa} - w_{,x}\hat{\gamma} \\ \hat{\kappa}x + \hat{\gamma} \\ \hat{\kappa} \end{Bmatrix} dx = \begin{Bmatrix} u_2 - u_1 \\ v_2 - v_1 - \phi_2 L \\ \phi_1 - \phi_2 \end{Bmatrix} \tag{36}$$

where u_i, v_i, ϕ_i are translations and rotations at the nodal points. Since the right hand side of Eq. (35) is independent of the approximation of the

displacement field, we may claim that the field resulting from the exact analytic solution of the problem has been selected and that the element will not lock.

The equations relating the nodal forces and the nodal displacements are obtained by solving Eq. (35) for β_1, β_2, β_3 and then making use of the following relationships

$$n_1^* = -\beta_1 \ , \ m_1^* = \beta_3 \ , \ q_1^* = -\beta_2$$

$$n_2^* = \beta_1 \ , \ m_2^* = -\beta_2 L - \beta_3 \ , \ q_2^* = \beta_2 \tag{37}$$

Mixed Formulation

For the cubic-linear element, the following internal force distributions were considered:

i. nQ - qC; this distribution conforms with the guideline of Ref. [19] that the internal force distribution be one order lower than that obtained from Eq. (26):

$$n = \beta_1 + \beta_2 (1 - \xi)^2 + \beta_3 \xi^2$$

$$m = \beta_4 L (1 - \xi)^2 + \beta_5 \xi^2 \tag{38}$$

$$q = \beta_6$$

ii. nQ - qL; in tnis element, the shear distribution is consistent in order with Eq. (26):

$$n = \beta_1 + \beta_2 (1 - \xi)^2 + \beta_3 \xi^2$$

$$m = \beta_4 L (1 - \xi) + \beta_5 L \xi \qquad (39)$$

$$q = \beta_6 + \beta_7 (1 - 2\xi)$$

iii. nD - qC; this element has a normal force distribution consistent with Eq. (26):

$$n = \beta_1 + \beta_2 (-6\xi^3 + 11\xi^2 - 6\xi + 1) + \beta_3 (-6\xi^3 + 7\xi^2 - 2\xi)$$

$$m = \beta_4 L (1 - \xi) + \beta_5 L \xi \qquad (40)$$

$$q = \beta_6$$

iv. nC - qL; this element has the simplest normal force and shear distribution consistent with a 5 parameter stress model:

$$n = \beta_1$$

$$m = \beta_2 L (1 - \xi) + \beta_3 L \xi \qquad (41)$$

$$q = \beta_4 + \beta_5 (1 - 2\xi)$$

In all the above elements, the displacement shape functions are given in Eq. (28c) and the $\underset{\sim}{B}$ matrix needed to evaluate Eq. (24c) is given in Eq. (29). In reduced membrane integration, the rows of $\overline{\underset{\sim}{B}}$ associated with the axial force n (e.g. rows 1 to 3 for nQ - qL) are underintegrated, while in the reduced shear integration, the rows of $\overline{B}$ associated with the shear q (i.e. rows 6 and 7 for nQ - qL) are underintegrated.

Numerical Results

Results were obtained for the deep arch shown in Fig. 4. The results for various integration schemes in displacement, mixed and hybrid formulations are summarized in Table 4.

The displacement method with full integration of both membrane and shear terms, it is apparent, is far too stiff. Reduced integration of either the membrane or shear terms leads to reasonable agreement with the analytic solution; this contrasts with the behavior of curved C^1 elements of this type, where reduced membrane integration is always necessary [1]. However, reduced membrane integration with full shear integration gives the best results. The reason for this is apparent from examining the membrane-flexural coupling terms $\hat{K}_{12}$, which vanish for shear underintegration, thus providing behavior similar to that of a straight element; this also is borne out by comparing cases 3 and 5.

The hybrid element does not lock and is in good agreement with the analytic solution. This was expected in view of the fact that for this element, the stiffness matrix is independent of the shape functions used; see comments following Eq. (36).

The mixed elements, as can be seen from Table 4, also exhibit locking when full integrated except for the constant membrane, linear shear element

(nC-qL). In the quadratic membrane, linear shear element (nQ-qL), various reduced integration schemes were tried. The best accuracy was attained for reduced membrane and full shear integration. Reduced shear integration yields results similar to that of the quadratic membrane, constant shear (nQ-qC) curved and straight elements, supporting the hypothesis that reduce shear integration diminishes flexural-membrane coupling.

This conjecture is also supported by the effects of reduced integration on the stiffness term $\hat{K}_{12}$ which is given for the various elements in Table 4. It is apparent that reduced membrane integration provides a good estimate of this stiffness term, while for reduced shear integration it often vanishes, as in a straight beam.

Examining the results and their implications in more detail provides some interesting insight into the relationship between reduced integration and shear/membrane locking. The element nQ-qC (quadratic n, constant q) was designed according to the recommendation of [19]; see Section 2. As can be seen from Table 4, nQ-qC possesss no flexural-membrane coupling and behaves like a straight element (compare with Case 13); this reflects the shear flexibility brought about by the constant shear approximation. The element with constant n, linear q (case 12) in fact performs better, for by reducing the order of n and increasing the order of q, an effect similar to membrane underintegration is brought about.

These results (cases 7 and 12; 9 and 10) again illustrate the interrelationship of membrane and shear underintegration in curved elements, and that it also occurs in the framework of mixed elements.

It is worth noting that when continuous distributions were used for the stress functions [18, 19], no locking was observed despite the fact that the order of $\underset{\sim}{S}$ was one order higher than that given by Eq. (26). We attribute

this to the fact that using continuous shape functions $\underset{\sim}{S}$ diminishes the number of independent parameters, and is thus in a sense equivalent to reducing its order.

Section 4

CURVED ISOPARAMETRIC ELEMENTS

Description of Elements

The element studied in Section 3 employed a linear axial and cubic transverse displacement. The purpose of this Section is to examine whether the behavior of isoparametric elements, where the axial and transverse displacements are of the same order, is similar.

Two elements were studied:

1. a quadratic isoparametric with 3 nodes
2. a cubic isoparametric with 4 nodes

In the quadratic and cubic elements, u, v, ϕ, and w were approximated by quadratic and cubic shape functions, respectively. Because the curvature is treated by shallow-shell theory, cf. Eqs. (1), all terms were integrated over the straight x-axis. Only displacement formulations with selective reduced integration were considered. The number of Gauss points required for exact quadrature of the relevant terms is given in Table 1.

Some of the reduced quadrature schemes introduced kinematic modes; wherever this occured, the element was stabilized by exactly integrating entries of the stiffness corresponding to the transverse displacements of the interior nodes. Although this scheme is not suitable for practical applications, it provided a convenient means to study low order quadrature. All results obtained in this manner have been identified.

Numerical Results

Results for the curved isoparametric elements are presented in Tables 5 and 6. It can be seen from Table 5 that the quadratic element exhibits severe

locking when full quadrature is employed; see Table 1 for the quadrature which is exact. Reduced membrane integration alone makes a big difference between 3 and 2 Gauss points but, still, some locking is present. Further reduction to one integration point practically introduces no additional change. If only shear terms are underintegrated, the big difference is between 2 and 1, with almost no difference between 3 and 2 Gauss points.

For one-point integration of the shear terms, the results are independent of the membrane integration. This suggests that bending of the element's midline is not involved in the deformation process and the membrane-bending coupling is almost eliminated. To verify this, the terms $\hat{K}_{12}$ and $\hat{K}_{22}$ are given in Table 7 (see Eq. (30)). It is clear that $\hat{K}_{12}$, which represents the membrane-bending coupling, vanishes for one point shear integration. It also vanishes if one point membrane integration is used; this stems from the fact that the initial shape of the element is symmetric and $w_{,x}$ in Eq. (1a) vanishes at the center of the element. Obviously, neither one point shear nor one point membrane integration is desirable.

The results for the cubic element are given in Table 6. The difference between full and reduced integration is quite small. This element is only mildly susceptible to membrane or shear locking, apparently, deformation modes which eliminate excessive membrane and shear energy are always possible. However, the accuracy is best for 3 point quadrature of both terms, which represents underintegration.

Recommended Quadrature Scheme

From the numerical results, it appears that quadrature schemes which in a sense filter out the higher order terms in Eqs. (1a) and (1b), are most accurate. For an isoparametric element, these terms

are $w_{,x}$ $v_{,x}$ and ϕ, respectively. The number of quadrature points would then be estimated by requiring exact quadrature of the energies associated with the lower order terms in Eqs. (1a) and (1b), namely $u_{,x}^2$ and $v_{,x}^2$, respectively.

For the quadratic isoparametric, this guideline suggests 2 point quadrature for the shear and membrane terms, while for the cubic isoparametric, it suggest 3 points. Tables 5 and 6 indicate that these quadrature scheme give the best results.

Remark 3. Both 2 x 2 quadrature in the quadratic element and 3 x 3 quadrature in the cubic element are associated with kinematic modes in the three dimensional shell element. These modes would require stabilization.

Section 5

CONCLUSIONS

1. Shear membrane locking are interrelated in curved C^0 elements. Reduced integration of either the shear or membrane terms can alleviate locking, but shear underintegration eliminates the membrane-flexural coupling which characterizes curved elements and thus results in elements whose performance closely approximates that of straight elements.

2. Mixed finite element formulations, when used with generalized stress fields local to the element, also exhibit membrane and shear locking.

3. In cubic isoparametric beam elements, almost no locking of either a membrane or shear type is detectable with full integration.

4. In quadratic isoparametric beam elements, both membrane and shear locking are present and the interrelationship between these types of locking described in the first conclusion is apparent.

5. Hybrid curved beam elements do not exhibit locking. This is probably a consequence of the fact that a general equilibrium solution can be obtained for this element; it is doubtful that this could be achieved for a curved shell element.

It is worth noting that these locking phenomena will occur regardless of the type of structural or continuum theory which is used. A shallow beam theory has been used here because it enables the order of the membrane terms

to be easily identified. In a continuum formulation, these terms appear through the variations in the Jacobian which are brought about by the curvature, and are not as easily identified. Nevertheless, the mechanical behavior of a slightly curved element will be identical. Thus in either context, the use of higher order integration, which incidentally, is often recommended for plastic problems, will result in poor element performance because of locking.

ACKNOWLEDGEMENT

The support of the Air Force Office of Scientific Research under Grant F49620-82-K-0013 under the direction of Dr. A. Amos is gratefully acknowledged.

Figure Captions

Fig. 1. Notation for the curved beam Element.

Fig. 2. Bending stiffness of the curved beam element as a function of aspect ratio normalized with respect to a straight beam; F and R designate full and reduced quadrature of membrane (M) and shear terms (S); EBA designates an analytical result for the Euler-Bernoulli beam.

Fig. 3. Bending stiffness of the curved beam element as a functin of the initial curvature (see Fig. 2 for nomenclature).

Fig. 4. Problem description for the elastic deep arch.

REFERENCES

1. H. Stolarski and T. Belytschko, "Membrane locking and reduced integration for curved element," J. Appl. Mech., 49 (1982) 172-176.

2. D.G. Ashwell and A.B. Sabir, "Limitations of certain curved finite elements when applied to arches," Int. J. Mech. Sci., 13 (1971) 133-139.

3. D.G. Ashwell, A.B. Sabir and T.M. Roberts, "Furtner studies in the application of curved finite elements to circular arches," Int. J. Mech. Sci. 13 (1971) 507-517.

4. A.B. Sabir and D.G. Ashwell, "A comparison of curved beam finite elements when used in vibration problems," J. Sound Vibr. 18 (1971) 555.

5. A.B. Sabir and A.C. Lock, "Large deflection, geometrically nonlinear analysis of circular arches," Int. J. Mech. Sci. 15 (1973) 37-47.

6. D.J. Dawe, "Curved finite elements for the analysis of shallow and deep arches," Computers and Structures 4 (1974) 559-580.

7. D.J. Dawe, "Numerical studies using circular arch finite elements," Computers and Structures 4 (1974) 729-740.

8. D.G. Ashwell and R.H. Gallagher, editors, Finite elements for thin shells and curved members, John Wiley & Sons, London, 1976.

9. T. Belytschko, "Explicit time integration of structure-mechanical systems," Advanced Structural Dynamics, ed. by J. Donea, Applied Science Publishers, 1980, 97-122.

10. O.C. Zienkiewicz, R.L. Taylor and J.M. Too, "Reduced integration techniques in general analysis of plates and shells," Int. J. Num. Meth. Eng. 3 (1971) 275-290.

11. G.A. Wempner, J.T. Oden and D. Kross, "Finite element analysis of thin shells," Journal of Engineering Mechanics Division, ASCE, Vol. 94, No. EM6, 1968, 1273-1294.

12. T.J.R. Hughes, R.L. Taylor and W. Kanoknukulchai, "A simple and efficient element for plate bending," Int. J. Num. Meth. Eng. 11 (1977) 1529-1543.

13. H. Parish, "A critical survey of the 9-node degenerated shell element with special emphasis on thin shell application and reduced integration," Comp. Meth. Appl. Mech. Eng. 20 (1979) 323-350.

14. T.J.R. Hughes and T.E. Tezduyar, "Finite elements based upon Mindlin plate theory with particular reference to the four-node bilinear isoparametric element," J. Appl. Mech., 48 (1981) 587-596.

15. G. Prathap and G.R. Bhashyam, "Reduced integration and the shear flexible beam element," Int. J. Num. Meth. Eng. 18 (1982) 195-210.

16. S.W. Lee and T.H.H. Pian, "Improvement of plate and snell finite elements by mixed formulations," AIAA Journal, 1, 16 (1978) 29-34.

17. A.K. Noor, W.H. Greene and S.J. Hartley, "Nonlinear finite element analysis of curved beams," Comp. Meth. Appl. Mech. Eng. 12 (1977) 289-307.

18. A.K. Noor and N.F. Knight, "Nonlinear dynamic analysis of curved beams," Comp. Meth. Appl. Mech. Eng. 23 (1980) 225-252.

19. A.K. Noor and J.M. Peters, "Mixed models and reduced/selective integration displacement models for nonlinear analysis of curved beams," Int. J. Num. Meth. Eng. 17 (1981) 615-631.

20. J.T. Oden and J.N. Reddy, "Some observations on properties of certain mixed finite element approximations," Int. J. Num. Meth. Eng. 9 (1975) 933-938.

21. D.S. Malkus and T.J.R. Hughes, "Mixed finite element methods-reduced and selective integration techniques: A unification of concepts," Comp. Meth. Appl. Mech. Eng. 1, 15 (1978) 63-81.

22. K. Marguerre, "Zur Theorie Der Gekrummten Platte Grosser Formenderung," Prof. 5th Int. Congress of Applied Mechanics, 1938, 93-701.

23. T. Belytschko and B.J. Hsieh, "Nonlinear transient finite element analysis with convected coordinates," Int. J. Num. Meth. Eng. 3 (1973) 255-272.

24. T. Belytschko and L.W. Glaum," Application of higher order corotational stretch theories to nonlinear finite element analysis," Computers and Structures, 10 (1979) 175-182.

25. J.L. Batoz, "Curved finite elements and shell theories with particular reference to the buckling of a circular arch," Int. J. Num. Meth. Eng. 14 (1979) 774-779.

TABLE 1

Order of Approximations and Gauss points required
for Exact Integration for Element

Element	Order of Approximation				Order of shear	Order of memb.	Gauss pts. for exact integ.	
	u	v	ϕ	w	$(v_{,x} - \phi)^2$	$(u_{,x} + w_{,x}v_{,x})^2$	shear	memb.
Linear-cubic	1	3	2	3	2*	8	2	5
Quadratic isoparametric	2	2	2	2	4	4	3	3
Cubic isoparametric	3	3	3	3	6	8	4	5

* see Eq. (28)

TABLE 2

Bending stiffness $\hat{K}_{22}$ (Eq. (30))

$$\hat{K}_{22} = \frac{Eh^3}{12L}\left\{4.0 + A_1\,\alpha^2 + A_2\left(\frac{h}{L}\right)^2 + \left(\frac{La}{h}\right)^2\left[A_3 + A_4\,\alpha^2 + a_5\left(\frac{h}{L}\right)^2\right]\right\}$$

Type of integration	A_1	A_2	A_3	A_4	A_5
EBA	0.0	0.0	0.5829	0.0	0.0
FNI	-0.8381	-8.0	0.9144	0.8316	1.8288
FS-RM	-1.7984	-2.6667	0.6744	0.0	0.0
FM-RS	-0.8381	-8.0	0.3143	-0.0878	-0.8381

Notation: EBA - Euler Bernoulli analytic solution, FNI - full integration, FS-RM - full shear and reduced membrane (2 Gauss points) integration, FM-RS - full membrane and reduced shear (1 Gauss point) integration.

TABLE 3

Bending stiffness $\hat{K}_{23}$ (Eq. (30))

$$\hat{K}_{23} = \frac{Eh^3}{12L}\left\{2.0 + C_1\alpha^2 + C_2\left(\frac{h}{L}\right)^2 + \left(\frac{L\alpha}{h}\right)^2\left[C_3 + C_4\alpha^2 + C_5\left(\frac{h}{L}\right)^2\right]\right\}$$

Type of Integration	C_1	C_2	C_3	C_4	C_5
EBA	0.0	0.0	-0.2500	0.0	0.0
FNI	-0.8381	-8.0	-0.2856	-0.8724	-0.8376
FS-RM	-1.7984	-2.6667	-0.6744	0.0	0.0
FM-RS	-0.8381	-8.0	0.3143	-0.0878	-0.8381

Notation the same as for Table 1.

TABLE 4

Numerical Results for a Deep Circular Arch
with Cubic-Linear Element

Case No	Method	Element Used	Further Specifications of the Element* (number of integration points in parenthesis)	Force/Displ lb/in	Stiffness terms**	
					K_{22}	K_{12}
1	Exact analytic	———	EBA	471.1	—	—
2	Displacement Method	8 curved shear flexible el.	full integration	694.9	1.25	1.10
3			FM-RS, full mem. (5) red. shear int.(1)	487.8	1.00	0
4			FS-RM full shear, (2) red. mem. int. (2)	473.3	1.01	1.12
5		8 straight EB el.	full int.	482.1	0.9	0.0
6	Hybrid stress	8 curved shear		473.3	1.00	1.00
7	Mixed Method	8 el. nQ - qC	curved; full int.(4,1)	484.5	0.94	0
8		8 el. nQ - qL	curved; full int.(4,2)	690.3	1.19	1.11
9			curved; full shear (2) red. mem. (2)	473.3	1.01	1.13
10			curved; full mem. (4) red. shear (1)	485.2	0.94	0
11		8 el. nD - qC	curved; full int. (4,1)	487.0	1.00	0
12		8 el. nC - qL	curved; full int. (3,2)	473.4	1.02	1.13
13		8 el. nC - qL	straight; full int.(1,2)	482.1	0.87	0

*Abbreviations: EB =Euler-Bernoulli; int. = integration; mem. = membrane; red. = reduced

**Normalized with respect to $\hat{K}_{22}$ and $\hat{K}_{12}$ for hybrid stress method respectively

TABLE 5

Ratio of Numerical to Analytic Results for a Circular Arch Solution with Quadratic Isoparametric Elements for Reduced Membrane and Shear Quadrature

n_G (memb) / n_G (shear)	Curved Element			Straight Element
	3	2	1	
3	1.575	1.063	1.084	1.084
2	1.449	1.004	1.023	1.023
1	0.939*	0.940*	0.940*	0.940*

*) Some entries of the stiffness matrix were integrated exactly to stabilize kinematic modes.

TABLE 6

Ratio of Numerical to Analytic Stiffness for a Deep Circular Arch with Cubic Isoparametric Element for Reduced Integration

Gauss quadrature points for membrane	Gauss quadrature points for shear	Ratio
5	4	1.010
5	3	1.007
5	2	1.004*
5	1	0.957*
4	4	1.010
3	4	1.004
2	4	1.004
1	4	1.023
3	3	1.004

*) Kinematic modes were stabilized.

TABLE 7

Stiffnesses $\hat{K}_{22}$ and $\hat{K}_{12}$ for Quadratic Isoparametric Element*

n_G (memb) / n_G (shear)	3		2		1	
	$\hat{K}_{22}$	$\hat{K}_{12}$	$\hat{K}_{22}$	$\hat{K}_{12}$	$\hat{K}_{22}$	$\hat{K}_{12}$
3	3.25	1.09	3.15	1.12	3.00	0.00
2	1.11	1.09	1.01	1.12	0.87	0.00
1	0.52	0.00	0.52	0.00	0.52	0.00

*) normalized with respect ot hybrid element in Table 3

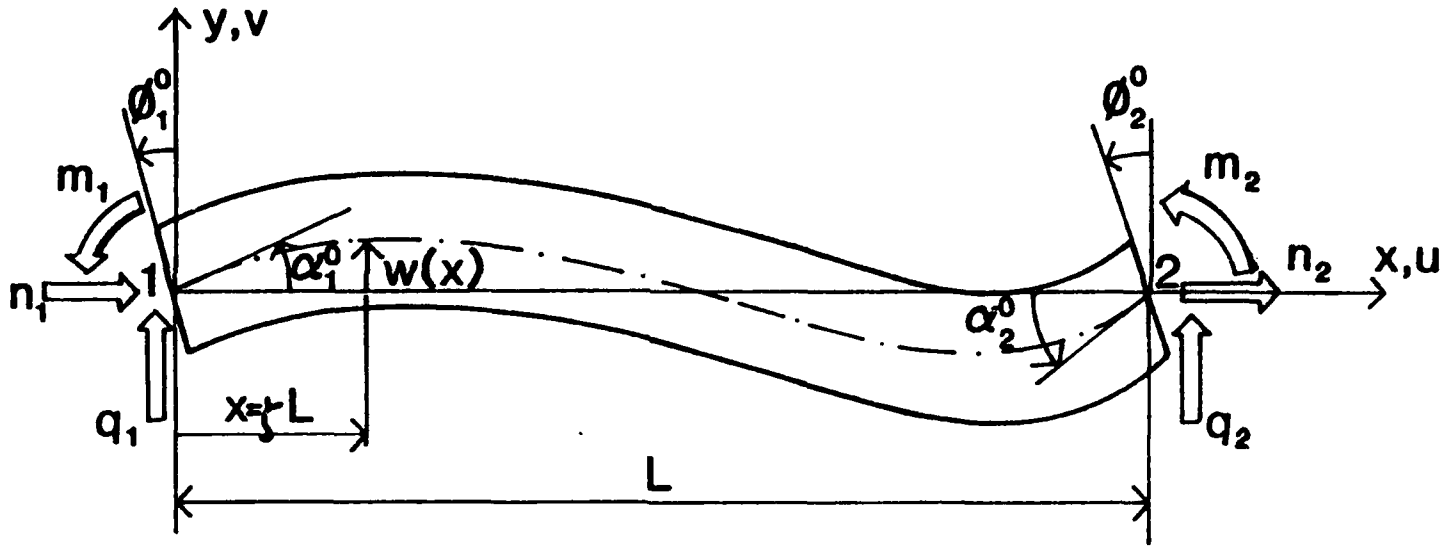
y,v
ϕ_1^0
ϕ_2^0
m_1
m_2
n_1
n_2
1
2
x,u
α_1^0
w(x)
α_2^0
q_1
q_2
x=ξL
L

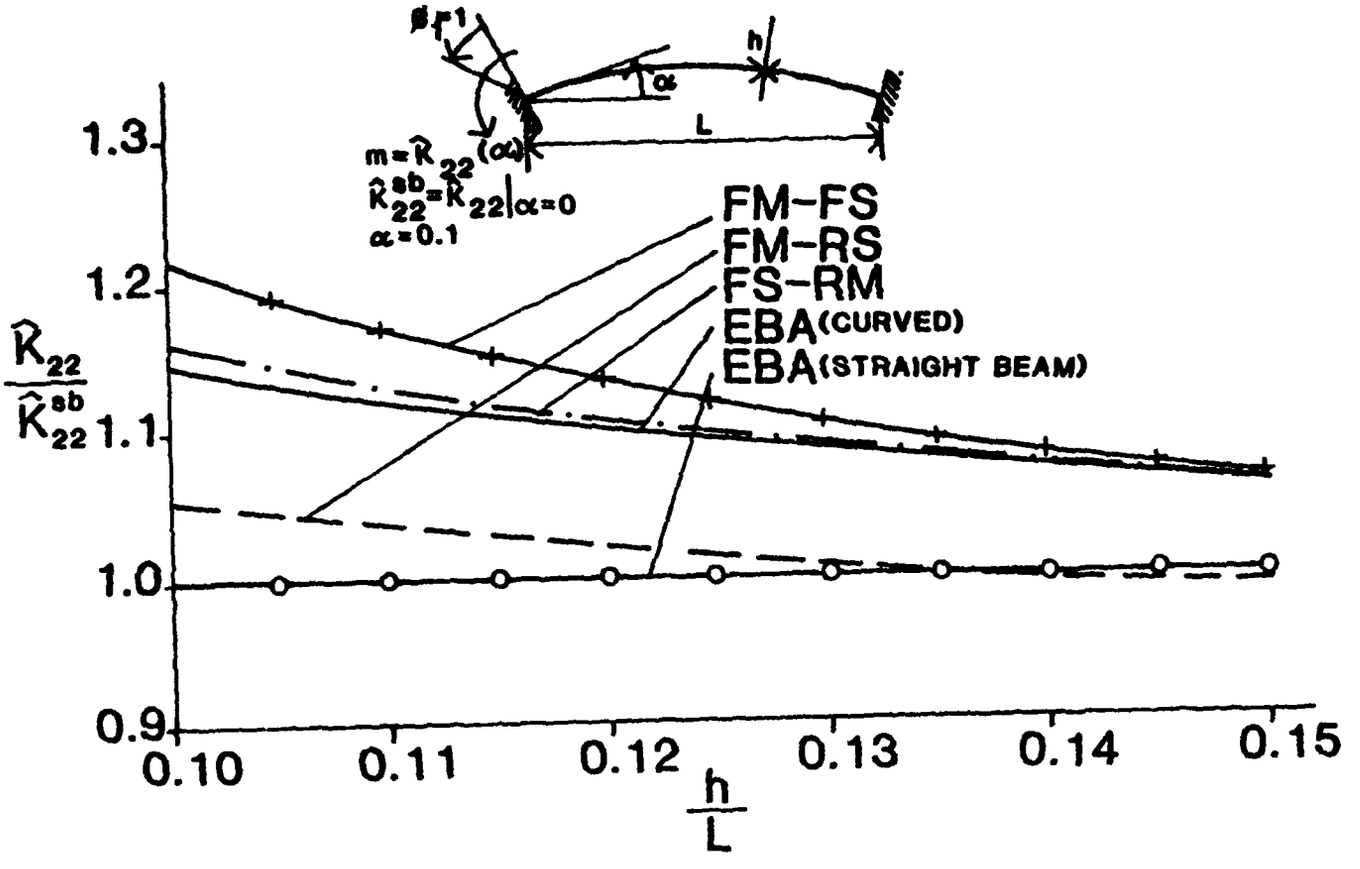
h
α
L
m=R̂22(α)
R̂22sb=R̂22|α=0
α=0.1
FM-FS
FM-RS
FS-RM
EBA(CURVED)
EBA(STRAIGHT BEAM)
R̂22 / R̂22sb
1.3
1.2
1.1
1.0
0.9
0.10
0.11
0.12
0.13
0.14
0.15
h/L

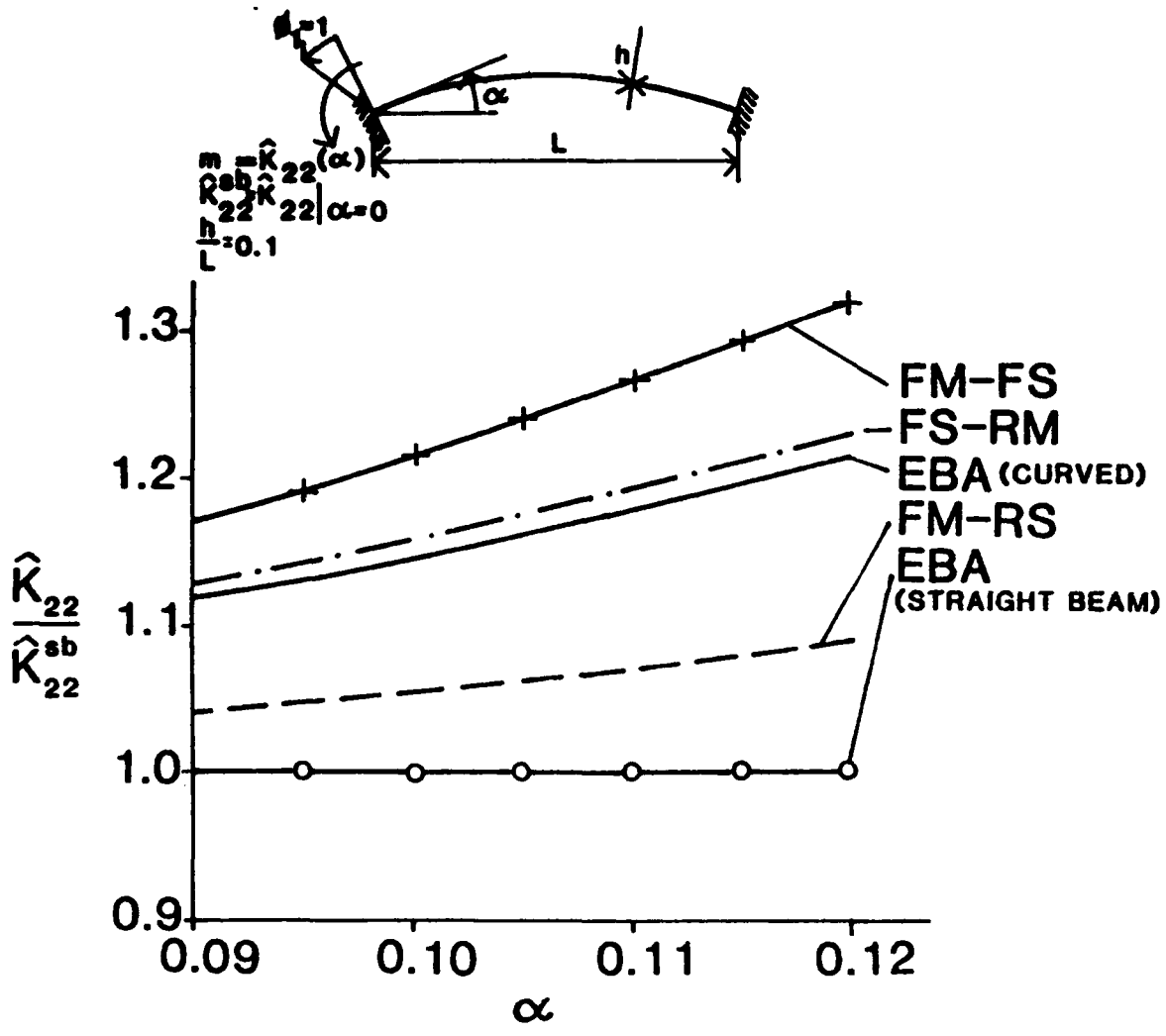
$\hat{K}_{22}$
$\frac{\hat{K}_{22}}{\hat{K}_{22}^{sb}}$
1.3
1.2
1.1
1.0
0.9
0.09
0.10
0.11
0.12
α
L
h
α
$\frac{h}{L}$=0.1
FM-FS
FS-RM
EBA (CURVED)
FM-RS
EBA
(STRAIGHT BEAM)

45°
2.935in
F
Δ
1.2in
0.125in
E = 1.05x10^7 psi
ν = 0.3
k = 1.0

END

FILMED

1-84

DTIC